Defining Protein Interactions With Small Heat Shock Proteins

Scott P Delbecq

A dissertation
Submitted in partial fulfillment of the
Requirements of the degree of

Doctor of Philosophy

University of Washington

2015

Reading Committee:

Rachel E. Klevit, Chair

Roland Strong

Dana Miller

Program Authorized to Offer Degree:

Department of Biochemistry

University of Washington

Abstract

Defining Protein Interactions With Small Heat Shock Proteins

Scott P. Delbecq

Chair of the Supervisory Committee:
Professor Rachel E. Klevit
Department of Biochemistry

Small heat shock proteins (sHSPs) are a class of molecular chaperones broadly observed across organisms where they play a central role in maintaining protein homeostasis under conditions of cellular stress. sHSPs are known to make protein-protein interactions that can be defined into two classes: 1) interactions with unfolded and aggregate-prone proteins (clients) to delay protein aggregation and 2) interactions with each other, leading to the formation of sHSPs oligomers. Here, progress in characterizing details of these interactions is presented.

sHSP are defined by three regions: an N-terminal region (NTR), a conserved Alpha Crystallin Domain (ACD), and a C-terminal region (CTR). All three regions are involved in sHSP oligomer formation. Here, we demonstrate the peptides mimicking CTRs of human sHSPs are able to interact with isolated ACDs. Using a strategy based on this observation, we are able to characterize the requirements for ACD/CTR binding and demonstrate this interaction can occur the context of human sHSP heterooligomers. Further, though other interactions are involved in forming sHSP oligomers, we are able to demonstrate ACD/CTR interactions plays a key role in recruiting an incoming subunit to a sHSP oligomer. These observations are relevant to understanding the details dynamic subunit exchange and heterooligomer formation in human sHSPs.

Defining how sHSPs interact with clients remains one of the pressing challenges in the sHSP field. It is unclear whether sHSPs interact with clients through a conserved mechanism. Using a variety of techniques, we set to compare and contrast how the human sHSP, HSPB5, and the wheat sHSP, wHSP16.9, interact with clients. Our observations suggest these sHSPs interact with clients through distinct binding modes. Further, the techniques presented were used to characterize other client/sHSP interactions including, client interactions with the HSPB5 disease-associated mutation, R120G.

Table of Contents

CHAPTER 1 An Introduction to small Heat Shock Proteins (sHSPs) and sHSP Oligomers

(Adapted from Delbecq, S.P, and Klevit R.E. (2013) One size does not fit all: the oligomeric states of αB crystallin. FEBS Lett. 587: 1073-1080.)

Small Heat Shock Proteins (sHSPs) are a diverse class of protein chaperones observed across all kingdoms of life [1]. Though the list of specific sHSPs functions continues to grow, sHSPs share an ability to interact with partly unfolded and aggregate-prone proteins to delay the formation of insoluble protein aggregates *in vitro* [2]. This so-called "holdase" function is held to be responsible for the increased viability sHSPs impart on cells under stress conditions and may explain the association of sHSPs with diseases tied to protein aggregation [3-5]. While the ability of sHSPs to delay protein aggregation has been known for decades, our current understanding of how sHSPs work remains limited due in large part to the fact that neither the sHSPs nor their aggregating "clients" are amenable to conventional structural and biochemical methods for characterizing protein structure and protein-protein interactions in detail. Recent developments in nuclear magnetic resonance spectroscopy (NMR), electron microscopy (EM), native mass spectrometry (MS), small angle x-ray scattering (SAXS), and other techniques are beginning to allow a more detailed view into the sHSPs and their interactions [6-10]. Among metazoan sHSPs, much of the recent effort has focused on human αB crystallin (HSPB5), which is highly expressed in eye lens, muscle, and brain [5,11,12]. The aim of this review is to highlight characteristics of αB crystallin (αB) that are key to understanding its structure and function. We present the current state of knowledge, inadequacies of current models, and identify outstanding questions that remain to be addressed and challenges to be overcome.

The sub-class of heat shock proteins known as the *small* heat shock proteins are defined by their shared architecture, composed of a conserved central domain called the "alpha crystallin domain" ("ACD") which is flanked by a highly variable N-terminal region ("NTR") and a variable C-terminal region ("CTR") that contains a small conserved motif known as the "IXI/V" (Figure 1). Despite their moniker of "small" (based on the size of the gene products), sHSPs are functionally very large because they assemble into oligomers. The diversity and properties of sHSP oligomers are highly unusual and are believed to be key to their broad holdase function. In particular, their tendency to form large polydisperse (variable number of subunits) oligomeric species that undergo dynamic subunit exchange is a distinguishing feature of this family of proteins. The properties of sHSPs and their cellular function involve two types of protein-protein interactions: 1) homomeric interactions responsible for the assembly of and dynamic equilibria among sHSP oligomers and 2) heteromeric interactions between sHSP species and their client proteins. An additional layer of complexity arises from the fact that metazoan sHSPs are thought to form hetero-oligomers (i.e., oligomers composed of more than one type of sHSP subunit), thereby allowing for hetero-homomeric interactions (i.e., sHSP-sHSP interactions). Furthermore, there is mounting evidence that some sHSPs including αB and HSP27 (HSPB1) interact with specific folded cellular proteins in addition to partly unfolded proteins, indicating that further parsing may be required in the heteromeric category of interactions [13,14]. An ultimate goal is a unifying model for the myriad interactions that define sHSP function.

Homomeric Interactions: A distribution of oligomeric states

There are two distinguishing features of sHSP oligomers. First, different sHSPs form oligomers with different numbers of subunits, with oligomers ranging from dimers to 40mers across all sHSPs. For example, the sHSP from the thermophile *Methoanococcus jannaschii*,

Hsp16.5, forms a spherical 24mer with octahedral symmetry and the sHSP from wheat, wHSP16.9, forms a dodecameric double disc with 3_2 symmetry [15,16]. Second, metazoan sHSPs such as αB form a polydisperse population of oligomers containing different numbers of subunits [17]. Species within the population are in a highly dynamic equilibrium, making it almost impossible to isolate or capture a single discrete species for detailed investigation. Furthermore, the species and the equilibria among them are strongly influenced by small changes in pH or by phosphorylation [18,19]. Thus, a realistic model for αB and its metazoan relatives must take into account the nature of all oligomeric species present. This requires answers to the following questions: Are there a finite number of states, i.e., are there upper and/or lower bounds to the number of subunits that exist in the oligomeric state? Is there a continuum of N, N+1, N+2, etc. oligomeric states? And what governs the interconversion among states? In addition, questions related to αB function include: Are there certain states responsible for holdase activity? Are there (inactive) storage forms? And do different forms interact with different clients? Although the field is far from having answers to all these questions, progress is being made at a growing pace.

In general, proteins belong to one of three categories, defined by their overall structural behavior: globular, fibrous, or intrinsically disordered. The first two categories include proteins that self-associate to form larger structures. Self-associating globular proteins adopt discrete tertiary and quaternary structures; fibrous proteins adopt repeating structures of indefinite size that are usually insoluble. αB is unusual in its tendency *not* to favor oligomers of a specific size while remaining one of the most highly soluble proteins known. In self-assembling systems, protein concentration is predicted to alter the population and/or size of oligomeric species observed. Notably, there are large differences in αB cellular concentrations: it is a major

component in the eye lens but exists at much lower concentrations in other tissues [12]. A number of studies have been directed towards understanding the size and distribution of αB oligomers. aB behaves as a very large species in the range of 600 kDa (corresponding to ca. 30 subunits) when analyzed using conventional methods such as size exclusion chromatography (SEC)[20]. Simple thermodynamic considerations would predict that larger species should be favored as the concentration of αB increases. It is therefore surprising that the distribution of αB oligomers has been shown to be concentration independent over a concentration range spanning three orders of magnitude by analytical SEC [20]. However, approaches such as SEC may not detect changes in 600 kDa species that correspond to differences of one or two 20 kDa subunits.

Unlike SEC, native Mass Spectrometry can provide fine-grained information regarding αB subunit distribution. αB oligomers ranging from 10-40mers have been detected by these methods [7]. The relative abundance of oligomers ranging from 22mers to 34mers was determined and used to model the full distribution of oligomeric states present under a specific condition [19]. Of particular note, the data appear to fit a Poisson distribution of species centered around 26mers to 28mers, in concordance with earlier SEC observations. Such a distribution is consistent with a model in which interactions responsible for each of the oligomeric species are isoenergetic [19,21]. It is notable that at physiological pH the mass distribution observed by native MS is biased to oligomers containing even numbers of subunits (i.e., 24mer, 26mer, 28mer. etc.)[19]. The bias for even numbered oligomers is lost under acidic conditions (pH 5)[19]. Global changes in the oligomeric state as a function of pH have also been observed by SAXS, where the ensemble of particles at low pH conditions have a larger radius of gyration and maximum diameter than under physiological conditions [21]. The MS observations are consistent with a dimeric building block being largely responsible for oligomer assembly under

physiological conditions. The data suggest that monomeric units exist, at least transiently, at lower pH and can be incorporated into and/or dissociate from αB oligomers. Thus, the homomeric interactions that define and determine αB dimers are fundamental to the structure and properties of αB oligomers. The dimer-monomer transition implied by the MS analysis suggests these interactions are pH dependent. Therefore, a model for αB at physiological pH should be based mainly on dimeric units whose dimer interface is sensitive to changes in pH.

MS analysis suggests that a continuum of oligomers exist simultaneously but provides no direct information about the existence of smaller species (<10mers) that might represent assembly intermediates. However, sedimentation velocity (SV) measurements by analytical ultracentrifugation offer additional insights. Concordant with the native MS, αB sediments as a broad distribution with sedimentation coefficients that correspond to a range between 18mers and 36mers [10]. Under slight destabilizing conditions (1.0 M guanidine), these large species are no longer detected and discrete species corresponding to dimers, hexamers, dodecamers, and 18mers are detected. Such species may represent structural intermediates from which larger species are assembled. These species are quite evanescent, as under an only slightly higher guanidine concentration of 1.5 M αB sediments entirely as monomer. Altogether the data suggest that αB exists as a distribution of oligomeric species that are built of units that include dimers, hexamers, and multiples of hexamers, but that the lifetime and population of the smaller species limit their detection under native conditions.

Homomeric Interactions: Structural Features.

The behavior of αB described poses a serious challenge to structural biology. Specifically, how much can we ever know about the structures that make up the distribution of species observed? What features do they have in common and how do they interconvert? In this section, we will

present current knowledge regarding αB structure and highlight the homomeric interactions that determine structure as well as those that appear to be responsible for the polydisperse nature.

THE ALPHA CRYSTALLIN DOMAIN (ACD)

Of the three regions that comprise a sHSP (Figure 1), the central ACD is the best characterized. As the only conserved element of sHSPs, the properties of ACDs are likely fundamental to function [15,22]. When expressed on their own, ACDs fold autonomously into a discrete structure, allowing atomic-level structures of many ACDs to be solved [23-26]. The fact that ACDs exhibit behavior more like a "normal" globular protein identifies the NTR and/or the CTR as determinants of polydispersity. In all (wild-type) sHSPs that have been structurally characterized, the ACD forms a homodimer and is therefore considered responsible for the lowest level of self-assembly, i.e., between monomer and dimer [23-26]. Protomer structures of the ~90-residue ACDs are highly similar from bacterial to human examples, while there is diversity at the level of dimer construction. All determined structures exhibit a 6-to-8-stranded β-sandwich structure for the ACD protomer, (Figure 2). The available structures of sHSP oligomers from non-metazoan organisms contain ACD homodimers built via domain-swapping. All metazoan ACD structures solved to date show an antiparallel homodimer with a dimer interface predominantly consisting of a long β6+7 strand [23-26](Figure 2). Structural differences among ACD structures have been previously discussed in detail [25].

Relevant to the topic of protein-protein interactions, a notable feature in available ACD structures is the remarkable plasticity they exhibit with respect to the register of the dimer interface. Three different strand registrations have been observed, one of which has been observed under neutral pH conditions [25]. Importantly, ACD crystals obtained at higher or lower pH have registers shifted by one residue in either direction. While it is not clear what

functional significance the observed dimers of differing strand register have, the plasticity that such behavior implies is likely relevant. The ability to form not just a single discrete anti-parallel intermolecular β-sheet but rather numerous ones (at least as captured in crystals) suggests that even the ACD region has evolved to allow for dynamic behavior that could contribute to polydispersity of oligomers. Whether the different dimer interfaces can interconvert directly via a strand-sliding mechanism or whether the conversion goes via a dimer-to-monomer dissociation is an open question. Relevant to this point, studies of the isolated αB ACD reveal that monomeric ACD becomes more favorable at lower pH [6]. Altogether, the structures and properties of the αB ACD homodimer discussed here are consistent with the pH-dependent dimer-monomer exchange proposed on the basis of distributions observed by native MS for oligomeric αB [19]. Thus, intrinsic properties that contribute to the special behavior of αB oligomers are recapitulated in isolated ACDs, allowing for their more detailed parsing using the more tractable ACD dimers for certain investigations.

THE C-TERMINAL REGION (CTR)

Unlike the ACD, the CTR does not fold autonomously. Available structural information regarding CTRs comes from crystal structures of ACDs that also contain a portion of the CTR and from NMR studies of αB oligomers. CTRs of metazoan sHSPs are diverse both in length and sequence, with the only identifiable conserved element being the so-called IXI/V motif, a three-residue sequence of alternating isoleucines (or valine)[22]. The IXI/V motif tends to be closer to the ACD than to the extreme C-terminal end of sHSPs, but the exact spacing between the end of an ACD and the IXI/V is not conserved among sHSPs. Existing information regarding the CTR of αB and its relatives highlights two main properties: 1) binding of the IXI/V motif into a

groove at the edge of an ACD called the β4/β8 groove (Figure 2) and 2) high flexibility of the extreme C-terminus.

The C-terminal IXI/V motif has been observed bound to the β4/β8 groove of an ACD in many experimentally determined structures of sHSPs. In all crystal structures where such an interaction is possible (i.e., the IXI/V region is contained in the protein constructs whose structures were determined) an interaction is observed [15,16,26]. Indeed, the bound state of this motif is observed across multiple kingdoms of life. In all but one example, (a truncated form of αA crystallin), the interaction is intermolecular, i.e., an IXI/V of one dimeric unit is bound to the ACD of another dimer (Figure 2). Although crystal packing could enable or enhance such "intermolecular" contacts, the inter-dimer contact is also observed in solid-state NMR studies of αB oligomer, making such an explanation less likely [27]. Furthermore, intermolecular binding of a peptide corresponding to the αB CTR to αB ACD homodimers has been observed in solution-state NMR studies [28]. That the interaction between the two isolated αB regions closely recapitulates what is observed in oligomers supports the idea that the ACD-CTR interaction contributes to the structure and properties of αB. Solid-state NMR spectra of αB oligomer reveal a pH-dependent alteration in the β4/β8 groove and IXI/Vmotif [27]. Specifically, single resonances are observed for residues in these structural elements under neutral conditions, while multiple resonances are detected at pH 6.5. The resonances at pH 7.5 correspond to the IXI-bound state, while the heterogeneity implied by multiple resonances at pH 6.5 points to a plasticity in the interaction. The observation of distinct multiple resonances as opposed to a single averaged resonance indicates that different structural copies of the β4/β8 groove and the IXI/V motif exist within oligomers, although the differences could be fairly subtle. As will be discussed in a later section, the ACD/CTR interaction serves to define the second level of

protein-protein interaction in αB oligomers, namely hexameric structures comprised of three αB dimers, each linked via their IXI/V motif to their neighbor (Figure 3b) Whether the interaction contributes thermodynamically to oligomer assembly is less clear. Notably, in many but not all sHSPs, mutation of the IXI/V motif results in reduced mass oligomers [29-32].

The CTR/ACD protein-protein interaction must be understood and interpreted not only in the context of structural properties but also in terms of the prevailing dynamics. Solution-based NMR methods on oligomeric sHSPs are able to detect resonances derived from the last 10-15 residues of the protein indicating this region is disordered and flexible relative to the rest of the protein [33]. Resonances detected by this method start at the extreme C-terminus and end in close proximity to the IXI/V motif. For example, the most N-terminal resonance detected in human αB is three residues after the second Ile in the IXI/V motif (Figure 1)[33]. However, in αA crystallin, the first detectable residue preceeds the first Ile of its IXI/V motif by one residue. The observations suggest that small differences in sequence and possibly solution conditions can affect the binding of the IXI/V motif and the flexibility of the CTR [33].

Solution NMR methods that specifically detect methyl groups in highly deuterated molecules are able to observe resonances for the Ile residues in αB oligomers. Among the nine resonances observed are two very strong resonances that have been assigned as the two Ile residues of the IXI/V motif. Relaxation data for these peaks are most consistent with the isoleucines existing in a predominantly flexible state [8]. Thus, similar to the observation that the homodimer interaction that defines the ACD homodimer exhibits dynamic and structural plasticity, the CTR/ACD interaction appears also to have a strongly dynamic character that is dependent on conditions including pH and temperature [27,34].

THE N-TERMINAL REGION (NTR)

The NTR remains the most enigmatic region of αB as its properties render it difficult to study biochemically and structurally. The NTR is the most divergent region among sHSPs both in length and sequence [15,22]. Nevertheless, it is clear that the NTR is largely responsible for the assembly of oligomers and their distribution. Truncation of the NTR yields an αB that forms oligomers that are both considerably smaller than normal (species ~40-180kDa can be observed) and that show a concentration dependence [20]. This assigns the role of driving the assembly of large αB oligomers and the dynamic distribution of oligomers to the NTR. Such a role hints at some special feature(s) of NTR sequences, but what these might be remains to be uncovered. Intriguingly, insertion of a small portion (14 residues) of the NTR of HSPB1/HSP27, which forms large, polydisperse oligomers like αB, into that of a bacterial sHSP that forms distinct 24mers that can be crystallized generated a chimeric sHSP that forms a 48mer [35]. The finding implies that the peculiar properties of NTRs are both context dependent and that one can evolve sHSPs that form different oligomers simply by altering the NTR. In this regard, we note that the NTR is subject to phosphorylation in αB and other human sHSPs (Figure 1)[36,37]. Serine phosphorylation or its mimicry by serine-to-aspartate substitutions is reported to shift the distribution of oligomers towards smaller species when analyzed by SEC [18, 37]. As phosphorylation is thought to produce more active αB, the result implies that smaller species may represent holdase-active forms, but this implication has not been confirmed experimentally. Native MS analysis of αB phosphomimics provides a slightly different picture. Here, oligomers within the same range as seen in the native species are observed, but there appears to be an effect on the distribution of species [40]. A single Ser-to-Asp phosphomimic was indistinguishable to the native αB whereas a double substitution (there are three phosphorylation sites recognized on

αB) shifts the distribution from the native dimer-biased distribution (i.e., oligomers with even numbers of subunits) to a smoother distribution in which odd numbered oligomers are also populated. The authors of this study suggest that phosphorylation of the NTR is associated with a weakening of the dimer interface but given current knowledge of the elements that define αB dimers it is difficult to propose a structurally sensible model for how this might be accomplished.

Presently, the only experimentally-derived structural information available for the αB NTR comes from ssNMR studies. The first five N-terminal residues are highly flexible and the remainder of the NTR displays significant heterogeneity [21]. While only single resonances are observed for ACD residues in spectra of αB oligomers at pH 7.6, multiple and/or lower intensity resonances are observed for many NTR residues, indicating the presence of heterogeneous states [21]. For example, there are eight distinct resonances apparent for nuclei from Met68 indicating there are at least 8 different environments for the residue [6]. Whether different environments exist simultaneously within a single oligomer species or are specific to different oligomeric species is unknown, but it is likely that both explanations are correct. Despite the heterogeneity, there are restraints observed by ssNMR consistent with helical structure (for residues 14-17 and 27-31) and with an antiparallel β-hairpin structure (for residues 48-50 and 61-63) (Figure 1)[21]. Though the NMR observations indicate that such secondary structure exists, the multiple resonances observed for these regions should be taken as an indication that they exist as an ensemble in different environments and possibly different conformations. Again, whether different NTR structures can interconvert within an oligomer or are oligomer-specific cannot be experimentally determined with available technology. Altogether, the data depict an NTR that cannot be described by a single structure or in a single unique environment.

Oligomer Models

The inherent size and polydispersity of sHSPs make them challenging targets to characterize structurally. The heterogeneity in structure and the distribution of oligomeric states imposes the reality that no single structure can accurately depict the "structure" of αB. Thus it is not (presently) possible to generate atomic-level structures of αB experimentally. However, pseudo-atomic models derived from the merging of data from different methodologies (listed below), have been proposed for the αB oligomer (Figure 3). The key technological breakthrough was the ability to obtain detailed information at atomic level from solid-state NMR on samples of αB oligomer. The first model, proposed by Jehle and colleagues in 2011, is based predominantly on ssNMR restraints along with SAXS data and previously reported negative-stain EM density [21, 46]. Braun et al. subsequently proposed a model in which they fit the ACD dimer structure determined from the ssNMR data and homology models for the CTR and NTR into higher resolution cryo-EM density [10,27]. Both groups used cross-linking to verify features of the models. A third model for αB oligomer has been proposed based on native MS measurements [8,9,19,34]. Rather than providing a pseudo-atomic model, it presents a residue-specific model for the kinetics of oligomer subunit exchange and the distribution of oligomers observed. It is important to keep in mind that none of these models propose that a single structure can represent the oligomeric state of αB. The models each aim to provide a structural rationale for known properties of αB. Consistent with the previous sections of this article, models should have the following features: 1) be built of dimeric units in which the ACD β6+7 strand forms the dimer interface, 2) place dimers in positions relative to each other that allows for the inter-dimer ACD-IXI/V interaction, and 3) provide a structurally reasonable explanation for the observed distribution of and dynamic interchange among oligomer species. Furthermore, realistic models should provide hints or insights regarding the "holdase" function of αB.

Jehle Model. The model proposed by Jehle et al. relies on ssNMR restraints to provide atomic level structural information and previously reported 20Å negative stain-EM density to define the overall architecture [21,46]. ssNMR restraints were sufficient to define the structure of the ACD homodimer and the interdimer contact between the C-terminal IXI/Vmotif and the ACD β4/8 Groove within the oligomer (Figure 2). Three copies of ACD dimers, each with its CTR IXI/V bound into the groove of a neighboring ACD fit into the prominent triangular torus feature observed in the EM density, thereby satisfying two of the requirements of a model as outlined above (Figure 3b). This provides an atomic-level model of a 3-fold symmetric hexameric (trimer of dimers) torus for αB residues 60-163 (~60% of the protein sequence). The negative-stain EM density indicates an arrangement of four hexameric rings in tetrahedral symmetry, thereby providing a way to form a 24-subunit oligomer (Figure 3c,d top). The inherent symmetry of the 24mer aided the modeling of the oligomer and therefore a pseudo-atomic model for the 24mer was generated rather than other more abundant species. In the 24mer model, all copies of the ACD dimer and the CTR through the IXI/V sequence are identical, consistent with the single set of ssNMR resonance observed for these regions.

As previously discussed, there are limited NMR restraints for the NTR and multiple conformations and/or environments exist simultaneously. For the sake of simplicity, secondary structure for the NTR was generated using homology modeling biased towards structures containing secondary structure consistent with sparse ssNMR restraints (Figure 1). Placement of these elements in the interior of the 24mer was based on the inability to fit experimental SAXS data of αB oligomer with a hollow particle model. Cysteine cross-linking was used to validate

the intermolecular proximity for regions of the NTR within the oligomer, suggesting that the placement of NTRs relative to each other is realistic.

A 24mer represents only ~5% of the oligomeric population of αB and is at the lower end of the distribution observed by native MS [19]. Does the Jehle model provide hints about how 26mers, 28mers, etc. are built and why their interchange is so facile? By placing the NTRs primarily on the inside of their model, Jehle et al., posited that additional αB dimers can pack in a region between hexameric rings to build larger oligomers from the 24mer scaffold. There are six such sites in the model, allowing for oligomers up to 36mers, encompassing the majority of the oligomeric population. Each site within the symmetrical 24mer is identical, providing a way to isoenergetically form 26mer, 28mer, and so on, consistent with the normal distribution of oligomers.

Braun Model: Braun and colleagues used cryo-EM density that afforded higher resolution (9.4 Å) than their earlier 20 Å negative-stain EM density [10]. Similar to the negative stain data, density corresponding to hexameric rings are a prominent feature of the cryo-EM density and trimers of the ssNMR-determined ACD dimers were placed into this density. New features observed in the cryo-EM density include density on the surface of the particles at the three-fold axes where hexameric rings converge and an absence of density in the core of the particle (Figure 3b-d bottom). To account for the density at the 3-fold axis NTRs were modeled into this region. The Jehle model does not satisfy this density. The resulting 24mer model is a hollow sphere compared to the more compact 24mer particle proposed in the Jehle model (Figure 3c,d). The NTR is where the two models are most divergent (Figure 1 and 3c,d). The NTRs differ between the two models not only in their placement within the oligomer but also in their

secondary structure, which Braun et al. chose to generate by homology modeling that does not account for observed sparse ssNMR restraints for the NTR (Figure 1). Thus, the modeled NTR in the Braun model differs from the Jehle model and does not satisfy ssNMR restraints. As the NTR is the most structurally heterogeneous element of a polydisperse oligomer population, it is perhaps not surprising that differences in this region arise in different models.

In an effort to characterize oligomers other than 24mers, single particle images were surveyed for projections consistent with a range of oligomers (biased towards hexamer-based oligomers). Images consistent with a broad range of oligomers were indeed observed, suggesting that though there is a bias towards the 24mer-based assembly and for oligomers with even numbers of subunits, other oligomeric structures are present in an αB oligomeric population at low, but detectable levels.

Baldwin model: A third model for αB oligomer is based on solution NMR relaxation and native MS measurements [8,9,19,34]. Rather than provide a structural picture, the goal of this model is to explain the underlying thermodynamics and kinetics that drive oligomer formation and subunit exchange. The experimental observations on which the model is based are 1) subunit exchange rate between αA and αB oligomers measured by MS and 2) measured relaxation properties of NMR peaks assigned to the C-terminal IXI/V motif in the context of oligomer in solution. Methyl-TROSY NMR data indicate that the IXI/V motif exists in two states, a highly populated dynamic flexible state and a lowly populated (~2% of the population) bound state [34]. The unobserved bound state is inferred to possess properties (i.e., NMR resonances) that would be consistent with bound states observed by ssNMR and crystallographic methods. The proposed predominance of a mobile IXI/V motif contrasts with previously observed ssNMR,

crystallographic data, and the observation of CTR peptide binding to αB ACDs in solution by NMR [27,15,16, 28,26]. It is presently unclear whether the discordance among these observations can be rationalized by the variable experimental conditions required for each specialized method and/or differences in what species are actually detected by the various techniques [34].

An exchange rate between the abundant flexible IXI/V and the inferred IXI bound state calculated from NMR relaxation measurements is similar to the rate of subunit exchange between αB and αA oligomers, if one assumes two IXI/V interactions must exist in the bound state for a monomer to leave the oligomer. From this observation, Baldwin et al. suggest that the on/off rate of the CTR IXI/V motif is rate-determining for subunit exchange. The model assumes that all protomers in an oligomer are equivalent and make the maximum number of inter/intramolecular contacts possible, including an intra-dimer interaction (i.e., the ACD dimer interaction) and two CTR interactions per subunit (i.e., accepting and donating a CTR IXI/V motif). The proposed requirement for bound IXI/V motif in subunit dissociation is novel and somewhat contrary to previous suggestions that the IXI/V motif makes interactions that define and/or stabilize oligomers.

The collision-cross section of αB oligomers derived from ion mobility MS was used to ascertain the overall oligomer architecture. In contrast to the EM density used as a basis for the two pseudo-atomic models, a MS-based 24mer model with octahedral symmetry has been proposed in which an ACD dimer makes each “edge”. The current model does not account for the αB NTR and offers no hypothesis or prediction of how this region contributes to subunit exchange or oligomer formation.

Given the inherent heterogeneity and polydispersity of αB oligomers, it should perhaps not be surprising that different models exist. It is likely that features of each realistically represent aspects of αB. Parsing out what those are is critical in generating a more unified picture and is a challenge to be met by future efforts.

Heteromeric Interactions: mixed oligomers.

Oligomers composed of subunits of more than one sHSP have been inferred to exist both in cells and *in vitro* [41-45]. Of the proposed sHSP heteroligomers, the lens sHSPs αA and αB crystallin heterooligomer is the best characterized [47,48]. However, we still have a poor understanding of how heteromeric species are assembled and the necessity of having to account for more than one type of subunit in what is already an extremely complicated system makes the prospect of generating atomic-level models seem a low probability. Nevertheless, it should be possible to identify which of the protein-protein interactions that define homomeric αB oligomers can also occur between two different types of subunit. At the lowest level, can heteromeric ACD dimers form? Such species have not been been observed directly, but given the high degree of conservation among at least some of the human sHSPs (αA and αB, for example), it seems likely that heterodimeric species are possible [22]. That heterooligomer could be composed of homodimers or of heterodimers further increases the possible diversity and complexity. Similarly, the high conservation of both the β4/β8 ACD groove and the IXI/V motifs among at least a subset of sHSPs predicts that it is possible to assemble heteromeric hexameric sub-structures. Indeed, it has been observed that peptides mimicking different IXI/V motifs from other sHSPs are able to bind the β4/β8 ACD groove of αB [28]. The next level of assembly raises the question of interactions involving NTRs. These are the most divergent and the least is known about what the determinants for NTR-directed assembly are. A likely scenario is that the

diversity among NTRs could serve as both positive and negative determinants that control the types and compositions of hetero-oligomers that can form [35].

Heteromeric Interactions: Client Binding.

The single most outstanding question regarding sHSPs is how they interact with client proteins to delay the formation of insoluble protein aggregates. Fundamental knowledge such as 1) what αB species interact with clients and is this client-specific, 2) what regions within an αB oligomer interact with clients and is this client-specific, 3) what properties of a client are recognized in this interaction and 4) what is the lifetime of an αB-client interaction is currently almost completely lacking. Reports that small sequences from αB on their own display the ability to chaperone aggregation-prone proteins raise the specter that the function derives from as yet undefined properties of interactions between disordered polypeptides [39]. Further, if and how dynamic properties of sHSPs contribute to function remains unclear. Given what is known about interactions involving αB, it is reasonable to expect that those involving client interactions will also be evanescent and highly dynamic. The sheer diversity of potential unfolded client proteins that αB may encounter in a cell under stress conditions argues that there will not be singular solutions and that once again, an inherent diversity of protein-protein interactions define the system. Although they represent an important step forward in our understanding of the structure of αB, the recent models discussed above have not revealed profound insight into how sHSPs function. Similar to studies that ultimately provided atomic-level information about αB, it is likely that the ability to glean information from simplified systems will allow for progress to be made in the future towards obtaining answers to the questions raised. This will no doubt require the use of model clients that can be characterized at the residue, if not atomic level.

Conclusion

The past several years have seen remarkable progress in information regarding how the sHSP αB is assembled into an array of oligomeric species. This has been made possible by technological developments and by the ability to combine information from multiple experimental details to overcome the intransigence of the system to conventional structural biology approaches. In this review, we have attempted to highlight both the new insights gained from these efforts and the challenges that remain to be met. It is clear that the inherent and highly unusual properties of αB put new demands on how we think about its structural biology. As the functional repertoire of αB and the human diseases and disorders in which it is implicated continue to expand, interest in these fascinating protein assemblies and their highly unusual properties will continue to grow apace.

Figures

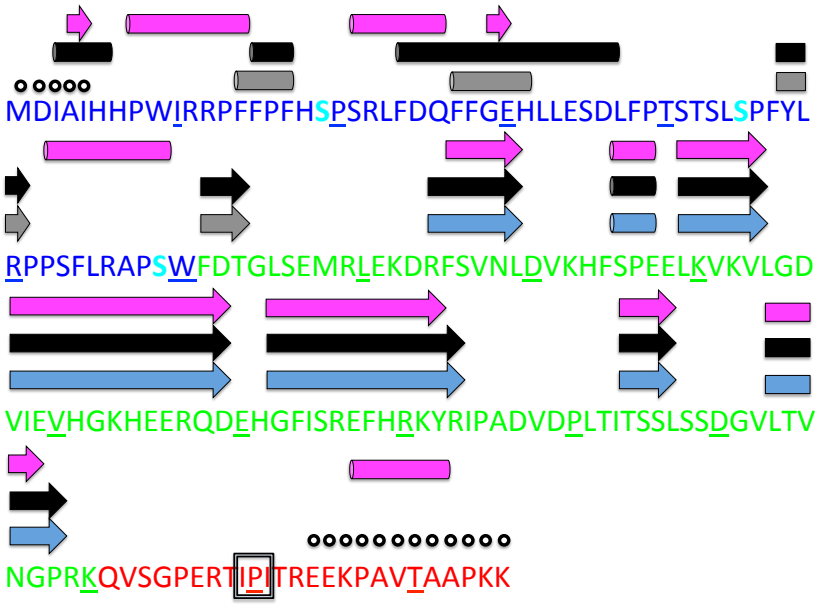

Figure 1. αB domain architecture, primary and secondary structure. The three domains/regions that define sHSPs are highlighted on the sequence of αB, with NTR residues in blue text, ACD residues in green, and CTR residues in red. Every tenth residue is underlined as a point of reference. In the NTR, three known phosphorylation sites are shown in cyan. The IXI/V motif in the CTR is shown in the black box. Secondary structure is summarized in three rows above the sequence, as cylinders (α-helix) and arrows (β-strand). TOP (magenta): secondary structure in the Braun model (PDB ID 2ygd). MIDDLE (black): secondary structure in the Jehle model. BOTTOM: experimentally-derived structural information, with secondary structure determined from ssNMR-based ACD structure shown in light blue, structure inferred from sparse ssNMR restraints shown in grey, and flexible regions measured by ssNMR and solution based NMR are shown in open circles.

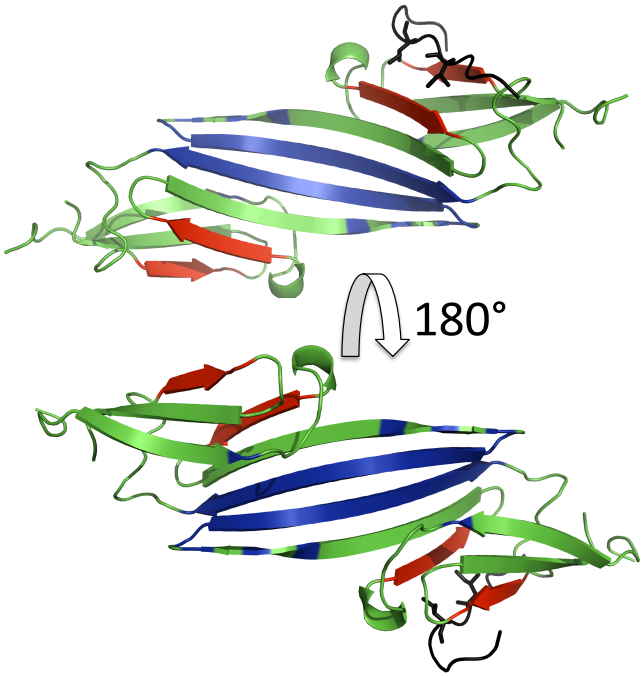

Figure 2. ssNMR structure of the αB ACD dimer (PDB 2klr) with the CTR IXI/V motif bound. Residues involved in intermolecular contacts are highlighted on both protomers. Regions involved in intra-dimer contacts that define the dimer interface are shown in blue and the β4/β8 grove involved in inter-dimer interactions with the CTR IXI/V motif (from a neighboring dimer) are shown in red. The CTR sequence PERTIPITREEK is shown in black (bound to one protomer for clarity) and the Iles of the IXI/V motif are rendered as sticks. Two views of the ACD are presented, rotated 180° about the x-axis.

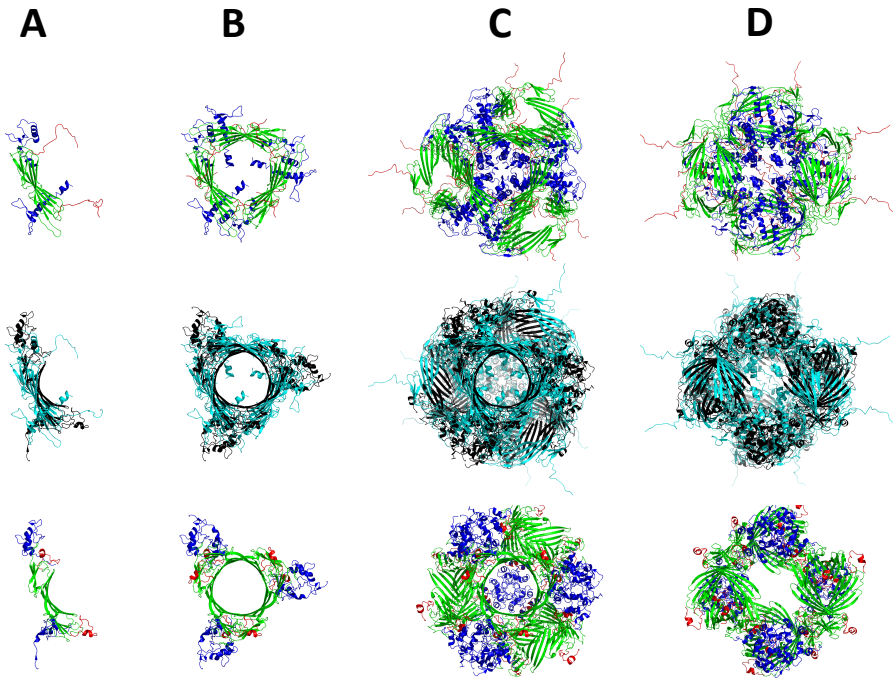

Figure 3. Comparison of the two pseudo-atomic models of an αB 24mer. The NTR (Blue), ACD (Green), and CTR (red) are displayed in different colors in the Jehle model (top row) and the Braun model (bottom row). The two models are aligned in the middle row, with the Jehle model in cyan and the Braun model in black. The hierarchy of assembly for the 24mer models is represented across columns A-D. The dimeric building block defined by intra-dimer contacts (A) are shown assembled into hexameric rings through CTR/ACD inter dimer interactions (B) and four hexamers are assembled through NTR interactions to form the 24mer oligomer (C and D). The models differ significantly in the placement of the NTR. The view in column D (rotated 55° about the y-axis relative to column C) clearly shows the Braun model to be a hollow particle with the NTR on the surface while the core of the particle is filled with the NTR in the Jehle model.

References

1. Haslbeck M, Franzmann T, Weinfurtner D & Buchner J & Buchner J (2005) Some like it hot: the structure and function of small heat-shock proteins. *Nat Struct Mol Biol* **10,** 842-846**.**

2. Horwitz J (1992) Alpha-crystallin can function as a molecular chaperone. *Proc Natl Acad Sci USA* **89**, 10449–10453.

3. Vicart P, Caron A, Guicheney P, Li Z, Prévost M, Faure A, Chateau D, Chapon F, Tomé F, Dupret J, Paulin D & Fardeau M (1998) A missense mutation in the αB-crystallin chaperone gene causes a desmin-related myopathy. *Nat Genet* **20**, 92–95.

4. Goldstein LE, Muffat JA, Cherny RA, Moir RD, Ericsson MH, Huang X, Mavros C, Coccia JA, Faget KY, Fitch KA, Masters CL, Tanzi RE, Jr LTC & Bush AI (2003) Cytosolic β-

amyloid deposition and supranuclear cataracts in lenses from people with Alzheimer's disease. *Lancet* **361**, 1258-1265.

5. Kato K, Inaguma Y, Ito H, Iida K, Iwamoto I, Kamei K, Ochi N, Ohta H & Kishikawa M (2001) Ser-59 is the major phosphorylation site in aB-crystallin accumulated in the brains of patients with Alexander's disease. *J Neurochem* **76**, 730–736.

6. Jehle S, van Rossum B, Stout JR, Noguchi SM, Falber K, Rehbein K, Oschkinat H, Klevit RE & Rajagopal P (2009) alphaB-crystallin: a hybrid solid-state/solution-state NMR investigation reveals structural aspects of the heterogeneous oligomer. *J Mol Biol* **385**, 1481-1497.

7. Aquilina JA, Benesch JL, Bateman OA, Slingsby C & Robinson CV (2003) Polydispersity of a mammalian chaperone: mass spectrometry reveals the population of oligomers in alphaB-crystallin. *Proc Natl Acad Sci USA* **100**, 10611-10616.

8. Baldwin AJ, Hilton GR, Lioe H, Bagneris C, Benesch JLP & Kay LE (2011) Quaternary Dynamics of αB-Crystallin as a Direct Consequence of Localised Tertiary Fluctuations in the C-Terminus. *J Mol Biol* **413**, 310–320.

9. Baldwin AJ, Lioe H, Hilton GR, Baker LA, Rubinstein JL, Kay LE & Benesch JLP (2011)The Polydispersity of aB-Crystallin Is Rationalized by an Interconverting Polyhedral Architecture. *Structure* **19**, 1855–1863.

10. Braun N, Zacharias M, Peschek J, Kastenmüller A, Zou J & Hanzlik M (2011) Multiple molecular architectures of the eye lens chaperone αB-crystallin elucidated by a triple hybrid approach. *Proc Natl Acad Sci U S A* **108**, 20491-20496.

11. Tallot P, Grongnet & David JC (2003) Dual perinatal and developmental expression of the small heat shock proteins [FC12]aB-crystallin and Hsp27 in different tissues of the developing piglet. *Biol Neonate* 83, 281-288.

12. WW de Jong H. Bloemendal (Ed.), Molecular and Cellular Biology of the Eye Lens, Wiley, New York (1981), pp. 221–278.

13. Kase S, He S, Sonoda S, Kitamura M, Spee C, Wawrousek E, Ryan SJ, Kannan R, Hinton DR. (2010). alphaB-crystallin regulation of angiogenesis by modulation of VEGF. *Blood* **115**, 3398-406

14. Hu WF, Gong L, Cao Z, Ma H, Ji W, Deng M, Liu M, Hu XH, Chen P, Yan Q, Chen HG, Liu J, Sun S, Zhang L, Liu JP, Wawrousek E & Li DW. (2012) αA- and αB-crystallins interact with caspase-3 and Bax to guard mouse lens development. *Curr Mol Med* **12**, 177-187

15. Kim KK, Kim R & Kim SH (1998) Crystal structure of a small heat-shock protein. *Nature* **394**, 595–599.

16. van Montfort RL, Basha E, Friedrich KL, Slingsby C & Vierling E (2001) Crystal structure and assembly of a eukaryotic small heat shock protein. *Nat Struct Biol* **8**, 1025–1030.

17. Haley DA, Horwitz J & Stewart PL (1998) The small heat-shock protein, alphaB-crystallin, has a variable quaternary structure. *J Mol Biol* **277**, 27–35.

18. Ito H, Kamei K, Iwamoto I, Inaguma Y, Nohara D & Kato K (2001) Phosphorylation-induced change of the oligomerization state of alpha B-crystallin. *J Biol Chem* **276**, 5346–5352.

19. Baldwin AJ, Lioe H, Robinson CV, Kay LE & Benesch JLP (2011) αB-crystallin polydispersity is a consequence of unbiased quaternary dynamics. *J mol biol* **413**, 297–309.

20. Horwitz J (2009) Alpha-Crystallin: The Quest For A Homogeneous Quaternary Structure. *Exp Eye Res* **88**, 190-194.

21. Jehle S, Vollmar BS, Bardiaux B, Dove KK, Rajagopal P, Gonen T, Oschkinat H & Klevit RE (2011) N-terminal domain of alphaB-crystallin provides a conformational switch for multimerization and structural heterogeneity. *Proc Natl Acad Sci U S A* **108**, 6409–6414.

22. Taylor RP & Benjamin IJ (2005) Small heat shock proteins: a new classification scheme in mammals. *J Mol Cellular Cardiol* **38**, 433–444.

23. Bagnéris C, Bateman OA, Naylor CE, Cronin N, Boelens WC, Keep NH & Slingsby C (2009) Crystal structures of alpha-crystallin domain dimers of alphaB-crystallin and Hsp20. *J Mol Biol* **392:** 1242-1252. (doi: 10.1016/j.jmb.2009.07.069)

24. Baranova EV, Weeks SD, Beelen S, Bukach OV, Gusev NB & Strelkov SV (2011) Three-dimensional structure of α-crystallin domain dimers of human small heat shock proteins HSPB1 and HSPB6. *J Mol Biol* **411:** 110-122 (doi: 10.1016/j.jmb.2011.05.024)

25. Clark AR, Naylor CE, Bagnéris C, Keep NH & Slingsby C (2011) Crystal structure of R120G disease mutant of human αB-crystallin domain dimer shows closure of a groove. *J Mol Biol* **408:** 118-134 (doi: 10.1016/j.jmb.2011.02.020)

26. Laganowsky A, Benesch JLP, Landau M, Ding L, Sawaya MR, Cascio D, Huang Q, Robinson CV, Horwitz J & Eisenberg D (2010) Crystal structures of truncated alphaA and alphaB crystallins reveal structural mechanisms of polydispersity important for eye lens function. *Protein Sci* **19**, 1031–1043.

27. Jehle S, Rajagopal P, Bardiaux B, Markovic S, Kühne R, Stout JR, Higman VA, Klevit RE, van Rossum BJ & Oschkinat H (2010) Solid-state NMR and SAXS studies provide a structural basis for the activation of alphaB-crystallin oligomers. *Nat Struct Mol Biol* **17**, 1037–1042.

28. Delbecq SP, Jehle S & Klevit R (2012) Binding determinants of the small heat shock protein, αB-crystallin: recognition of the "IxI" motif. *EMBO J*, Ahead of print.

29. Saji H, Iizuka R, Yoshida T, Abe T, Kidokoro S-I, Ishii N & Yohda M (2008) Role of the IXI/V motif in oligomer assembly and function of StHsp14.0, a small heat shock protein from the acidothermophilic archaeon, Sulfolobus tokodaii strain 7. *Proteins* **71**, 771–782.

30. Studer S, Obrist M, Lentze N & Narberhaus F (2002) A critical motif for oligomerization and chaperone activity of bacterial alpha-heat shock proteins. *Eur J Biochem* **269**, 3578–3586.

31. Pasta SY, Raman B, Ramakrishna T & Rao CM (2004) The IXI/V motif in the C-terminal extension of alpha-crystallins: alternative interactions and oligomeric assemblies. *Mol Vis* **10**, 655–662.

32. Giese KC & Vierling E (2004) Mutants in a small heat shock protein that affect the oligomeric state. *J Biol Chem* **279**, 32674–32683.

33. Treweek TM, Rekas A, Walker MJ & Carver JA (2010) A quantitative NMR spectroscopic examination of the flexibility of the C-terminal extensions of the molecular chaperones, αA- and αB-crystallin. *Exp Eye Res* **91**, 691–699.

34. Baldwin AJ, Walsh P, Hansen DF, Hilton GR, Benesch JLP, Sharpe S & Kay LE (2012) Probing dynamic conformations of the high-molecular-weight αB-crystallin heat shock protein ensemble by NMR spectroscopy. *J Am Chem Soc* **134**, 15343–15350.

35. McHaourab HS, Lin Y-L & Spiller BW (2012) Crystal structure of an activated variant of small heat shock protein Hsp16.5. *Biochemistry* **51**, 5105–5112.

36. Miesbauer LR, Zhou X, Yang Z, Yang Z, Sun Y, Smith DL & Smith JB (1994) Post-translational modifications of water-soluble human lens crystallins from young adults. *J Biol Chem* **269**, 12494–12502.

37. Stokoe D, Engel K, Campbell DG, Cohen P & Oaestep M (1992) Identification of MAPKAP kinase 2as a major enzyme responsible for the phosphorylation of the small mammalian heat shock proteins *FEBS Lett* **313**, 307–313.

38. McDonald ET, Bortolus M, Koteiche HA & Mchaourab HS (2012) Sequence, structure, and dynamic determinants of Hsp27 (HspB1) equilibrium dissociation are encoded by the N-terminal domain. *Biochemistry* **51**, 1257–1268.

39. Bhattacharyya J, Udupa EGP, Wang J & Sharma KK (2006) Mini-αB-Crystallin : A Functional Element of αB-Crystallin with Chaperone-like Activity. Biochemistry **45**, 3069–3076.

40. Aquilina JA, Benesch JLP, Ding LL, Yaron O, Horwitz J & Robinson CV (2004) Phosphorylation of alphaB-crystallin alters chaperone function through loss of dimeric substructure. *J Biol Chem* **279**, 28675–28680.

41. Zantema A, Verlaan-De Vries M, Maasdam D, Bol S, van der Eb A (1992) Heat shock protein 27 and alpha B-crystallin can form a complex, which dissociates by heat shock. *J Biol Chem* **267**, 12936–12941

42. Kato K, Goto S, Inaguma Y, Hasegawa K, Morishita R, Asano T (1994) Purification and characterization of a 20-kDa protein that is highly homologous to alpha B crystallin. *J Biol Chem* **269**, 15302–15309

43. Sugiyama Y, Suzuki A, Kishikawa M, Akutsu R, Hirose T, Waye MMY, Tsui SKW, Yoshida S & Ohno S (2000) Muscle develops a specific form of small heat shock protein complex composed of MKBP/ HSPB2 and HSPB3 during myogenic differentiation. *Biochemistry* **275**, 1095–1104

44. Bukach OV, Glukhova AE, Seit-Nebi AS & Gusev NB (2009) Heterooligomeric complexes formed by human small heat shock proteins HspB1 (Hsp27) and HspB6 (Hsp20). *Biochim Biophys Acta* **1794**, 486–495

45. Engelsman J, Boros S, Dankers PYW, Kamps B, Vree Egberts WT, Bo¨de CS, Lane LA, Aquilina JA, Benesch J, Robinson CV, de Jong WW & Boelens WC (2009) The small heat-shock proteins HSPB2 and HSPB3 form well-defined heterooligomers in a unique 3 to 1 subunit ratio. *J Mol Biol* **393**, 1022–1032

46. Peschek J, Braun N, Franzmann TM, Georgalis Y, Haslbeck M, Weinkauf S & Buchner J (2009) The eye lens chaperone alpha-crystallin forms defined globular assemblies. *Proc Natl Acad Sci U S A* **106**, 13272-13277

47. Siezen RJ, Bindels JG & Hoenders HJ (1980) The quaternary structure of bovine alpha-crystallin. Chemical crosslinking with bifunctional imido esters. *Eur J Biochem* **107,** 243-249

48. van den Oetelaar PJ, Van Someren PF, Thomson JA, Siezen RJ & Hoenders HJ (1990) A dynamic quaternary structure of bovine alpha-crystallin as indicated from intermolecular exchange of subunits. *Biochemistry* **29**, 3488-3493

CHAPTER 2 Binding determinants of the small heat shock protein, αB-crystallin: recognition of the "IxI" motif

(adapted from Delbecq, S.P., Jehle, S., and Klevit R.E. (2012) Binding determinants of the small heat shock protein, αB-crystallin: recognition of the "IxI" motif. EMBO J 31: 4587-4594.)

Introduction

Small heat shock proteins (sHSPs) help to maintain protein homeostasis by interacting with partly-unfolded, aggregate-prone proteins to prevent cell damage (Haslbeck et al., 2005; Bukau et al., 2006). In humans, there are ten members of the ATP-independent sHSP family (HSPB1, HSPB2, etc.) of which αB-crystallin ("αB" or HSPB5) is a paradigm example (Horwitz 1992). Though originally discovered in eye lens as a protein essential for maintaining lens transparency, αB is additionally expressed in muscle and brain. Specific biological roles for αB continue to emerge. In mice, knockout of αB reduces life span by half whereas its over-expression protects cardiac tissue from necrosis and myocardial infarction following ischemic stress (Brady et al., 2001; Ray, et al., 2001). Dysfunctions of αB in humans are associated with the occurrence of neurodegenerative diseases such as Alzheimer's disease and Alexander disease (Kato et al. 2001; Goldstein et al, 2003). Inherited missense mutations in αB are associated with desmin-related cardiomyopathy, congenital cataracts, and myopathy (Vicart et al., 1998; Selcen & Engel 2003; Liu et al., 2006;Rajasekaran et al., 2007). Furthermore, high expression of αB in cancer cells confers resistance to chemotherapy and is correlated with poor clinical outcomes (Vargas-Roig et al., 1998; Moyano et al., 2006). Yet despite its critical roles in maintaining healthy cells, understanding of αB structure and function remains rudimentary.

As is common for mammalian sHSPs, αB exists as large polydisperse assemblies containing variable numbers of subunits (Aquilina et al, 2003). The inherent dynamics of the assemblies is a defining feature and is likely linked to αB function. For decades, high-resolution structural studies on functional, full-length αB and mammalian sHSPs in general were confounded by both polydispersity and dynamics. Developments in solid-state NMR, solution-state NMR, and electron microscopy are finally providing experimental means to obtain atomic-level information on αB. Each approach has its strengths and weaknesses and each requires quite different experimental conditions under which a measurement can be made. Thus, a unifying model should be congruent with all observations to the extent possible.

As a class, sHSPs are defined by the presence of a conserved α-crystallin domain (ACD) that mediates formation of dimeric building blocks. The central ACD is flanked by highly variable N- and C-termini that mediate formation of the larger oligomeric assemblies (Jehle et al, 2009; Laganowsky et al, 2010; Bagnéris et al, 2009; Baldwin et al, 2011). sHSP oligomers may be comprised of a single type of subunit or of a combination of different subunits (Sun & Liang, 1998; Zantema et al, 1992; Engelsman et al, 2009; Bukach et al, 2009; Sugiyama et al, 2000; Kato et al, 1994). Atomic-level structures of ACDs from a number of mammalian sHSPs including αB have been determined by x-ray crystallography and solid-state NMR (ssNMR) (Laganowsky et al, 2010, Bagnéris et al, 2009; Clark et al, 2011; Baranova et al, 2011; Jehle et al, 2010). Atomic-level structures are available for non-mammalian sHSP oligomers (Montfort et al, 2001; Kim et al, 1998; Stamler et al, 2005; Hilario et al, 2011). Pseudo-atomic models for αB have been generated using data from a combination of methods including solid-state NMR, SAXS, negative-stain EM and cryo-EM (Jehle et al, 2011; Braun et al, 2011). The growing

database of structural information provides a rich resource for studies aimed at understanding how sHSP structure is related to function.

Structures of sHSP oligomers and of isolated ACDs reveal some common features. The ACD is a 6-8 stranded β-sandwich structure and two ACDs usually associate in an anti-parallel fashion to form homodimeric units that serve as the building block for higher-order structures (see Supplemental Figure S1) (Laganowsky et al, 2010, Bagnéris et al, 2009; Jehle et al, 2011; Clark et al, 2011; Baranova et al, 2011; Jehle et al, 2010). In addition, sequences from outside the ACD have been observed to be in contact with the ACD both in crystalline samples and by solid-state NMR. The interactions involve three ACD regions: 1) the β3 strand, 2) a groove on the edge of the ACD structure known as the β4/β8 groove, and 3) the surface formed by the dimer interface (Laganowsky et al, 2010, Bagnéris et al, 2009; Montfort et al, 2001; Kim et al, 1998; Jehle et al, 2011) (see Supplementary Figure S1 for strand nomenclature).

In what is by far the most frequently observed interaction, a small conserved sequence motif called the IxI/V motif found in the C-terminal region of many sHSPs is bound in the β4/β8 groove of an ACD. The motif is comprised of two Ile (or Val) residues separated by one residue. The interaction has been observed both in the context of homo-oligomers such as αB-crystallin, MjHSP16.5, and wheat HSP16.9, and in the context of ACD crystals, where the interactions take place among neighboring dimers in the crystal lattice (Laganowsky et al, 2010; Montfort et al, 2001; Kim et al, 1998; Jehle et al 2011). Heteromeric IxI/V-β4/β8 interactions have been detected in solution between human sHSPs, αB and αA-crystallin (αA) by FRET experiments (Pasta et al, 2004). That the ACD-IxI/V interaction is observed in so many contexts implies some shared structural and/or functional role. To varying degrees, the interaction has been implicated in oligomer formation (Pasta et al, 2004; Studer et al, 2002). Deletions spanning the C-terminal

motif result in a loss of higher-order oligomeric structure in multiple sHSPs and mutation of the conserved motif residues Ile/Val (IxI/V) to Gly (GxG), Ala (AxA), or to Phe (FxF) also appears to abrogate the interaction (Pasta et al, 2004; Studer et al, 2002; Hayes et al, 2008; Takeda et al, 2011). Altogether, the observations suggest that the ACD-IxI/V interaction has a role in oligomer structure. While solution-state NMR studies at 25°C, designed to specifically detect highly flexible regions detect the IxI/V motifs in some sHSP oligomers the same experiments fail to observe this region in αB, implying the region is either bound within oligomer or is exchanging among multiple states (Treweek et al, 2010; Benesch et al, 2010; Ghahghaei et al, 2009). In contrast, a ^{13}C-methyl -TROSY solution-state NMR study on αB oligomers at temperatures ranging from 24-50°C contained signals assigned to the IxI/V motif congruent with the residues being highly flexible and in an unbound state (Baldwin et al, 2011). This observation led the authors of that study to propose that the IxI/V interactions observed in structural studies of sHSPs in the solid-state or crystalline form may not accurately reflect the oligomer in solution (Baldwin et al, 2011). Here, we assess the inherent binding properties of an ACD and an IxI/V motif outside an oligomeric or crystalline context. Towards this end, we have tested the ability of peptides that mimic sequences from human sHSPs to bind to αB-ACD and identify determinants for the interaction using solution-state NMR.

Results

An ACD Can Bind A CTR Outside The Oligomeric Context

The isolated ACD of αB (residues 64-152; called αB-ACD) forms well-behaved dimers that are amenable to solution-state NMR (Jehle et al, 2009). NMR resonance assignments for the αB-ACD have been previously reported and provide the ability to obtain residue-specific

information regarding potential peptide binding to an isolated ACD dimer (Jehle et al, 2009). Solution-state ^{1}H-^{15}N HSQC NMR spectra provide both a peak position (^{15}N and ^{1}H chemical shift) and peak intensity for ^{15}N-labeled proteins. Comparison of spectra collected on samples that contain increasing amounts of a putative binding partner will reveal perturbations in either the position, the intensity of a peak, or both. Perturbations are caused by a change in the local environment of the nuclei responsible for the peak. In this way, events such as peptide or protein binding can be detected, quantified, and mapped onto known structures of the protein under investigation.

NMR binding experiments were performed by titrating peptides with sequences containing the C-terminal IxI motif of αB or other human sHSPs into NMR samples of ^{15}N-αB-ACD. The effect of peptide addition was monitored in the ^{1}H-^{15}N HSQC NMR spectra of αB-ACD collected at 22°C. As illustrated in figure 1, significant changes in specific peak positions are observed as a consequence of addition of C-terminal αB-IxI peptide (Ac-PERTIPITREEK-NH2). Thus, the spectra confirm that isolated ACD dimers in solution can interact with a C-terminal sequence outside an oligomeric context. Notably, only a subset of resonances is affected by the presence of peptide, indicating that binding is not accompanied by a significant conformational change in the ACD dimer. Inspection of individual peaks in spectra collected throughout a titration revealed that some peaks exhibit intermediate exchange behavior: a phenomenon in which peaks broaden under conditions where the bound state is not saturated and reappear as observable resonances at saturating peptide concentrations (Supplementary Figure S2). In addition, a subset of affected peaks titrate to multiple resonance positions (up to 3) indicating these nuclei exist in multiple environments as a result of peptide binding (Figure 2). The observation of multiple resonances rather than one averaged resonance indicates that distinct

ACD-peptide complexes exist and that they do not interconvert rapidly. The observed exchange behavior allows us to estimate the exchange rate, k_{ex}, from the magnitude of the chemical shift differences among species. The chemical shift perturbations (CSPs) between the free and bound states are all quite similar for the amide group resonance for residue L94, which has well-resolved multiple peaks. This indicates a similar rate of exchange for each observed species. Under conditions where distinct resonances are observed for different forms present, the exchange rate ($k_{ex} = k_{on} + k_{off}$) between two forms is given by $k_{ex} < \Delta\omega$, where $\Delta\omega$ is chemical shift difference between the two forms. In the case of αB-IxI peptide bound to αB-ACD, we have determined the upper limit for k_{ex} to be 60 s^{-1} for the multiple states observed.

As mentioned above, resonance assignments for peaks in the αB-ACD spectrum provide residue-specific information from the titration data. For each peak that could be followed through the titration series, the difference between its peptide-free chemical shift and its peptide-bound position was measured, as shown in the histogram in Figure 3. For peaks that titrate to multiple peptide-bound states, the position of the most intense peak in the peptide bound spectrum was used in this analysis. A histogram in which the CSPs are ranked according to their magnitude reveals a group of peaks with CSPs significantly larger than all others (> 0.25 ppm). For a subset of peaks, the final positions in the peptide-bound spectrum could not be readily assigned because their resonances could not be followed due to intermediate exchange behavior or limited peak intensity. Nevertheless, the fact that they are in intermediate exchange indicates that their CSP values are even larger than those peaks whose positions shift gradually throughout the titration. The residues that experience the largest perturbations as a consequence of peptide binding reside in the β4/β8 groove and the loop between β4 and β5 (β4/5 loop) of the αB-ACD. Less affected peaks are clustered at the C-terminal end of the β3 strand (Figure 3). Peaks that are unaffected by

the addition of peptide derive from residues outside these regions (Figure 3). The large CSPs observed within the β4/β8 groove are consistent with the peptide binding to a surface similar to that observed in ssNMR and X-ray crystallographic studies (Figure 4). Thus, there is an intrinsic affinity between the αB-ACD and the αB C-terminal sequence that promotes their binding even outside the context of solid-state or crystalline samples.

The small CSPs (0.14-0.24 ppm) observed for residues at the C-terminal end of the β3 strand may arise from two possible scenarios: 1) this region may comprise a second, lower affinity peptide binding site or 2) the observed CSPs may be due to small changes in the chemical environment of these residues caused by binding in the β4/β8 groove. To distinguish between the two possibilities, a point mutation in the β8 residue Ser135 was designed with the goal of disrupting the β4/β8-peptide interaction. In αB structures derived from ssNMR data and crystal structures, the side chain of Ser135 sits between two pockets into which the side chain of Ile159 and Ile161 of the IxI motif are bound (Laganowsky et al, 2010; Jehle et al, 2010). Substitution of Ser135 with a longer Gln side chain (S135Q) should occlude the binding pockets without significantly perturbing other elements of the structure. The ^{1}H-^{15}N HSQC spectrum of S135Q-αB-ACD is highly similar to the wt-ACD spectrum indicating that the mutation has not significantly altered the overall structure (Supplemental figure S3). Spectra from a peptide titration carried out for ^{15}N -S135Q-αB-ACD reveal that S135Q-ACD binds peptide with significantly lower affinity: even a 10-fold molar excess does not achieve saturation with the mutant ACD whereas for the wt-ACD, saturation was attained at a 4-fold excess. Furthermore, the observed CSPs are much smaller in the mutant ACD and all affected peaks exhibit fast exchange rather than intermediate/slow exchange (Figure 5). Altogether, the observations indicate that the C-terminal peptide binds with lower affinity to the S135Q-ACD mutant and has

a shorter lifetime in the bound state. Notably, CSPs at the C-terminal end of the β3 strand also fail to reach saturation at 10-fold excess peptide in the S135Q mutant. If these perturbations were due to a second, independent binding event, they would not be expected to be disrupted by the S135Q mutation. The apparent coupling of the CSPs observed within the β4/β8 groove and the β3 region is strong evidence that they arise from the same binding event. Together with our previously published ssNMR data, the data presented here lead us to conclude that the IxI motif within the C-terminal peptide has an intrinsic affinity for the β4/β8 groove of αB-ACD and that alterations to the groove can modulate the affinity of this interaction.

Does the interaction between an isolated C-terminal peptide and an ACD dimer recapitulate that observed in the αB oligomer? To address this question, we compared the measured ^{15}N chemical shifts for the isolated αB-ACD dimer in solution with those measured within the oligomer. The calculated difference is plotted for each residue in the histogram, shown as gray bars in Figure 6. The largest differences occur at the termini of the excised ACD construct, the β3 strand, and at positions within the β4/β8 groove, suggesting that these regions differ in structure and/or environment between the ACD dimer alone in solution and in an oligomer. The calculation was repeated using ^{15}N chemical shifts measured for the peptide-saturated state of the ACD in solution and the ssNMR oligomer, shown as black bars in Figure 6. Notably, in the presence of peptide all observable β4/β8 residues in the ACD in solution have shifted significantly towards their solid-state ^{15}N chemical shifts (compare black and red bars). This remarkable concordance suggests the interaction between the αB-IxI peptide and the αB-ACD in the absence of oligomeric context recapitulates native intermolecular contacts within the αB oligomer. We note that a few peaks move away from their solid-state chemical shifts with the addition of peptide. The most significant of these deviations involves the perturbed positions at

the C-terminal end of the β3 strand of the ACD. Thus, the secondary effects of peptide binding observed for this region in solution may not reflect a native effect and should be interpreted with caution.

An I/V X I/V Motif Is A Determinant Of Binding The β4/β8 Groove

To test the direct involvement of the IxI sequence in binding the β4/β8 groove, NMR experiments were performed using αB C-terminal peptides in which the **I**P**I** sequence was mutated either to **G**P**G** or **A**P**A**. No detectable binding was observed for either mutant peptide even at high molar excess of peptide, consistent with the two Ile residues being the major determinants for the interaction (data not shown). This result raises the question as to whether other IxI/V sequences that exist (i.e., VxI or IxV) are capable of binding to the groove in αB. To address this question, NMR binding experiments were performed using peptides mimicking C-terminal sequences of HSPB1, HSPB2, and αA-crystallin (HSPB4), each of which contain an I/VxI or IxI/V motif (table 1). The NMR titrations confirm that each of these peptides binds to αB–ACD and produces CSPs that map to the β4/β8 groove. Differences in affinity and exchange behavior are apparent in the heterologous titrations. For example, binding of the αA-IxV peptide and the HSPB2-VxI peptide exhibit fast exchange behavior instead of the intermediate exchange observed with the αB-IxI peptide (Supplementary Figure S2). In a manner similar to the αB-IxI peptide titration, a subset of peaks in the αA-IxV peptide spectra titrates to multiple well populated resonances throughout the titration. Throughout the HSPB2-VxI peptide titration, peaks titrate along a vector to a dominant saturated state. Additional multiple resonances are apparent at saturation, but are much more lowly populated than those observed in the αB-IxI or αA-IxV peptides (Figure 2). The observations permitted approximation of a $K_{d\ app}$ value of ~90uM for HSPB2 peptide based on the dominant binding state CSPs (Supplementary Figure

S4). This value should be viewed only as an upper limit estimate $K_{d\ app}$ because alternative lowly populated bound states effectively serve as competitors to the dominant binding mode and therefore contribute to the observed binding isotherm. Further, our inability to detect additional binding modes for this peptide does not mean they do not exist, but rather that if they do exist they exchange rapidly. Altogether the data indicate that peptides that contain either an IxV or a VxI motif can bind the β4/β8 groove of the αB-ACD. In contrast, peptides that correspond to other regions of sHSPs that have been observed to make contact with an ACD in other structures display no detectable binding to αB-ACD under the conditions of our experiments (table 1)(Bagnéris et al, 2009; Jehle et al, 2010). Thus, the binding observed in the solution-state NMR experiments is specific and cannot be attributed to a general promiscuity of αB-ACD for unstructured polypeptides.

Discussion

The αB-ACD binds αB C-terminal IxI motif outside the oligomeric context.

Our results demonstrate that the αB-ACD has an inherent affinity for its C-terminal IxI motif and that the interaction can take place outside the context of either an oligomer or a crystal lattice. The major determinants for binding are the two Ile side chains, which interact directly with the β4/β8 groove of the ACD, yielding a bound state that is remarkably similar to that detected by ssNMR studies (Jehle et al, 2009). In addition to the β4/β8 groove, the β4/5 loop is strongly affected by peptide binding, while loops on the opposite end of the groove are not significantly perturbed. In the αB oligomer structure determined from ssNMR, the C-terminal region of a neighboring dimer contacts the β4/5 loop but not the loops on the other end of the β4/β8 groove (Jehle et al, 2010). Similar binding modes are observed in crystal structures: the

sequence N-terminal to the IxI motif is in close proximity to the β4/5 loop of a neighboring subunit while sequences C-terminal to the motif exit the groove without making contact with β6+7/8 or β3/4 loops (Laganowsky et al, 2010; Montfort et al, 2001; Kim et al, 1998; Jehle et al, 2010). Thus, the solution-state NMR data reported here are consistent with observations made for numerous sHSPs using multiple techniques. Solution-state NMR spectra that contain signals only from highly flexible and mobile residues failed to observe resonances from the IxI motif on αB crystallin oligomers at 25°C. This is consistent with the sequence being less flexible than residues more C-terminal to it, whose signals were detected (Treweek et al, 2011). In contrast, the IxI motif was deemed highly flexible based on a solution-state NMR study on oligomeric αB in which Ile resonances were selectively detected by the methyl-TROSY approach (Baldwin et al, 2011). Altogether the available observations are most consistent with a model in which the IxI motif exists in an equilibrium between a free, flexible state and a bound state. In the context of αB oligomers that contain between 24 and 32 subunits, free and bound IxI motifs, and empty and filled β4/β8 grooves, will exist simultaneously. Our results indicate a bound-state lifetime of 17ms ($k_{ex} \cong 60s^{-1}$) and a dissociation constant below 90μM for the binding of αB's IxI C-terminal sequence. These numbers are for a bimolecular binding reaction. In the context of the oligomer, the effective local concentrations of both binding components will be significantly higher than the conditions of our bimolecular, peptide based NMR experiments. So, it is reasonable to conclude that the population of bound C-termini at any given time will be significant. As we have previously proposed, the equilibrium free and bound states may be shifted towards one state or the other by a change in conditions such as pH and temperature (Jehle et al, 2010).

Finally, we note the presence of multiple bounds states for αB IxI peptide at saturation in the NMR spectrum. Two IxI/V motif binding orientations in the β4/β8 groove have been

observed in crystallographic studies ("parallel" and "antiparallel" to the β8 strand (Laganowsky et al, 2010). Due to the presence of two β4/β8 grooves per ACD dimer, if the two peptide orientations are independent and of approximately similar affinity in solution, three bound species would be predicted: parallel/parallel, antiparallel/antiparallel, and parallel/antiparallel in a 1:1:2 ratio. It is notable that for the very limited number of examples where three resonances can be clearly and unambiguously observed, their ratios appear to be approximately as predicted. Thus, the simplest interpretation of the observed behavior is that the αB-IxI peptide can bind in two orientations in solution. The slow exchange behavior observed between binding modes indicates that a slow step, presumably peptide dissociation, governs the inter-conversion between binding modes. We cannot, however, rule out other possible explanations for the presence of multiple bound states. For example, if binding to the ACD is not restricted to a single peptide conformation, the multiple bound states observed by NMR may originate from variability in the bound peptide conformation as opposed to its orientation. Whether the observed data result from one or a combination of these two possibilities cannot be unambiguously distinguished from the data at hand.

Binding to the β4/β8 groove requires an I/VxI/V motif.

Of the peptides tested, only peptides with I/VxI/V motifs were observed to bind to the αB-ACD. Substitution of both Ile sidechains with the smaller hydrophobic sidechain Ala abolished all detectable binding. Whether all combinations of I/V in the two positions and whether Leu or other residues are also allowable in one or both positions will require a more thorough and systematic study. The structure of the β4/β8 groove is defined by the side chains that face into the groove from the two β-strands. Substitution of the β8 residue, Ser135, with a

larger side chain (Gln) significantly inhibited IxI binding. This result is consistent with the structure derived from ssNMR in which Ser135 resides between the two hydrophobic binding pockets and may provide a functional explanation to the strong conservation of small amino acid residues observed at this position in sequence alignments (Kim et al, 1998; Baldwin et al, 2011; Haslbeck et al, 2005). Furthermore, the lowered affinity of the S135Q mutant for the IxI-peptide and the much shorter lifetime of the mutant bound state suggest that interpretation of studies in which this residue is mutated and/or modified should be approached with care (Baldwin et al, 2011).

Hetero-oligomers and C-terminal peptide binding

Hetero-oligomerization of αB with αA crystallin and HSPB1 has been reported and αB/HSP20 hetero-oligomers have been indirectly observed (Sun & Liang, 1998; Zantema et al, 1992; Engelsman et al, 2009; Bukach et al, 2009; Sugiyama et al, 2000; Kato et al, 1994). In contrast, attempts to observe αB/HSPB2 hetero-oligomers have failed to detect these species (Engelsman et al, 2009; Sugiyama et al, 2000). Such observations raise the question of what determines formation of sHSP hetero-oligomeric species. Given the high degree of conservation within the β4/β8 sequences of human sHSPs and the variability of sequences flanking the IxI motifs in the C-terminal regions, an appealing possibility is that β4/β8-to-IxI interactions help to define hetero-oligomers. If this were the case, we would expect to detect interactions with the C-terminal peptides from αA and HSPB1, but not from HSPB2. As summarized in Table 1, the prediction is not supported by our results. Nevertheless, interactions between the IxI motifs from αA crystallin and HSPB1 and the αB-ACD suggest such an interaction is possible in hetero-

oligomers. Whether and how the interaction contributes to hetero-oligomer formation or function must await further investigation.

Conclusion

It is possible to recapitulate interactions that normally occur within the context of an sHSP oligomer using a simplified system of isolated parts. The remarkable concordance of the NMR data acquired in solution on isolated ACD dimers and unstructured peptides with those data collected on oligomers in the solid-state indicate that important and relevant insights can be obtained using either approach. This provides a powerful strategy with which to study functionally relevant interactions involving sHSPs and their binding partners, be they other sHSPs or partly folded client proteins.

Materials and Methods

Expression and purification of ^{15}N labeled αB-ACD

Expression of a TEV cleavable N-terminally His tagged αB-ACD (64-152) was carried out using methods and conditions previously described for the αB-ACD (Jehle et al, 2009). Cultures were pelleted then resuspended in a buffer solution containing 20mM Tris (pH 8) 100mM NaCl, 1mM PMSF and EDTA Free Protease Inhibitor Cocktail (Sigma-Aldrich) and were lysed by French Press. Lysate was diluted 5-fold in 6M Urea, 100mM NaCl and centrifuged at 43,000g. The supernatant was applied to a Ni-NTA Agarose column (Invitrogen). Protein bound to the column was refolded by 3 column volumes (CV) of 25mM Tris, 150mM NaCl (Buffer A), 10mM Imidazole, pH 7.6 and His-tagged αB-ACD was eluted with the addition of Buffer A containing 250mM Imidazole, pH 7.6. The TEV cleavable His-tag was removed by dialyzing overnight into Buffer A containing 5mM DTT in the presence TEV protease. Following TEV digestion, the

protein was reapplied to a Ni-NTA column and eluted with the addition of Buffer A containing 50mM Imidazole pH 7.6. αB-ACD was further purified by anion exchange using a MonoQ column (GE) and SEC as previously described (Jehle et al, 2009). Purified αB-ACD was dialyzed into water and lyophilized for storage.

Peptides

Peptides were generated by Life Tein Custom Peptide Synthesis Services with acetylated N-termini and amidated C-termini. Additional αB-IxI peptide was generously provided by the *Gestwicki Lab (University of Michigan)*. Peptides were initially solubilized in water and the pH was adjusted to neutral, before the addition of phosphate and salt. Peptide concentrations were calculated based on the dry weight of lyophilized peptide and final peptide stock solutions ranged from 30-65mM peptide, in 25mM sodium phosphate and 150mM NaCl pH 7.5.

NMR Data Collection and Analysis

NMR experiments were performed on a Bruker 500MHz Avance III spectrometer equipped with a 5mm z-axis gradient, triple resonance probe. ^{15}N labeled, lyophilized αB-ACD was resuspended in 25mM sodium phosphate (pH 7.5), 150mM NaCl. Peptide titration spectra were collected on 600μM αB ACD (300μM ACD dimer) samples in 25mM sodium phosphate, 150mM NaCl, 10% D_2O at 295K. Titration points at 1-fold (600μM), 2-fold, and 4-fold peptide were collected for all peptides that bound the ACD. Additional titration points were collected with the αB-IxI peptide and the αA-IxI peptide to confirm titration assignments and saturation points. Peptides that did not perturb the αB-ACD spectrum at 4-fold excess were defined as peptides that do not bind the ACD and their presence in solution was confirmed by ^{1}H-1D NMR.

Because of the inherent acidity of peptide solutions used, the pH of all NMR samples was confirmed prior to data collection.

All spectra were processed using NMRPipe and data analysis was performed with NMRViewJ (Johnson & Blevins, 1994; Delaglio et al, 1995). Assignments for amide resonances in peptide-bound αB-ACD were obtained by following the resonances during the course of the titration. Some resonances in the spectra of αB-ACD bound to αB-IxI peptide could not be assigned unambiguously due to intermediate exchange behavior where the resonances disappear during the intermediate titration points and reappear at the excess peptide concentration. To resolve ambiguities in αB-IxI peptide bound αB-ACD assignments, peak trajectories were compared to trajectories in αA-IxI and HSPB2 peptide titrations where the resonances could be followed unambiguously. Chemical shift perturbations (CSP) were calculated based on the formula $\{(\Delta\delta_{HN}^2+(\Delta\delta_N/5)^2)\}^{1/2}$ where $\Delta\delta_{HN}$ and $\Delta\delta_N$ are the chemical shift differences in amide proton and nitrogen resonances in ppm, respectively. $\Delta\delta_N$ is divided by 5 since the spectral width in ^{15}N-dimension is 5-fold greater than the spectral width in the ^{1}H dimension. CSPs were plotted onto a model of 2KLR using Pymol.

The $K_{d\ app}$ for the HSPB2-VxI peptide binding to αB-ACD was determined using NMRViewJ (Johnson & Blevins, 1994). Six peaks from the HSPB2-VxI peptide titration were fit to a quadratic binding curve using a base 10 quadratic fit and 250 simulations and an average $K_{d\ app}$ for all peaks fit was calculated.

Acknowledgements.

We thank Jason Gestwicki and Leah Makley for their generous gift of peptide. We thank Ponni Rajagopal, Peter Brzovic, and Jonathan Pruneda for informative discussions and Ponni

Rajagopal for critical evaluation of the manuscript. This work was funded by NIH grant 1R01 EY017370 (to R. E. K.). S. D. is supported in part by NIGMS 2T32 GM008268.

Figures

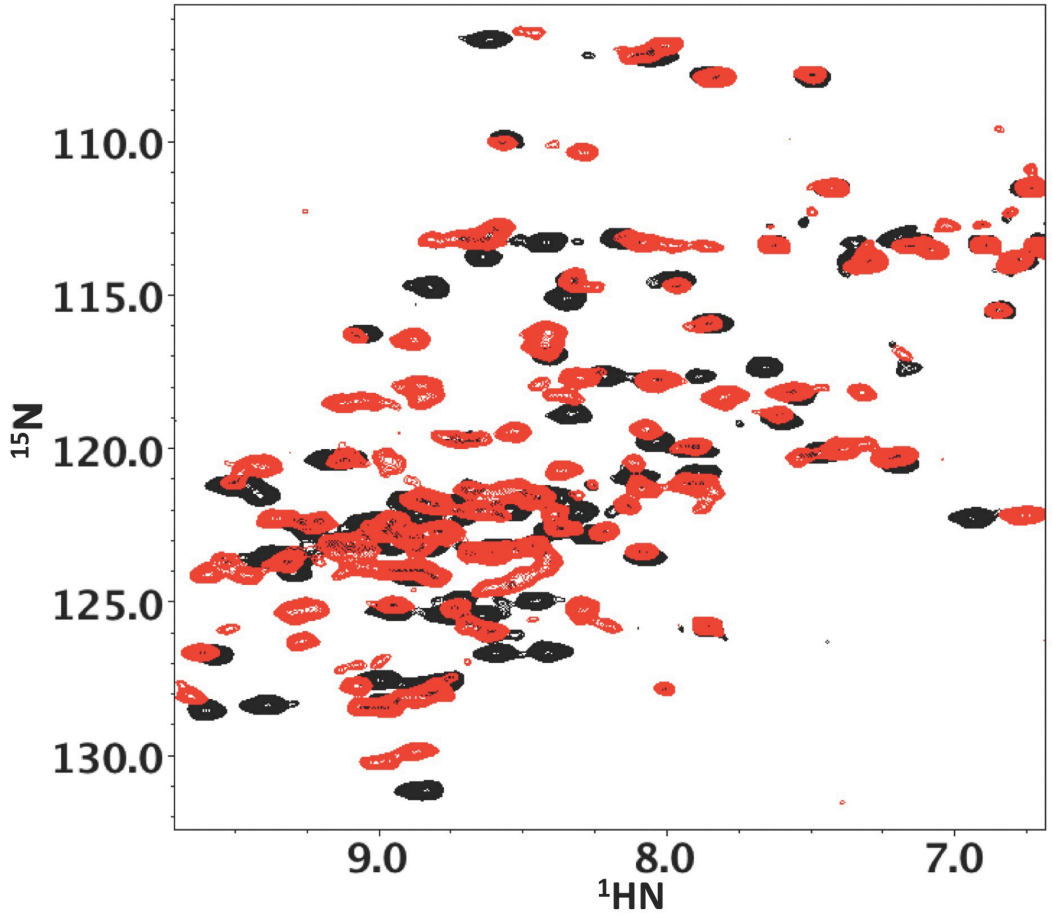

Figure 1. Overlay of ^{1}H-^{15}N HSQC spectra of ^{15}N αB-ACD collected at 22°C, in the absence (black) and at saturating concentrations (5-fold) of αB-IxI peptide (red).

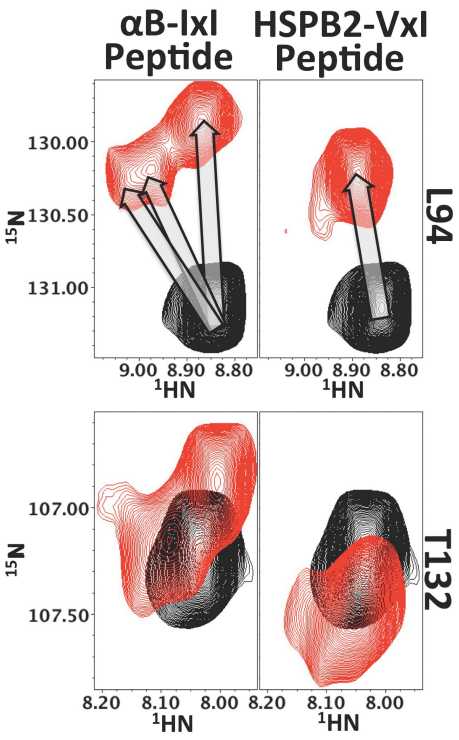

Figure 2. αB-ACD peaks titrate to multiple resonances at saturating concentrations of αB-IxI peptide. Three distinct resonances are observed for the amide of L94 in the presence of αB-IxI peptide (upper left arrows), while a single dominant peak is observed in the presence of the HSPB2-VxI peptide. The resonance for T132 also titrates to multiple positions in the presence of αB-IxI peptide (lower left) while a single dominant peak is observed in the presence of the HSPB2-VxI peptide. Spectra of the peptide-free and peptide-saturated ACD are shown in black and red, respectively.

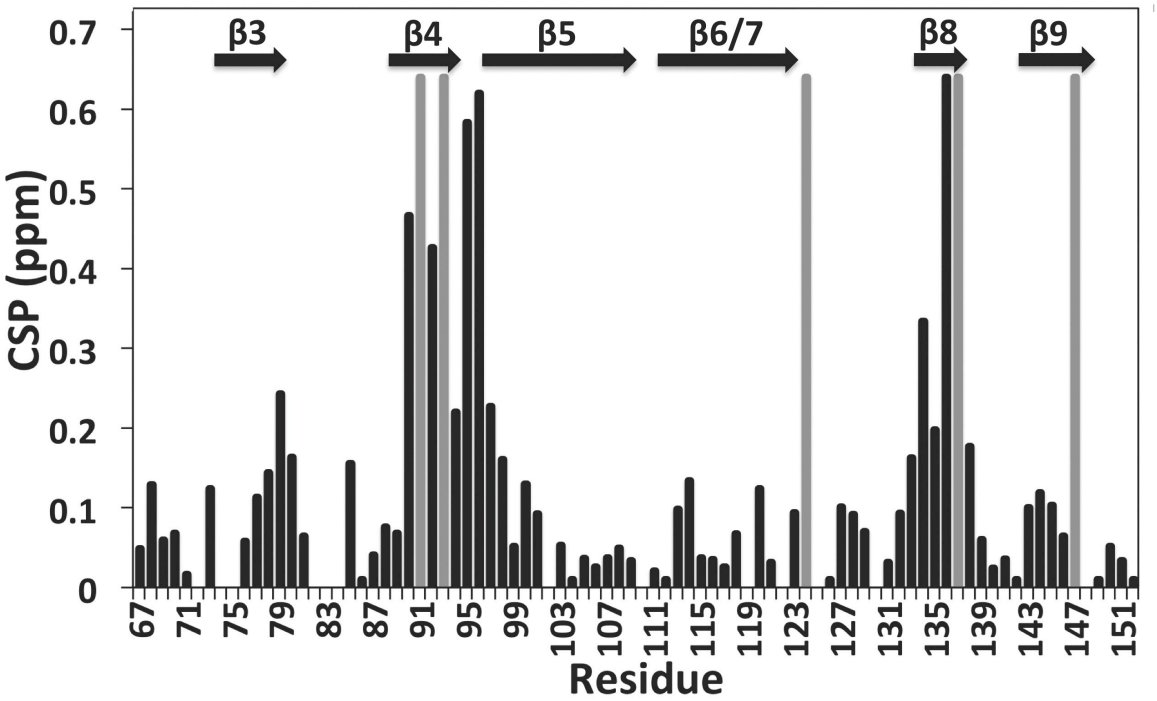

Figure 3. Histogram of calculated CSPs (Black) for the αB-ACD in the presence of saturating concentrations of αB-IxI peptide. Positions where CSPs could not be determined due to exchange behavior (and therefore have very large chemical shifts) are indicated in gray. Secondary structure elements are shown above.

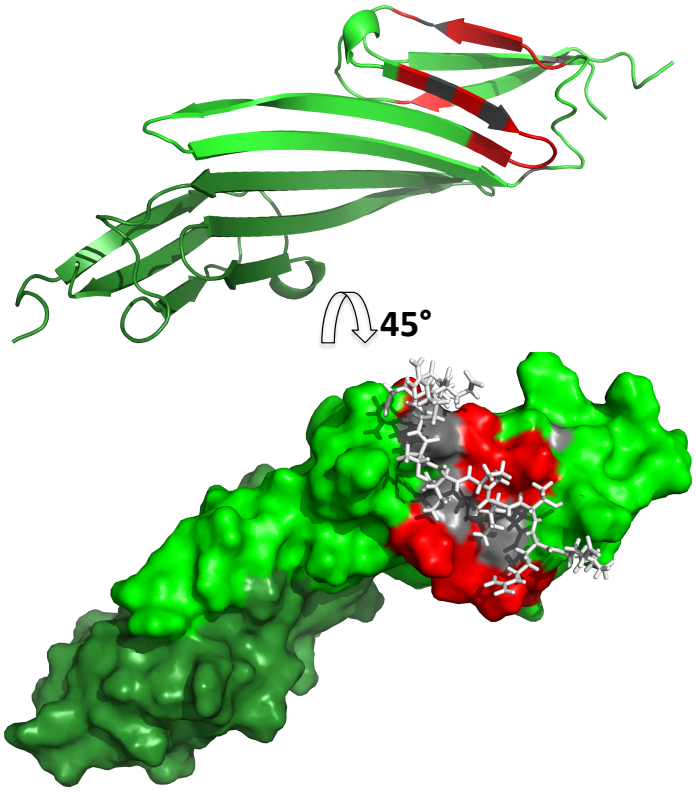

Figure 4 The chemical shift perturbations due to αB-IxI peptide binding map to the β4/β8 groove on the edge of the ACD. (Top) CSPs are mapped onto a secondary structure representation of the αB-ACD dimer (green and gray) (2klr). The most affected peaks (CSP > 0.16) are shown in magenta on one monomer (green) and map to the β4/β8 groove and β4/5 loop. Residues where CSPs could not be quantitated due to exchange over large chemical shifts are shown in red. (Bottom) Surface representation of the αB-ACD dimer (2klr) rotated 45° with the same residue coloring as above. The C-terminal αB sequence PERTIPITREEK (white) is shown as modeled previously with ssNMR restraints to illustrate the congruence between the chemical shifts observed for binding outside the oligomeric context and the structure observed in the context of αB oligomer.

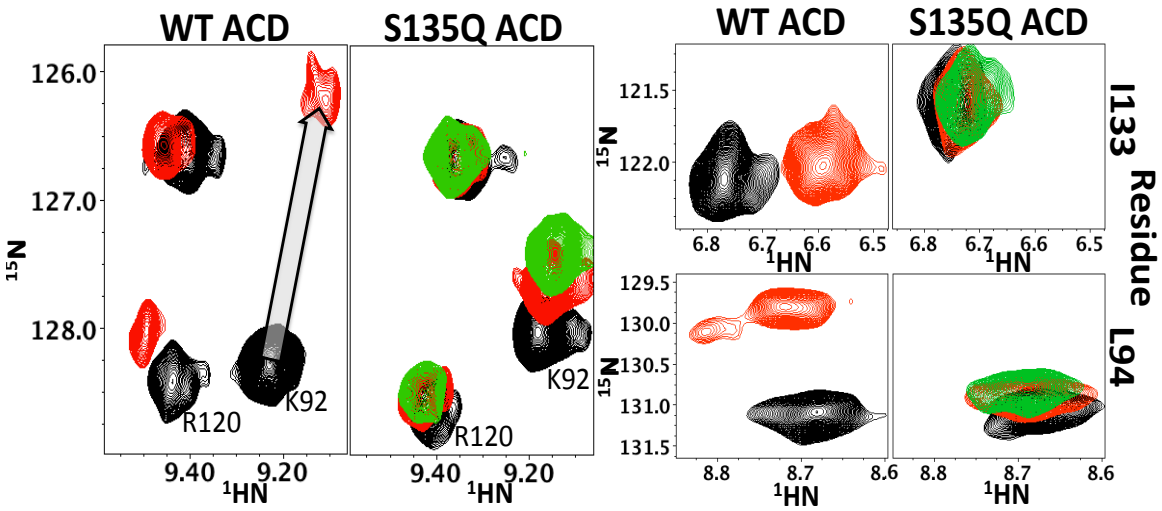

Figure 5. Mutation of residue S135 in the β4/β8 groove disrupts IxI peptide binding. a. Selected resonances from ^{1}H-^{15}N HSQC of WT ACD (left) and the Mutant S135Q ACD (Right) in the absence and presence of αB-IxI peptide are compared. Spectra collected in the absence of peptide are shown in black. Spectra collected in the presence of 6-fold αB-IxI peptide (red) for the WT and S135Q ACD and 10-fold (green) peptide for S135Q are shown. In the S135Q mutant, residues K92 from the β4 strand and R120 (which is close to and behaves similarly to perturbed residues on the β3 strand) show a decrease in peptide-dependent chemical shift perturbation. The titration vector for the resonance of K92 in the WT spectra is shown as a gray arrow. b. Peptide-induced CSPs observed for resonances of L94 and I133 are compared, with the same conditions and coloring as in (a).

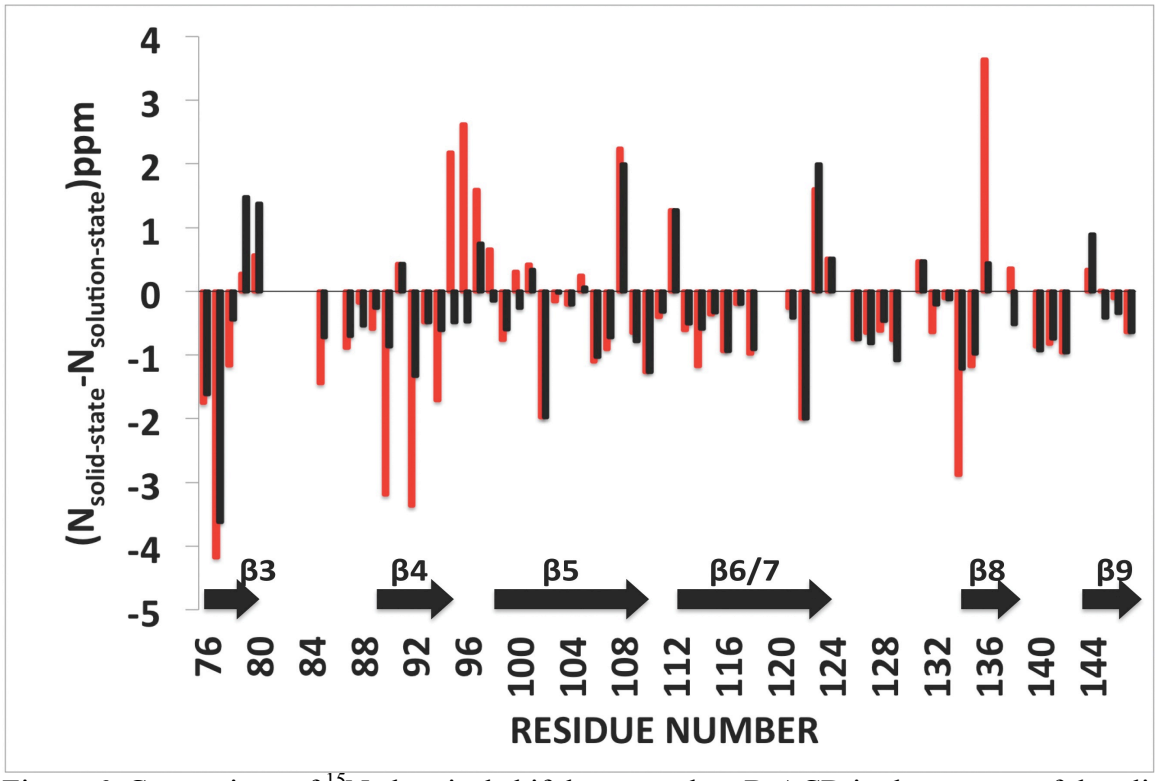

Figure 6. Comparison of ^{15}N chemical shift between the αB-ACD in the context of the oligomer observed by ssNMR and isolated αB-ACD in solution. ($^{15}N_{solid\text{-}state}$-$^{15}N_{solution\text{-}state}$) differences were measured using the solution-state values observed both in the absence of peptide (red bars) and in the presence of saturating αB-IxI peptide (black bars). Note the greatly reduced values for ($^{15}N_{solid\text{-}state}$-$^{15}N_{solution\text{-}state}$) in the presence of peptide in the β4 strand and β4/5 loop (residues 89-98) and the β8 strand (residues 133-137). Positions where ($^{15}N_{solid\text{-}state}$-$^{15}N_{solution\text{-}state}$) could not be determined are assigned the value of 0.0 ppm for clarity. For residues where multiple states were observed in the peptide saturated spectrum, the position of the most intense peak in the saturated spectrum was used.

SEQUENCE ORIGIN	PEPTIDE SEQUENCE**	BIND ACD?
αB crystallin(HSPB5) CT*	PERT**IPI**TREEK	YES
αB crystallin(HSPB5) CT IXI Mutants	PERTAPATREEK PERTGPGTREEK	NO NO
αA Crystallin(HSPB4) CT	AERA**IPV**SREEK	YES
MKBP(HSPB2) CT	DTEVNE**VYI**SL	YES
HSP27(HSPB1) CT	QSNE**ITIPV**TFESR	YES
HSP20(HSPB6) CT HSP20(HSPB6) NT*	SAQAPPPAAAK VAQVPTDPGH	NO NO
αB crystallin(HSPB5) NT	RAPSWFDTG	NO

Table 1. Summary of C-terminal peptide sequences from different sHSPs binding to αB-ACD. *Where the peptide originates relative to the ACD within the sHSP is denoted N-terminal (NT) or C-terminal (CT).
**V/IxI/V motifs are shown in bold text.

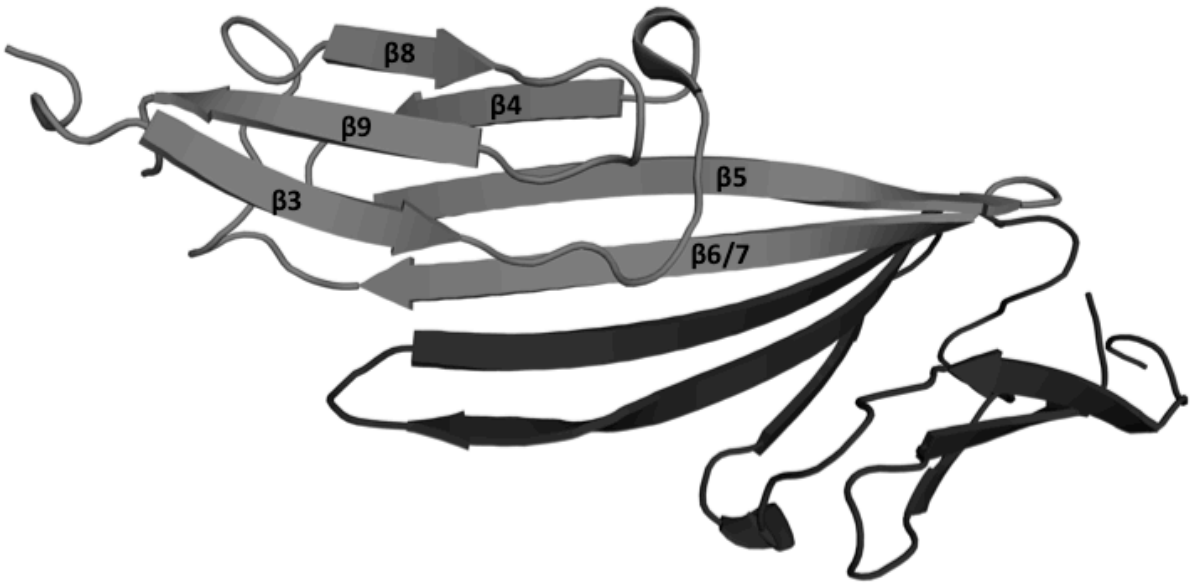

Supplemental Figure S1. Secondary structure representation of the αB-ACD determined by ssNMR (2KLR). The two monomers are shown in different shades of gray and β strands are labeled.

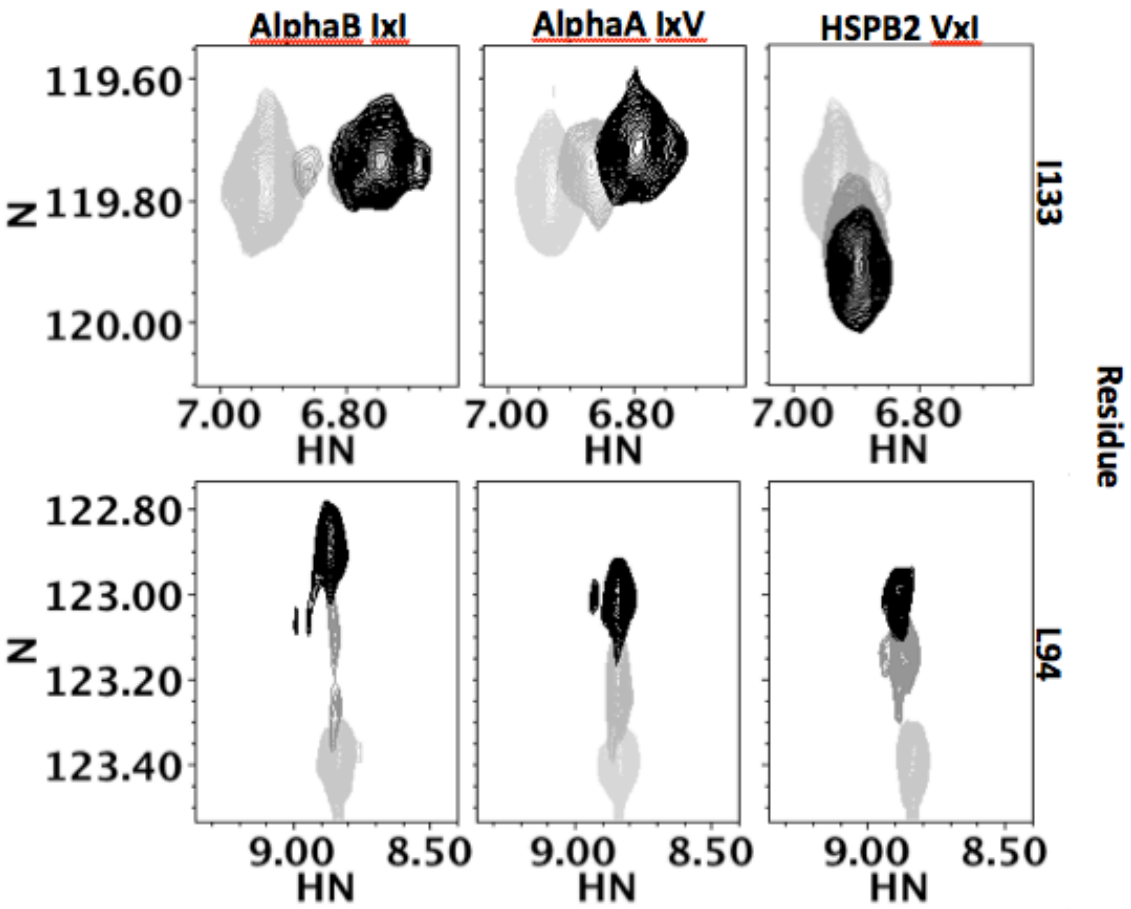

Supplemental figure S2. αB-IxI peptide, αA-IxV and HSPB2-VxI peptides show different affinities and residence times. The resonances of residue I133 (Top) from the β8 strand and L94 (Bottom) from the β4 strand of the αB ACD are plotted in the absence of peptide and in the presence of 1-fold and 4-fold αB-IxI-peptide (Left) and αA-IxV peptide (Middle) and HSPB2 peptide (Right). Overlay of spectra measured from αB-ACD samples containing no peptide, 1-fold, 2-fold and 4-fold excess peptide are shown in progressively darker shades of gray. Broadening in the spectrum collected with 1 -fold αB-IxI reflects the longer lifetime (Left Bottom) of the bound state relative to the other peptides.

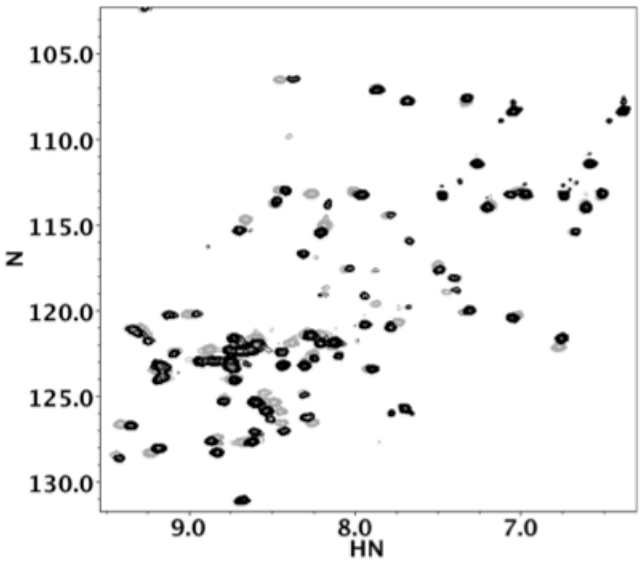

Supplemental Figure S3. ^{1}H-^{15}N HSQC Spectra of wt αB-ACD (Gray) and the β8 mutant S135Q αB-ACD indicate the mutant does not disrupt the ACD structure (Black). Peaks that show a chemical shift greater than .1 as a result of the mutation are V77, V91, L131, I133, T134, S136 and V145.

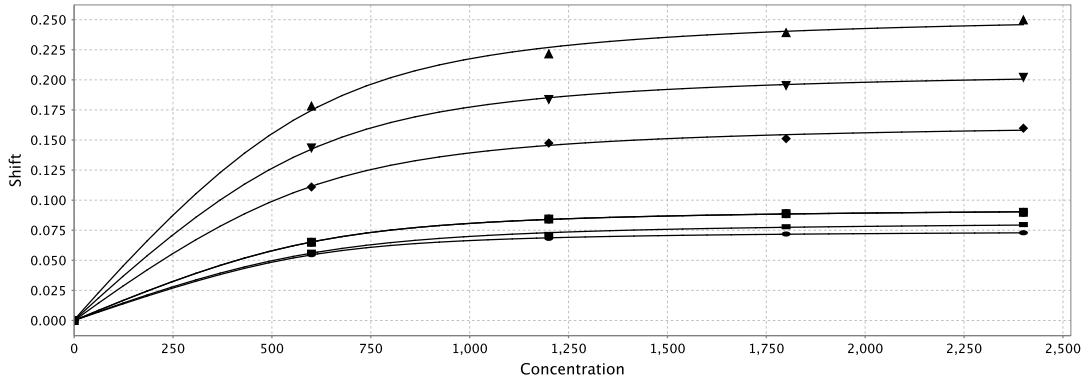

Supplemental Figure S4. Chemical shift perturbations fit to quadratic binding curves for the HSPB2 peptide. 6 peaks were fit for the HSPB2 peptide (92, 94, 136, 95, 78, 127 and 97) yielding an average K_d of 87 +/- 12 μM. Chemical shift perturbation is plotted on the y-axis and total peptide concentration(μM) is plotted on the x-axis.

References

Aquilina JA, Benesch JL, Bateman OA, Slingsby C, Robinson CV (2003) Polydispersity of a mammalian chaperone: mass spectrometry reveals the population of oligomers in alphaB-crystallin. Proc Natl Acad Sci USA **19:** 10611-10616

Bagnéris C, Bateman OA, Naylor CE, Cronin N, Boelens WC, Keep NH, Slingsby C (2009) Crystal structures of alpha-crystallin domain dimers of alphaB-crystallin and Hsp20. *J Mol Biol* **392:** 1242-1252. (doi: 10.1016/j.jmb.2009.07.069)

Baldwin AJ, Hilton GR, Lioe H, Bagneris C, Benesch JLP, Kay LE (2011) Quaternary Dynamics of αB-Crystallin as a Direct Consequence of Localised Tertiary Fluctuations in the C-Terminus. *J Mol Biol* **413**: 310-320 (doi: 10.1016/j.jmb.2011.07.017)

Baldwin AJ, Lioe H, Hilton GR, Baker LA, Rubinstein JL, Kay LE, Benesch J (2011) The Polydispersity of aB-Crystallin Is Rationalized by an Interconverting Polyhedral Architecture. *Structure* **19:**1855–1863

Baranova EV, Weeks SD, Beelen S, Bukach OV, Gusev NB, Strelkov SV (2011) Three-dimensional structure of α-crystallin domain dimers of human small heat shock proteins HSPB1 and HSPB6. *J Mol Biol* **411:** 110-122 (doi: 10.1016/j.jmb.2011.05.024)

Benesch JLP, Aquilina JA, Baldwin AJ, Rekas A, Stengel F, Lindner RA, Basha E, Devlin GL, Horwitz J, Vierling E, Carver JA, Robinson CV (2010) The quaternary organization and dynamics of the molecular chaperone HSP26 are thermally regulated. *Chem Biol* **17:** 1008-1017 (doi: 10.1016/j.chembiol.2010.06.016)

Brady JP, Garland DL, Green DE, Tamm ER, Giblin FJ, Wawrousek EF (2001) AlphaB-crystallin in lens development and muscle integrity: a gene knockout approach. *Invest Ophthalmol Vis Sci* **42:** 2924-2934

Braun N, Zacharias M, Peschek J, Kastenmüller A, Zou J, Hanzlik M, Haslbeck M, Rappsilber J, Buchner J, Weinkauf S (2011) Multiple molecular architectures of the eye lens chaperone αB-crystallin elucidated by a triple hybrid approach. *Proc Natl Acad Sci USA* **108**, 20491-20496

Bukach OV, Glukhova AE, Seit-Nebi AS, Gusev NB (2009) Heterooligomeric complexes formed by human small heat shock proteins HspB1 (Hsp27) and HspB6 (Hsp20). *Biochim Biophys Acta* **1794:** 486-495 (doi: 10.1016/j.bbapap.2008.11.010)

Bukau B, Weissman J, Horwich A (2006) Molecular chaperones and protein quality control. *Cell* **125:** 443–451

Clark AR, Naylor CE, Bagnéris C, Keep NH, Slingsby C (2011) Crystal structure of R120G disease mutant of human αB-crystallin domain dimer shows closure of a groove. *J Mol Biol* **408:** 118-134 (doi: 10.1016/j.jmb.2011.02.020)

Delaglio F, Grzesiek S, Vuister GW, Zhu G, Pfeifer J, Bax A (1995) NMRPipeL a multidimensional spectral processing system based on UNIX pipes. *J Biomol NMR* **6:** 277-293

Engelsman J, Boros S, Dankers PYW, Kamps B, Vree Egberts WT, Böde CS, Lane LA, Aquilina JA, Benesch J, Robinson CV, de Jong WW, Boelens WC (2009) The Small Heat-Shock

Proteins HSPB2 and HSPB3 Form Well-defined Heterooligomers in a Unique 3 to 1 Subunit Ratio. *J Mol Biol* **393:**1022-1032 (doi: 10.1016/j.jmb.2009.08.052)

Ghahghaei A, Rekas A, Carver JA, Augusteyn RC (2009) Structure / function studies of dogfish α-crystallin, comparison with bovine α-crystallin. *Mol Vis* **15:** 2411-2420

Goldstein LE, Muffat JA, Cherny RA, Moir RD, Ericsson MH, Huang X, Mavros C, Coccia JA, Faget KY, Fitch KA, Masters CL, Tanzi RE, Chylack LT Jr, Bush AI (2003) Cytosolic β-amyloid deposition and supranuclear cataracts in lenses from people with Alzheimer's disease. *Lancet* **361:** 1258–1265

Haslbeck M, Franzmann T, Weinfurtner D, Buchner J (2005) Some like it hot: the structure and function of small heat-shock proteins. *Nat Struct Mol Biol* **12:** 842-846

Hayes VH, Devlin G, Quinlan RA (2008) Truncation of alphaB-crystallin by the myopathy-causing Q151X mutation significantly destabilizes the protein leading to aggregate formation in transfected cells. *J Biol Chem* **283:** 10500-10512 (doi: 10.1074/jbc.M706453200)

Hilario E, Javier F, Martin M, Bertolini MC, Fan L (2011) Crystal Structures of Xanthomonas Small Heat Shock Protein Provide a Structural Basis for an Active Molecular Chaperone Oligomer. *J Mol Biol* **408:** 74-86

Horwitz J (1992) α-crystallin can function as a molecular chaperone. *Proc Natl Acad Sci USA* **89:** 10449–10453

Jehle S, Rajagopal P, Bardiaux B, Markovic S, Kühne R, Stout JR, Higman VA, Klevit RE, van Rossum BJ, Oschkinat H (2010) Solid-state NMR and SAXS studies provide a structural basis for the activation of alphaB-crystallin oligomers. *Nat Strucl Mol Biol* **17:** 1037-1042

Jehle S, van Rossum B, Stout JR, Noguchi SR, Falber K, Rehbein K, Oschkinat H, Klevit RE, Rajagopal P (2009) alphaB-crystallin: a hybrid solid-state/solution-state NMR investigation reveals structural aspects of the heterogeneous oligomer. *J Mol Biol* ***385*:**1481-1497 (doi: 10.1016/j.jmb.2008.10.097)

Jehle S, Vollmar BS, Bardiaux B, Dove KK, Rajagopal P, Gonen T, Oschkinat H, Klevit RE (2011) N-terminal domain of alphaB-crystallin provides a conformational switch for multimerization and structural heterogeneity. *Proc Natl Acad Sci USA* **108:** 6409-6414 (doi: 10.1073/pnas.1014656108)

Johnson BA, Blevins RA (1994) NMR View: A computer program for the visualization and analysis of NMR data. *J Biomol NMR* **4:** 603-614

Kato K, Goto S, Inaguma Y, Hasegawa K, Morishita R, Asano T (1994) Purification and characterization of a 20-kDa protein that is highly homologous to alpha B crystallin. *J Biol Chem* **269:** 15302-15309

Kato K, Inaguma Y, Ito H, Iida K, Iwamoto I, Kamei K, Ochi N, Ohta H, Kishikawa M (2001) Ser-59 is the major phosphorylation site in αB-crystallin accumulated in the brains of patients with Alexander's disease. *J Neurochem* **76:** 730–736

Kim KK, Kim R, Kim SH (1998) Crystal structure of a small heat-shock protein. *Nature* **394:** 595-599 (doi: 10.1038/29106)

Langanowsky A, Benesch J, Landau M, Ding L, Sawaya M, Cascio D, Huang Q, Robinson C, Horwitz J, Eisenberg D (2010) Crystal structures of truncated alphaA and alphaB crystallins reveal structural mechanisms of polydispersity important for eye lens function. *Protein Sci* **19:**1031-1043 (doi: 10.1002/pro.380)

Liu Y, Zhang X, Luo L, Wu M, Zeng R, Cheng G, Hu B, Liu B, Liang JJ, Shang F (2006) A novel αB-crystallin mutation associated with autosomal dominant congenital lamellar cataract. *Invest Ophthalmol Vis Sci* **47:** 1069–1075

Moyano JV, Evans JR, Chen F, Lu M, Werner ME, Yehiely F, Diaz LK, Turbin D, Karaca G, Wiley E, Nielsen TO, Perou CM, Cryns VL (2006) AlphaB-crystallin is a novel oncoprotein that predicts poor clinical outcome in breast cancer. *J Clin Invest* **116:** 261-270

Pasta SY, Raman B, Ramakrishna T, Rao CM (2004) The IXI/V motif in the C-terminal extension of alpha-crystallins: alternative interactions and oligomeric assemblies. *Mol Vis* **10**: 655-662

Petkova AT, Ishii Y, Balbach JJ, Antzutkin ON, Leapman RD, Delaglio F, Tycko R (2002) A structural model for Alzheimer's beta-amyloid fibrils based on experimental constraints from solid state NMR. *Proc Natl Acad Sci USA* **99:**16742–16747

Rajasekaran NS, Connell P, Christians ES, Yan LJ, Taylor RP, Orosz A, Zhang XQ, Stevenson TJ, Peshock RM, Leopold JA, Barry WH, Loscalzo J, Odelberg SJ, Benjamin IJ (2007) Human α B-crystallin mutation causes oxido-reductive stress and protein aggregation cardiomyopathy in mice. *Cell* **130:** 427–439

Ray PS, Martin JL, Swanson EA, Otani H, Dillmann WH, Das DK (2001) Transgene overexpression of alphaB crystallin confers simultaneous protection against cardiomyocyte apoptosis and necrosis during myocardial ischemia and reperfusion. *FASEB J **15*:** 393-402

Selcen D, Engel AG (2003) Myofibrillar myopathy caused by novel dominant negative α B-crystallin mutations. *Ann Neurol* **54:** 804–810

Stamler R, Kappe G, Boelens W, Slingsby C (2005) Wrapping the α-Crystallin Domain Fold in a Chaperone Assembly. *J Mol Biol* **353:** 68-79

Studer S, Obrist M, Lentze N, Narberhaus F (2002) A critical motif for oligomerization and chaperone activity of bacterial alpha-heat shock proteins. *Euro J Biochem* **269:** 3578-3586 (doi: 10.1046/j.1432-1033.2002.03049.x)

Sugiyama Y, Suzuki A, Kishikawa M, Akutsu R, Hirose T, Waye MMY, Tsui SKW, Yoshida S, Ohno S (2000) Muscle Develops a Specific Form of Small Heat Shock Protein Complex Composed of MKBP / HSPB2 and HSPB3 during Myogenic Differentiation. *Biochemistry* **275:** 1095-1104

Sun TX, Liang JJ (1998) Intermolecular Exchange and Stabilization of Recombinant Human alphaA- and alphaB-Crystallin. *Biochemistry* **273:** 286 -290

Takeda K, Hayashi T, Abe T, Hirano Y, Hanazono Y, Yohda M, Miki K (2011) Dimer structure and conformational variability in the N-terminal region of an archaeal small heat shock protein, StHsp14.0. *J Struct Biol* **174**: 92-99 (doi: 10.1016/j.jsb.2010.12.006)

Treweek TM, Rekas A, Walker M J, Carver JA (2010) A quantitative NMR spectroscopic examination of the flexibility of the C-terminal extensions of the molecular chaperones, αA- and αB-crystallin. *Exp Eye Res* **91:** 691-699 (doi: 10.1016/j.exer.2010.08.015)

van Montfort RL, Basha E, Friedrich KL, Slingsby C, Vierling E, (2001) Crystal structure and assembly of a eukaryotic small heat shock protein. *Nat Struct Biol* **8:** 1025-1030 (doi: 10.1038/nsb722)

Vargas-Roig LM, Gago FE, Tello O, Aznar JC, Ciocca DR (1998) Heat shock protein expression and drug resistance in breast cancer patients treated with induction chemotherapy. *Int J Cancer* **79:** 468-475

Vicart P, Caron A, Guicheney P, Li Z, Prévost MC, Faure A, Chateau D, Chapon F, Tomé F, Dupret JM, Paulin D, Fardeau M (1998) A missense mutation in the αB-crystallin chaperone gene causes a desmin-related myopathy. *Nat Genet* **20:** 92–95

Zantema A, Verlaan-De Vries M, Maasdam D, Bol S, van der Eb A (1992) Heat shock protein 27 and alpha B-crystallin can form a complex, which dissociates by heat shock. *J Biol Chem* **267:** 12936-12941

CHAPTER 3 A Mechanism of Subunit Recruitment in Human Small Heat Shock Protein Oligomers

(adapted from Delbecq, S.P, Rosenbaum J.C., and Klevit, R.E. (2015) A Mechanism of Subunit

Recruitment in Human Small Heat Shock Protein Oligomers. Biochemistry 54:4276-4284.)

Introduction

Small heat shock proteins (sHSPs) are molecular chaperones that maintain protein homeostasis and protect cells from stress (1-3). Members of this protein family occupy various biological niches and are found in all kingdoms of life (2). The human sHSP family includes ten members, each with distinct gene expression patterns and presumably distinct roles (4,5). Of these, HSPB5 (αB-crystallin) is among the most abundant, with especially high levels of expression in the eye lens, heart, brain, and skeletal muscle (4). Highlighting its importance in maintaining cellular function, deleterious mutations in HSPB5 cause a number of known congenital disorders, including cataracts, cardiomyopathies, and myofibrillar myopathies (6-9). Furthermore, overexpression of HSPB5 is linked to the progression of numerous cancers, including prostate and breast carcinomas (10,11).

Because of its significance, HSPB5 has been the focus of intense study, yet many aspects of its structure and function remain poorly understood. HSPB5 contains structural elements common to all sHSPs, with a highly conserved alpha-crystallin domain (ACD) that is flanked by variable N- and C-terminal regions (NTR and CTR). In the absence of the NTR and CTR, ACDs form stably folded dimers (12-15). The C-terminal region of HSPB5 contains a three-residue isoleucine-proline-isoleucine/valine ("IXI/V") motif that is found in many sHSPs. Though their monomeric mass is relatively small, many metazoan sHSPs form large, polydisperse (oligomers contain variable numbers of subunits) structurally heterogeneous, oligomers that undergo dynamic subunit exchange. The distribution of oligomers and exchange dynamics are unique for different sHSPs and can be attributed to the variability observed in N- and C-terminal regions (16-18).

Though homomeric sHSP oligomers have been best characterized, many human sHSPs are known to form heterooligomers (containing more than one type of sHSP). HSPB5 is known

to form heterooligomeric complexes with HSPB1, HSPB4, and HSPB6, sHSPs that are expressed in tissues where HSPB5 is also present (19-21). That heterooligomeric sHSPs exist in cells provides impetus to understand properties of sHSPs in the context of mixed oligomers. Defining structural details of heterooligomers assembly proves complicated due to the inherent heterogeneity observed in sHSP oligomers (16, 22). We postulated that interactions that drive heterooligomer formation are common to those that drive homooligomer formation, which have been more thoroughly characterized. In this way, we can draw on the insights gained from many previous studies on homooligomers.

Because of their size and polydispersity, HSPB5 oligomeric complexes have proven challenging to study using conventional biophysical and structural techniques. Attaining structural information for HSPB5 has thus proceeded through a piecemeal approach, beginning with domain-level structures of the HSPB5-ACD solved by NMR and x-ray crystallography (12-15). Pseudo-atomic models of HSPB5 oligomers have been generated using hybrid approaches that combine information from solid-state NMR, small angle x-ray scattering, and electron microscopy (22,23).

Although they differ in certain respects, the two pseudo-atomic models of HSPB5 share several important features that highlight putative intermolecular contacts that may occur within oligomers. In both cases, dimers form the basic building block of an HSPB5 oligomer, where the dimer interface is formed by the antiparallel alignment of the β6+7 strands of the ACD. Dimers form hexameric rings through the interaction of a C-terminal IXI motif from one dimer with a hydrophobic groove formed by the β4/8 strands in the ACD of a neighboring dimer. A model of a 24mer with tetrahedral symmetry can be generated through the assembly of four hexameric rings through extensive contacts between NTRs (Figure 1) (22,23). The resulting models

represent a considerable advancement in our understanding of HSPB5 structure. However, each represents only a single state within the ensemble of HSPB5 oligomers that exist in solution and do not explain dynamic subunit exchange properties.

Multiple studies have demonstrated that subunit exchange occurs between HSPB5 oligomers with subunit exchange rates on the scale of 10^{-3} Sec^{-1} at 37 ^{0}C (18, 24). Recent studies using native mass spectrometry and solution-state NMR attribute the global exchange rate of HSPB5 subunits to structural changes that occur on millisecond time scale (25). Based on these kinetic models, the rate of subunit dissociation from the oligomer is proposed to be limited by interactions involving CTRs within the oligomers. These observations are a first step in linking structural details to the observed subunit exchange. However, the kinetic data do not speak to oligomer assembly and subunit recruitment into an oligomer.

Here we demonstrate that an ACD-only (i.e., the domain without its flanking NTR and CTR) can interact with an HSPB5 oligomer, identifying the minimal and most conserved domain of a sHSP as sufficient for interactions with a sHSP oligomer. The interaction is detected only when the ACD-only can first bind to a CTR from an HSPB5 oligomer and accessibility of CTRs in the HSPB5 oligomer dictates the extent and rate of exchange. Further, we demonstrate that an ACD-only can exchange at the dimer interface within an oligomer, but only when an ACD-only can first bind the CTR, illustrating interactions that dictate oligomer formation are interdependent. Finally, we extend the observations made using an HSPB5 ACD-only and oligomers to the formation of the HSPB5/HSPB6 heterooligomers to gain further insight into the roles of the ACD, CTR, and NTR in oligomer assembly.

Results

An ACD-Only Can Interact With The HSPB5 Oligomer

On the basis of previous structural and biochemical studies, interactions within HSPB5 oligomers can be classified into three types, shown schematically in Figure 1 (22,23). Two of the interaction classes involve the ACD, namely 1) interactions across the ACD dimer interface ("ACD-ACD") and 2) interactions between the β4/β8 groove at the edge of an ACD β-sandwich and the IXI motif within the C-terminal region ("ACD-CTR"). The third type of interaction is poorly defined: the N-terminal region interacts with other NTRs and/or with an ACD. Both the "ACD-ACD" and "ACD-CTR" interactions observed in HSPB5 oligomers can be recapitulated with an ACD devoid of NTRs and CTRs (ACD-only) (12-15, 26). As at least two classes involve the ACD, we asked whether ACD-only can be incorporated into an oligomer and, if so, which interactions are critical?

To determine whether an ACD-only can interact with an oligomer, mixtures of HSPB5-ACD-only and HSPB5-oligomer were incubated at 37°C for 1hour and the distribution of the two species was characterized by analytical size exclusion chromatography (aSEC) (Figure 2A). The mixture reaches equilibrium within the 1-hour incubation (data not shown). As shown in Figure 2A, the elution profile obtained for the mixture is different from that of the oligomer and ACD-only in isolation in two ways. When mixed with an ACD-only, the earliest-eluting peak that corresponds to HSPB5 oligomers elutes slightly later, indicating a smaller average hydrodynamic radius, and the slow-eluting peak, associated with the ACD-only dimer is broader and elutes earlier. Although the differences are subtle, they are reproducible and indicate that the two species interact with sufficient affinity to alter the SEC distributions. SDS-PAGE analysis of fractions from the elution confirms that ACD-only is present in earlier-eluting fractions in the

mixture than when applied and eluted on its own (Figure 2D i). Thus, aSEC provides a simple way to detect an interaction between an ACD-only and an oligomer.

As mentioned above, there are two well-defined ways in which an ACD-only might interact with an oligomer: 1) an ACD-only subunit could exchange with a full-length subunit at the ACD-ACD interface and/or 2) an ACD-only subunit could bind the CTR of an oligomer through ACD-CTR interactions. To determine whether either of these known interactions mediates the ACD-only/oligomer binding detected in the mixing experiment, we performed additional mixing experiments using mutations in the ACD-only that either inhibit CTR binding in the ACD β4/β8 groove, or lock the ACD-only into a dimer unable to exchange subunits. It has been previously demonstrated that mutation of Ser135 to Gln in the ACD effectively blocks binding of a CTR-IXI motif without distorting the ACD structure (26). Remarkably, the IXI-binding mutation in the ACD-only subunit (S135Q-ACD-only) abrogates observable interactions with the oligomer. The elution profile of the mixture is indistinguishable from that of the individual components and there is no sign of mixing in the SDS-PAGE analysis of fractions (Figure 2B and Dii).

To block exchange that might occur though the dimer interface, a Cys residue was introduced at the center of symmetry in the ACD dimer interface (E117C-ACD-only). The E117C-ACD-only robustly forms a disulfide-locked dimer under non-reducing conditions (30). While not as dramatic as the S135Q-ACD-only mixing result, the aSEC profile obtained for WT-HSPB5 oligomer incubated with locked ACD-only dimers is reproducibly different from the mixing experiments shown in Figures 2A. The elution volume of the oligomer species does not shift upon mixing with E117C-ACD-only, but there is a slight broadening and shift of E117C-ACD-only dimers toward earlier elution (Figure 2C and D). This suggests that a locked ACD-

only dimer retains some ability to interact with large oligomers, but not in a way that detectably changes the hydrodynamic properties of the oligomer (as seen in Figure 2A). An explanation for the combined observations is that a CTR-ACD interaction is required for the recruitment of subunits to an oligomer (i.e. the ACD-only associates with the oligomer, without altering the distribution of the oligomer) but is not sufficient for incorporation of a subunit into an oligomer, which requires exchange at the ACD-ACD interface and results in an altered distribution of the oligomer.

To further define and confirm the CTR-ACD interaction is responsible for subunit recruitment, NMR spectra of ^{15}N-labeled HSPB5 oligomers were collected in the presence and absence of the ACD-only. In solution, the large oligomers tumble slowly and therefore most of the resonances are too broad to observe. There are, however, approximately twenty peaks visible in a TROSY-HSQC spectrum that are derived from the highly mobile and dynamic CTR (31). Consistent with this, the spectrum contains a single peak in the region that uniquely contains glycine resonances. The final glycine in the HSPB5 sequence, Gly154, is twenty-one residues from the C-terminus. This indicates that residues back as far as Gly154 are flexible and dynamic and can be observed in the TROSY-HSQC spectrum. As illustrated in Fig. 3A, addition of HSPB5-ACD-only to a ^{15}N-HSPB5-oligomer sample results in broadening of ~14 resonances, confirming that the interaction between the ACD-only and oligomer involves the flexible C-terminal region. Among the observable peaks are ten resonances that have been previously assigned to residues 164 to the C-terminus, residue 175 (31). Ile 159 and Ile161 of the CTR IXI motif precede the assigned region of the spectrum. In the presence of ACD, assigned resonances proximal to the IXI motif (residues 164-170) broaden significantly, while the last 5 C-terminal resonances (171-175) are relatively unaffected (Figure 3B). Additionally, the Gly154 peak is

among those affected by the ACD-only, providing additional support that the region most proximal to the structured portion of the oligomer including the IXI motif (Ile^{159}-Pro-Ile^{161}) is involved in ACD binding to oligomers. Additionally, eight of the nine unassigned peaks broaden significantly with the addition of ACD-only (Figure 3B, red bars). These peaks are likely resonances from residues falling between Gly 154 and the first assigned residue Glu164, but these resonances have not been unambiguously assigned. This region is where we would predict the ACD-only to bind based on previous studies (14, 26, 32)

To directly survey the extent of exchange at the dimer interface between an ACD-only and an oligomer, the "locked" dimer mutation E117C was introduced into both full-length (oligomeric) HSPB5 (E117C-FL) and into the ACD-only construct (E117C-ACD-only). The two species were mixed under reducing conditions for 1 hour to allow exchange and then dialyzed into non-reducing conditions at room temperature, where the disulfide bond can form. Exchange at the dimer interface was detected by the presence of a disulfide-linked FL/ACD-only heterodimer, and visualized by non-reducing SDS-PAGE. By this method, it is apparent that exchange at the dimer interface occurs between an ACD-only subunit and a full-length subunit (Figure S2 in supporting information). Because we observed that initial recruitment of ACD-only into oligomers required the ACD-CTR interaction, we introduced the ACD-CTR-blocking mutation into the E117C-ACD-only to determine if recruitment was required for exchange at the ACD-ACD interface observed by this method. When E117C-FL is equilibrated with the double mutant E117C/S135Q-ACD-only, very little heterodimer is formed, indicating that exchange at the dimer interface does not occur without the binding of a C-terminus from the oligomer (Figure 4A, Figure S2).

Given the results above, conditions or mutations that enhance ACD-CTR interactions may facilitate subunit exchange. Introduction of the S135Q mutation into full-length E117C-HSPB5 inhibits binding of IXI motifs between full-length subunits within an oligomer and should increase the accessibility of CTRs in the oligomer. We predicted this would enhance formation of mixed dimers and indeed we observe an increase in the extent of exchange observed at the dimer interface in the dimer trapping experiments with the S135Q-E117C-oligomer (Figure 4A, S2). As shown in Figure 4B, the effect is particularly apparent in aSEC mixing experiments where the majority of the peak corresponding to free ACD-only is shifted and broadened, as more ACD-only subunits associate with the S135Q-HSPB5 oligomer than we observe associating with the WT HSPB5 oligomer (Figure 2A). Furthermore, when both the oligomer and the ACD-only carry the S135Q mutation little mixing at the dimer interface is observed, demonstrating that if the ACD-only cannot bind the oligomer CTR, subunit exchange does not readily occur (Figure 4A, S2).

Assembly Of HSPB5/HSPB6 Heterooligomers

Mammalian HSPB6 is a small heat shock protein originally co-purified with HSPB5 from skeletal muscle extract (19). HSPB5 and HSPB6 are expressed in many other tissues, such as the heart, lungs, kidney, and brain (4). HSPB6 has been shown to form heterooligomeric complexes with HSPB5, *in vitro* (21). HSPB6 possesses both an NTR and CTR, although its CTR does not contain an IXI motif. Consistent with the lack of IXI motif, a peptide with the HSPB6-CTR sequence does not interact with the ACD of HSPB5 in contrast to peptides mimicking CTRs from other sHSPs that contain an IXI motif (26). Despite lacking its own IXI motif, the sequences that compose the β4/β8 groove are conserved between HSPB6 and other IXI-

containing sHSPs. This raised the question of whether the HSPB6 retains the ability to bind IXI motifs found in heterooligomeric partners. Analogous to the ACD-only from HSPB5, ^{15}N HSQC NMR spectra can be collected on the HSPB6 lacking its NTR (ΔN-HSPB6). To determine whether HSPB6 can bind CTRs containing IXI motifs, ^{15}N HSQC spectra of ΔN-HSPB6 were collected in the absence and presence of a peptide mimicking the HSPB5-CTR. Large perturbations in the HSQC spectrum of ΔN-HSPB6 are observed upon addition of the CTR peptide, demonstrating that though HSPB6 lacks a CTR IXI motif, it is able to bind to peptides mimicking IXI-containing CTRs (Figure S3 in supporting information). Based on the results in the previous section, we hypothesized that binding the CTR of HSPB5 may be critical in the formation of HSPB5/HSPB6 heterooligomers.

To study incorporation of HSPB6 into HSPB5 oligomers, we performed aSEC mixing experiments similar to those previously described (21). The aSEC profile of full-length HSPB6 alone shows it forms much smaller homooligomers (dimer-tetramer) than HSPB5 (Figure 5A). As shown in Figure 5A, aSEC profiles of an equimolar mixture of HSPB5 and HSPB6 reveals the formation of HSPB5/HSPB6 heterooligomers. Assembly of the heterooligomer was observed over a time course of 120 minutes at 37°C. The peak that corresponds to HSPB6 homooligomer decreased over time and a peak that contains both HSPB5 and HSPB6 subunits appears at an intermediate elution time.

The ability to observe formation of HSPB5/HSPB6 heterooligomers by aSEC provides a platform to assess the importance of the ACD-CTR interaction in the formation of a native oligomeric complex, where all subunits contain their native NTRs and CTRs. To address whether binding of the HSPB5-CTR by the ACD-β4/β8 groove of HSPB6 plays a determinant role in the formation of the heterooligomer, the mutation S134Q was introduced into HSPB6 to

block the binding of HSPB5 CTRs (analogous to S135Q-HSPB5). S134Q-HSPB6 is dramatically inhibited in its ability to form HSPB5/HSPB6 heterooligomers: there is only a very small decrease in the HSPB6 peak and the HSPB5/HSPB6 peak observed when WT subunits are incubated is not readily formed (Figure 5B). Thus, as observed with the simplified ACD-only mixing experiments, the ability of an incoming HSPB6 subunit to bind an HSPB5-CTR is a strong determinant for heterooligomer assembly.

To further test this conclusion, mixing experiments were performed with WT-HSPB6 and S135Q-HSPB5 oligomers, the mutation that increases the accessibility of HSPB5 CTRs (Figure 6). Comparison of a 30-minute incubation of WT-HSPB5/WT-HSPB6 and S135Q-HSPB5/WT-HSPB6 shows the latter to incorporate HSPB6 subunits to a greater extent. Importantly, both heterooligomers compared in this experiment are equivalent in their hydrodynamic radii. This is consistent with the notion that the accessibility of oligomer CTRs (i.e., the relative population of CTRs in the free versus bound state) dictates both the rate and extent of subunit recruitment in the formation of both homo- and hetero-oligomers.

NTR Role In Oligomer Formation

Because of its enigmatic and heterogeneous structure, understanding the role of the NTR in oligomer formation remains a formidable challenge. The HSPB6 NTR drives neither formation of large HSPB6 homomeric species nor the incorporation of HSPB6 into pre-existing HSPB5 oligomers. However, once incorporated, an HSPB6 NTR may contribute to the global oligomer distribution and/or stability of the heterooligomer. To further assess a contribution of the HSPB6-NTR to the final oligomeric distribution of HSPB5/HSPB6 heterooligomers, we compared the incorporation of HSPB6 with the incorporation of the NTR deletion ΔN-HSPB6.

Over a two hour time course, ~60% of FL HSPB6 was incorporated into HSPB5/HSPB6 heterooligomers based on the decrease in the aSEC peak volume observed for HSPB6 (Figure 7). In contrast, only ~25% of ΔN-HSPB6 was incorporated, based on peak volume. Additionally, when FL-HSPB6 subunits are incorporated, the resulting HSPB5/HSPB6 heterooligomer elutes later than when the smaller ΔN-HSPB6 subunits are incorporated, demonstrating the presence of the HSPB6 NTR has a detectable impact on the heterooligomer that is formed. Altogether the results confirm that while the HSPB6 NTR does not drive oligomerization *per se*, it makes significant contributions to the stability of heterooligomer and the energetics and extent of incorporation.

Discussion

All sHSPs are composed of an NTR, an ACD, and a CTR. Despite their heterogeneity, three types of interactions have been observed or inferred in sHSP oligomeric structures; an ACD-ACD dimer interface, a CTR-ACD interaction, and ill-defined interactions involving NTRs. We used an ACD-only construct that forms a dimer on its own to parse out the importance and interplay of these interactions in subunit recruitment and oligomer assembly. We detected two classes of interactions between an ACD-only and an HSPB5-oligomer (Figure 2): 1) a weak oligomer-ACD complex manifest as broadening of the ACD elution peak towards shorter elution times without a detectable change in the elution of the oligomer peak (Figure 2C), that we could attribute to ACD-CTR interactions and 2) incorporation of ACD-only subunits into an oligomer to form a "mixed" oligomer that elutes later than the original oligomer (Figure 2A). This incorporation into the oligomer is dependent on the formation of ACD-ACD interactions between the ACD-only and the full-length HSPB5 oligomer. That "locked" ACD-only dimers are recruited but not incorporated into the oligomer is most consistent with exchange occurring at

the dimer interface (Figure 2C). Thus, incorporation of ACD-only into an HSPB5 oligomer proceeds through exchange of monomeric subunits. Importantly, the ACD-CTR interaction is a prerequisite for exchange at the ACD-ACD interface. This implies that subunit exchange occurs with subunits recruited to the oligomer and that the interactions within an oligomer are interdependent. Our observations with HSPB5/HSPB6 heterooligomers are consistent with the observations of ACD-only interactions with HSPB5 oligomers and those made by others (Figures 5 and 6)(21).

We propose that the accessibility of CTRs (i.e., CTR_{free} : CTR_{bound}) dictates both the extent and rate of subunit recruitment to the HSPB5 oligomer. That we can both enhance or diminish both ACD-only and HSPB6 hetero-oligomer formation with HSPB5 by modulating the ACD-CTR interaction underscores the importance of this interaction in sHSP subunit recruitment and incorporation (Figures 2, 4, 5, and 6). Thus, conditions known to increase CTR_{free} such as heat shock or a small decrease in pH will enhance subunit exchange (32, 33). Others have proposed the ACD-CTR interaction is relevant for subunit dissociation and may destabilize the ACD-ACD interface to promote subunit exchange (25, 34). Whether CTR-ACD binding *per se* has a direct affect on the intrinsic rate of exchange at the dimer interface can neither be confirmed nor disputed by the results presented here. However, by bringing a subunit to the oligomer, ACD-CTR binding increases the effective local concentration of non-oligomeric subunits, which will manifest in an observed increase in dimer exchange. Though ACD-CTR binding is of lower affinity than ACD-ACD binding (K_d values of ~100μM vs 2μM, respectively) the ~1000 sec^{-1} rate of exchange at the dimer interface is substantially higher than the ~60 sec^{-1} for ACD-CTR binding (26, 34, and 35). Thus, once bound by a CTR, ACDs of incoming and oligomer-bound subunits can rapidly exchange. The values quoted are for HSPB5; if other human sHSPs have

appreciably different affinities and/or exchange rates, they could impact these steps in subunit recruitment/exchange.

The precise nature of the NTR role in oligomer recruitment and assembly remains enigmatic. Although we did not set out explicitly to study the NTR, our results do shed light on some possible roles. Specifically, our results show that the NTR plays a deterministic role in the stability and distribution of HSPB5/HSPB6 heterooligomers (Figures 5 and 7). By extrapolation, we conclude that the NTR plays a thermodynamic role in oligomer assembly. This conclusion is consistent with studies on phosphorylated states of HSPB1 and HSPB5, in which phosphorylation of NTR residues promotes disassembly of large oligomers into smaller species and with studies on non-mammalian sHSPs, which also demonstrate that alterations in NTRs result in changes in the size and/or stability of their respective oligomers (36-39).

Altogether, observations reported here support a stepwise model by which subunits are incorporated into HSPB5 oligomers (Figure 8). First, a subunit is recruited via its β4/β8 groove to an oligomer CTR through an ACD-CTR interaction. A mutation or conditions such as increased temperature or decreased pH that increase the fraction of CTRs in the "free" state will therefore have a direct effect on both the rate and extent of subunit incorporation (29, 30). Next, exchange at the ACD dimer interface occurs to form a new dimer composed of one original subunit and one newly recruited subunit. A key implication of this step is that subunit exchange in and out of an oligomer occurs (predominantly) via monomeric subunits, even though sHSP dimers are presumed to be the structural building blocks of oligomers. Likely, displaced monomers from this step are able to form new dimeric species off the oligomer, based on reported exchange rates and dimer affinities for the ACD-ACD interaction (35). Finally, the

NTR of an incoming subunit is likely sequestered in the interior of the oligomer where it contributes to the thermodynamic stability and size of the newly formed heterooligomer.

The model presented here implies there are two requirements for sHSP recruitment into an oligomer. First, it must have sufficient sequence complementarity to bind a CTR displayed by an oligomer through an ACD-CTR interaction. The ability to bind a CTR's IXI motif is defined by four residues in the β4/β8 groove of the ACD, which are conserved in all human sHSP except ODF1 (Figure S4 in supporting information). Second, a recruited subunit must be capable of forming a heteromeric ACD-ACD dimer interface to be fully incorporated into an oligomer. The long β-strand that makes the dimer interface is also remarkably well conserved (Figure S4 in supporting information), implying that a majority of human sHSPs may be able to form heterodimers through their ACDs. Therefore, formation of the heterooligomers observed to date (e.g., HSPB1/HSPB5, HSPB4/HSPB5, HSPB1/HSPB6, and HSPB5/HSPB6) likely proceeds via a similar mechanism to the one proposed here, though the explicit role(s) of the highly variable NTRs remain to be defined (19-21, 24, 40).

Our observations here suggest a dominant route in subunit recruitment. It is likely that alternative, though less kinetically favorable modes of subunit recruitment exist, that do not require interactions with the CTR. That S135Q-HSPB5, which cannot bind IXI motifs, is able to form oligomers and that the S134Q-HSPB6, though at a rate much slower than wt-HSPB6, forms heterooligomers with HSPB5, suggest that alternate interaction modes do exist. Identifying and characterizing other modes of recruitment and their role(s) in processes such as the initial steps in the assembly of an oligomer, will require further study and new approaches.

In sum, we have assigned roles for the interactions observed to exist in sHSP oligomers in the process of assembly and subunit exchange. Given the conservation in the relevant

sequences, we imagine that most human sHSPs will assemble using these rules, albeit with inevitable variations that remain to be defined. We note that the insights obtained here stem from simple biochemical approaches using versions of sHSPs designed based on our structural understandings of them. Similar approaches applied to other sHSPs should make them similarly tractable and forthcoming, allowing for a fuller understanding of the mechanism(s) and diversity of sHSP oligomer assembly.

Materials and Methods

HSPB5 and HPB5-ACD-only constructs and mutants have been previously described (23, 26). ΔN-HSP20 (residues 65-160) was expressed from the pPROEX HT(b) vector. HSPB6 was expressed from the pET23b vector. Under non-reducing conditions the formation of disulfide bonds are apparent in HSPB6. HSPB6 has one native cysteine (C46), which was mutated to serine (C46S) in all constructs. Mutagenesis was accomplished using the primer 5'-TGGCTGCGCTCAGCCCCACCACG-3'. Additionally, the mutation S134Q was introduced into HSPB6 constructs using the primer 5'-GGCTGCCGTGACGCAGGCGCTGTCCCCCG-3'.

Protein Expression and Purification

All sHSPs constructs were expressed in BL21(DE3) *Escherichia coli* cultured in Luria-Bertaini media containing 100ug/ml Ampicillin. Protein expression was induced with the addition of Isopropyl thio-β-D-thiogalactoside to a final concentration of 0.5mM at 22°C for 16 hours. All sHSPs constructs purified from BL21(DE3) *Escherichia coli* by methods previously described (12, 17, 23, 26). Briefly, wt and mutant full-length HSPB5 and HSPB6 were purified by an ammonium sulfate precipitation, followed by anion exchange chromatography. Full-length proteins were further purified by size exclusion chromatography in 25mM sodium phosphate and

150mM sodium chloride, pH 7.5 (PBS 7.5). Purification of HSPB5-ACD-only (residues 64-152), HSPB5-ACD-only mutants and ΔN-HSPB6 (residues 65-160) was accomplished by methods previously described (12, 26). Briefly, TEV cleavable, N-terminally His-tagged HSPB5-ACD-only or ΔN-HSPB6 were initially purified from lysate using a Ni^{2+} affinity column. The His-tag was removed by TEV-protease and separated from the ACD using a Ni^{2+} affinity column. Proteins were further purified by anion exchange chromatography and size exclusion chromatography in PBS 7.5.

Analytical Size Exclusion Chromatography (aSEC)

All aSEC experiments were performed on an GE akta Purifier equipped with a Superose 6 10/300 GL column (GE Life Sciences) and a 200µl sample loop in PBS 7.5. aSEC experiments were performed at room temperature (~25°C) with samples preincubated at 37°C. Elution volumes for molecular weight standards and proteins in this study are available in figure S1.

HSPB5 AND ACD-only aSEC. Mixtures of 200µM HSPB5 oligomers and 200µM ACD-only in PBS pH7.5 were incubated at 37°C for 1hour prior to aSEC (monomer concentrations). Mixtures of mutant HSPB5 oligomers and mutant ACD-only constructs were made in the same manner. Fractionated mixtures from these experiments were visualized by SDS-PAGE.
HSPB5 and HSPB6 aSEC. Mixtures of 50µM HSPB5 oligomers and 50µM HSPB6 mutants were incubated at 37°C for 1hr and 2hrs prior to aSEC (monomer concentrations). All full-length HSPB6 proteins contained the mutation C46S to eliminate confounding disulfide bond formation. Mixtures of HSPB5 and ΔN-HSPB6 were made and in the same manner.

Detection of ACD interface exchange. To detect mixing at the ACD-ACD interface E117C-HSPB5 and E117C-ACD-only were reduced in PBS pH 7.5 containing 15mM DTT for 1 hour at 37°C. Reduced E117C-HSPB5 and E117C-ACD-only were then mixed for 1 hour at 37°C. Reducing agent was removed by a 16 hours dialysis into PBS pH 7.5, at room temperature (~25°C). Additionally, mixing experiments with either E117C-HSPB5 and/or the E117C-ACD-only containing the S135Q mutation, were done using the same methodology. Non-reduced mixtures were then visualized by non-reducing SDS-PAGE. The extent of exchange at the ACD-ACD interface was quantified by the appearance of a band corresponding to a disulfide locked mixed FL/ACD-only dimer. Mixing experiments were done in triplicate and gels were imaged using a LI-COR Odyssey CLx and band intensities were quantified using the imaging software ImageJ (27). Band intensities were normalized to the mean band intensity observed for the E117C-HSPB5/E117C-ACD-only mixture.

NMR. ^{15}N TROSY-HSQC spectra of ^{15}N-HSPB5 oligomers were collected on a Bruker Avance II 600 MHz spectrometer equipped with a triple resonance, z-gradient cryoprobe. Spectra were collected on samples containing 300μM ^{15}N HSPB5 in the presence and absence of 600μM HSPB5-ACD-only in PBS pH7.5 and 10%D_2O, at 22°C. ^{15}N HSQC-spectra of 500μM ΔN-HSPB6 we were collected in identical buffer conditions with a Bruker 500 MHz AVANCE II NMR spectrometer. HSQC spectra of ΔN-HSPB6 were collected in the presence of a 6-fold excess of a peptide with the sequence PERTIPITREEK that mimics a region HSPB5 CTR, by methods described previously (26). Spectra were processed using the NMR-Pipe/NMRDRaw and visualized with NMRView (28,29).

ACKNOWLEDMENTS. We thank Christine Slingsby (Birkbeck College) and Nikolai Gusev (Moscow State University) for generously providing HSPB6 plasmids for this work. We thank Dr. Peter Brzovic, Dr. Vinyak Vittal, and Amanda Clouser for their discussions and critical reading of this manuscript.

Figures

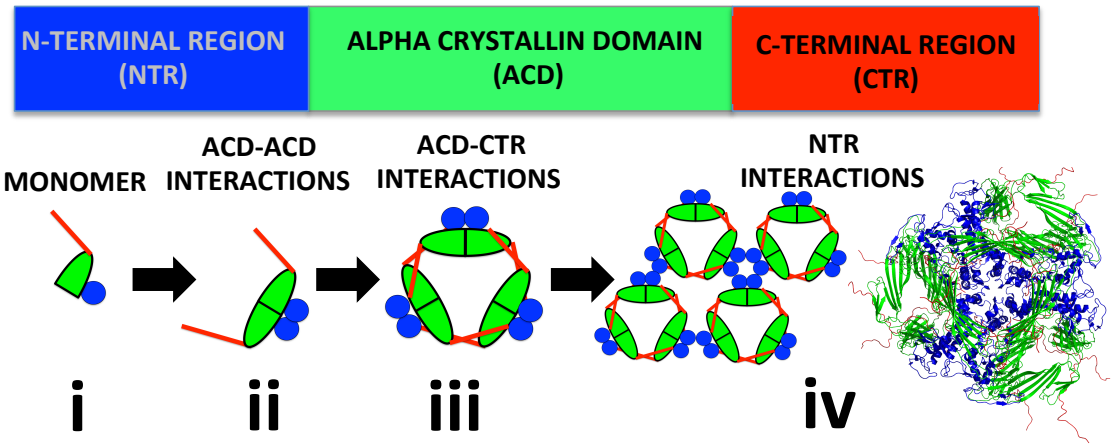

Figure 1. A) The three regions of sHSPs are the conserved alpha-crystallin domain (ACD, green), flanked by variable N-terminal regions (NTR, blue) and C-terminal regions (CTR, red). B) A cartoon diagram of interactions observed in pseudo-atomic models of HSPB5 (same colors as defined in (A)). sHSP monomers (i) assemble into dimers through ACD-ACD interactions (ii). Higher-order assemblies occur through CTR-ACD interactions (iii, hexamer shown), and poorly defined NTR interactions drive the assembly of the final oligomer (iv). Rather than the formation of an expanded array (iv, left cartoon), sHSPs assemble into oligomers with defined assemblies/distributions (iv). A pseudo-atomic model of a 24mer HSPB5 oligomer is shown in colors described above (12).

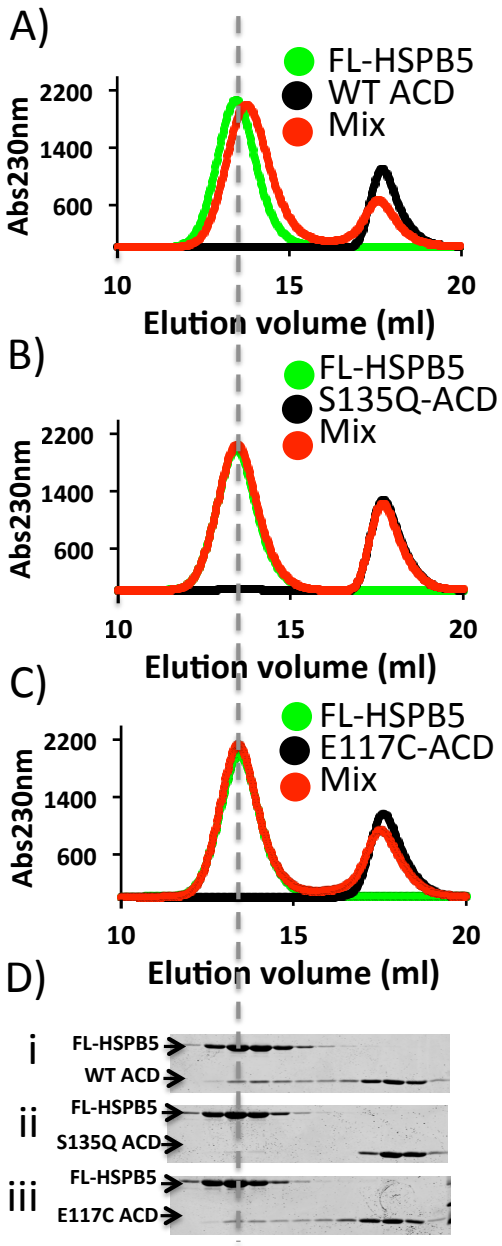

Figure 2. ACD-only interactions with HSPB5 oligomers detected by aSEC. A) aSEC traces of HSPB5-oligomers (green) and ACD-only alone (black), as well as an equimolar mixture of HSPB5-oligomer/ACD-only incubated at 37°C for 1hour prior to aSEC (red). B) aSEC traces of HSPB5-oligomers, S135Q-ACD-only, and their equimolar mixture (same colors as A.). C) aSEC traces of HSPB5-oligomers, E117C-ACD-only, and their equimolar mixture (same colors as A.). D. SDS-PAGE gels of aSEC fractions from HSPB5-oligomer/ACD mixtures: i) HSPB5-oligomers with wt –ACD-only; ii) HSPB5-oligomers with S135Q-ACD-only; iii) HSPB5-oligomers with E117C–ACD-only.

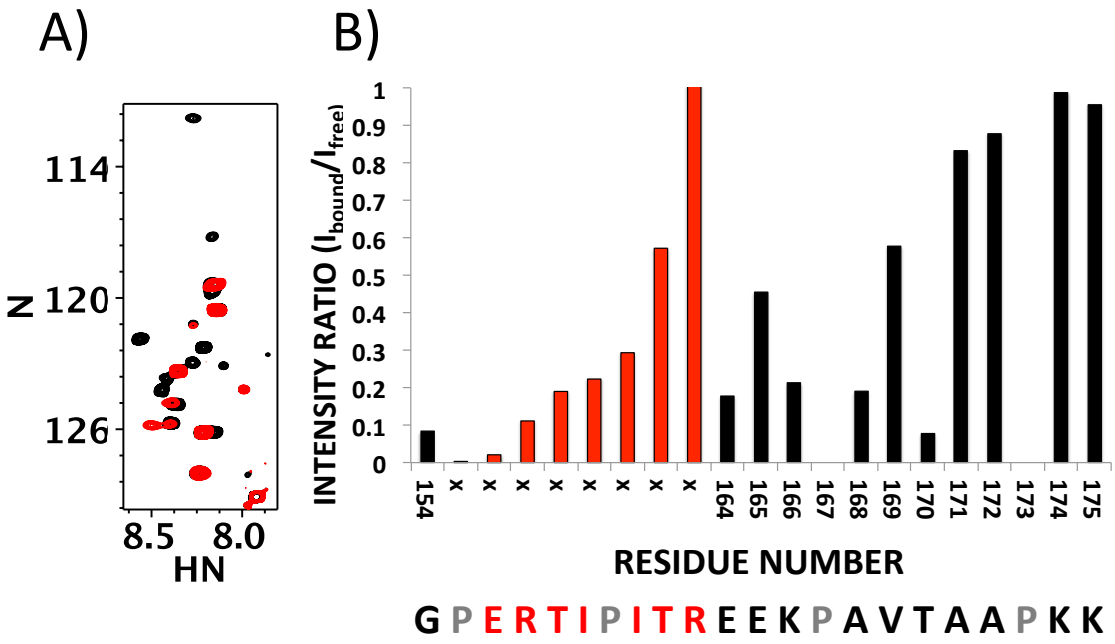

Figure 3. ACD-only Binding to CTRs of ^{15}N-HSPB5 Oligomers. A) ^{15}N-HSQC spectra of HSPB5-oligomers in the absence (black) and presence (red) of 2 mol equivalents of HSPB5-ACD-only. B) Histogram of intensity ratios (I_{bound}/I_{free}) for HSPB5-oligomer CTR residues, with and without HSPB5-ACD-only bound. Intensity ratios for assigned residues are shown in black. Intensity ratios for unassigned residues are shown in red in ranked order as the peaks are not attributed to specific residues. Nevertheless, it is likely unassigned resonances arise from residues 155-163. The CTR sequence is shown below. Prolines (shown in gray) are not observed by this method and are denoted with intensity ratios of zero.

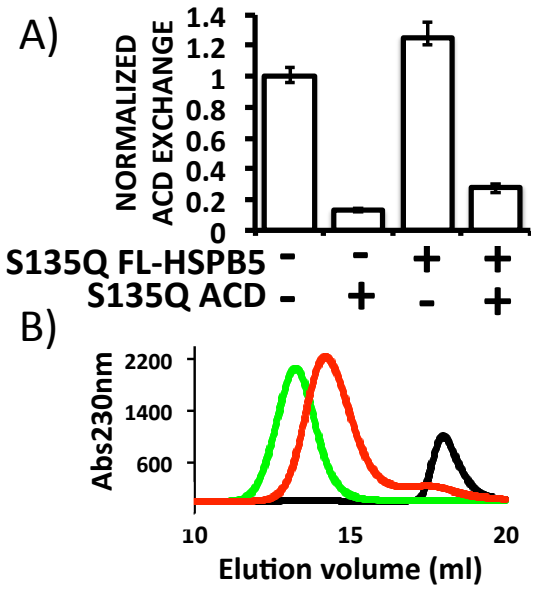

Figure 4. A) Normalized SDS-PAGE band intensities for the disulfide-locked FL/ACD-only mixed dimer from E117C-fl-HSPB5 and E117C-ACD-only mixtures, incubated under reducing conditions and subsequently dialyzed into non-reducing conditions. Mixtures were visualized by non-reducing SDS-PAGE. Intensities for disulfide-locked FL/ACD-only mixed dimer were determined with mixtures where either or both E117C-fl-HSPB5 and E117C-ACD-only had the additional mutation, S135Q. Mixing experiments were done in triplicate and intensities were normalized to the mean intensity for the E117C-fl-HSPB5 and E117C-ACD-only mixture (left bar). Mean normalized intensities are plotted for each mixture, as are the minimum and maximum observed normalized intensities (error bars). B) aSEC traces of S135Q HSPB5-oligomers (green) and HSPB5-ACD-only (black) alone, as well as an equimolar mixture of S135Q HSPB5-oligomer/HSPB5-ACD-only incubated at 37°C for 1hour prior to aSEC (red).

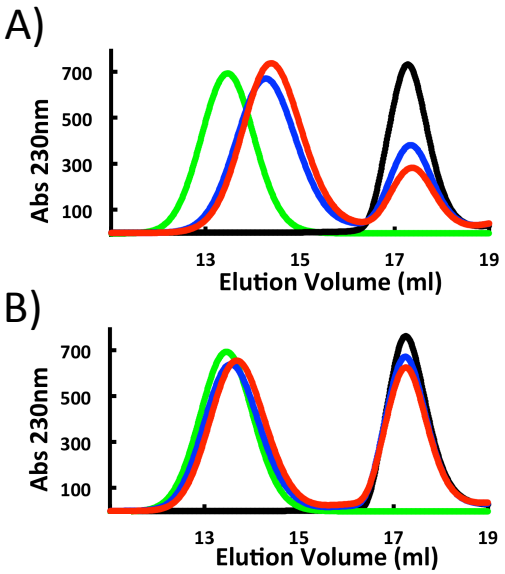

Figure 5. Formation of HSPB5/HSPB6 heterooligomers. A) aSEC traces of HSPB5-oligomers (green) and HSPB6 (black) alone, and as an equimolar mixture incubated at 37°C for 1hour (blue) and 2 hours (red) prior to aSEC. B) aSEC traces of HSPB5-oligomers (green) and S134Q-HSPB6 (black) alone, and as an equimolar mixture incubated at 37°C for 1hour (blue) and 2 hours (red) prior to aSEC.

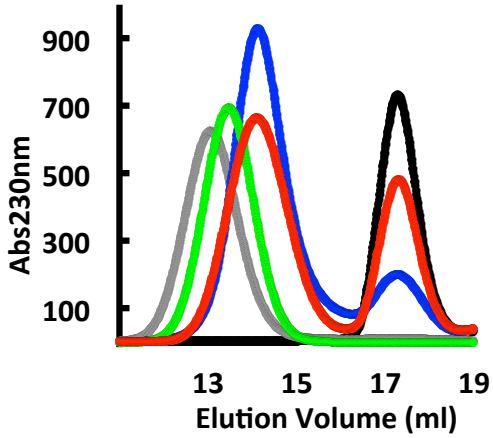

Figure 6. S135Q-HSPB5 interactions with HSPB6. aSEC traces of HSPB5-oligomers (green) and HSPB6 alone (black), and as an equimolar mixture incubated at 37°C for 30 minutes (red) prior to aSEC compared to equimolar mixture of S135Q-HSPB5 and HSPB6 incubated at 37°C for 30 minutes (blue) prior to aSEC. The aSEC trace for S135Q-HSPB5 is shown in gray.

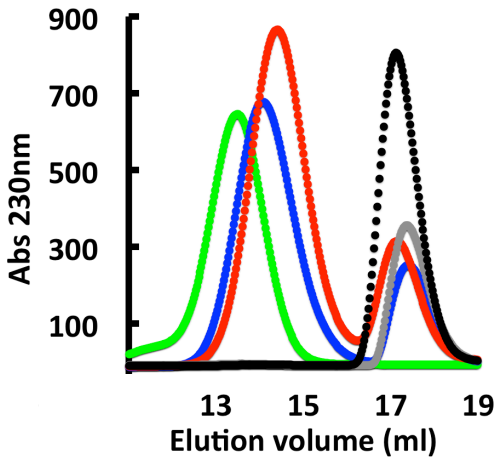

Figure 7. NTR role in HSPB5/HSPB6 interactions. aSEC traces of HSPB5-oligomers (green) and HSPB6 (black) alone, and as an equimolar mixture incubated at 37°C for 2 hours (red) prior to aSEC is compared to an equimolar mixture of HSPB5-oligomer and ΔN-HSPB6 incubated at 37°C for 2 hours (blue) prior to aSEC. The aSEC profile for ΔN-HSPB6 alone is shown in gray.

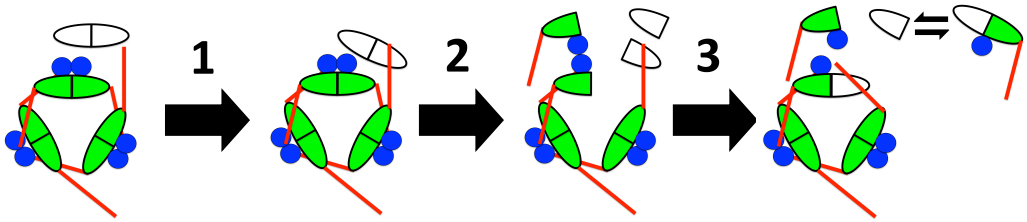

Figure 8. Model for subunit recruitment and incorporation. 1) Through an ACD-CTR interaction an ACD-only (white) is recruited to the oligomer though interactions with CTRS that are "free" in the oligomer (Shown as a hexamer; NTR (blue), ACD (green), CTR (red)). 2, 3 Association through the CTR permits mixing at the ACD-ACD interface through monomer exchange and results in the subsequent dissociation of a subunit previously bound to the oligomer.

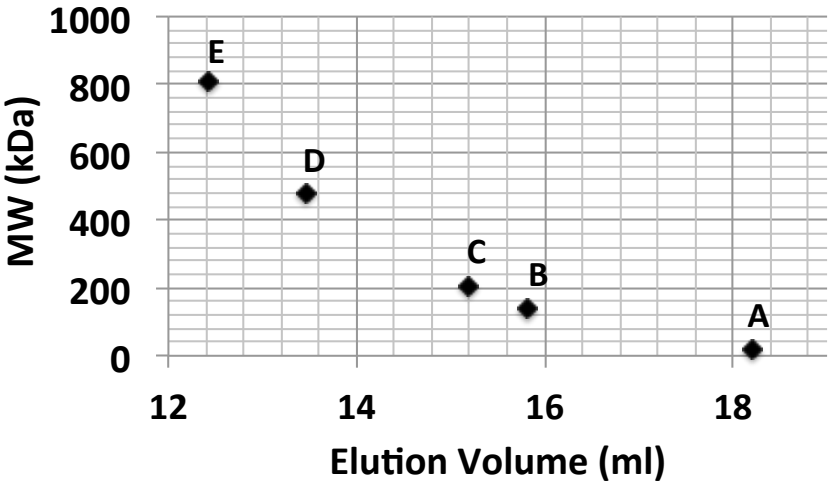

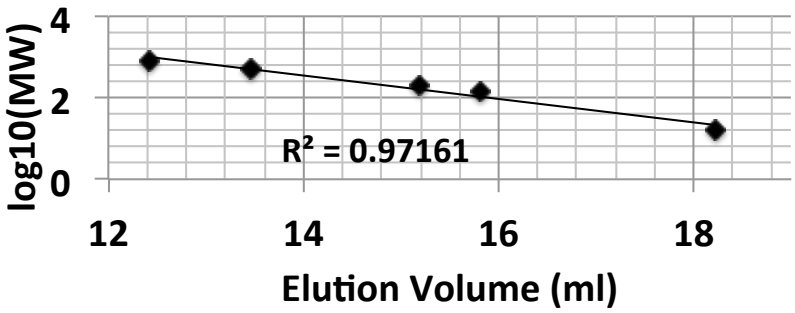

Protein or Protein Mixture	Elution Volume	Apparent Molecular Weight
HSPB5-ACD only	17.7 ml	~30kDa
HSPB6	17.3 ml	~40kDa
ΔN-HSPB6	17.4 ml	~40kDa
S135Q-HSPB5	13.1 ml	~650kDa
HSPB6/S135Q-HSPB5 MIXTURE (Figure 6)	14.1 ml	~330kDa
HSPB6/HSPB5 MIXTURE (Figure 7)	14.4 ml	~270kDa
ΔN HSPB6/HSPB5 MIXTURE (Figure 7)	14.0 ml	~350kDa

S1. Molecular weights versus elution volumes for aSEC: A αlactalbumin (16kDa), B Yeast Alcohol Dehydrogenase (141kDa), C wheatHSP16.9 (200kDa), D WT-HSPB5 (~480kDa) and E H104K HSPB5 (~810kDa). Average molecular weights for HSPB5 and H104K HSPB5 oligomers are based on reported SEC-MALS values (35). Observed elution volumes and calculated apparent molecular weights for relevant proteins are presented below the plot. Apparent molecular weights calculated based on a linear fit of the log(MW) versus elution volume are given.

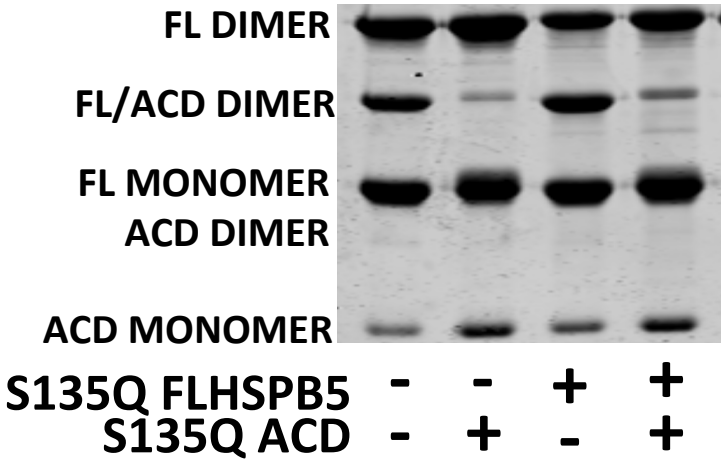

S2. Non-reducing SDS-PAGE of E117C HSPB5-oligomers and E117C HSPB5-ACDs mixed under reducing conditions, followed by dialysis into oxidizing conditions. Exchange at the ACD-ACD interface is observed by the formation of a mixed FL/ACD locked dimer. Lane 1, the E117C HSPB5-oligomer and E117C-ACD mixture; Lane 2, mixing when the ACD additionally carries the S135Q mutation; Lane 3, mixing when the HSPB5 oligomer additionally carries the S135Q mutation; Lane 4, mixing when both oligomer and ACD additionally carry the S135Q mutation.

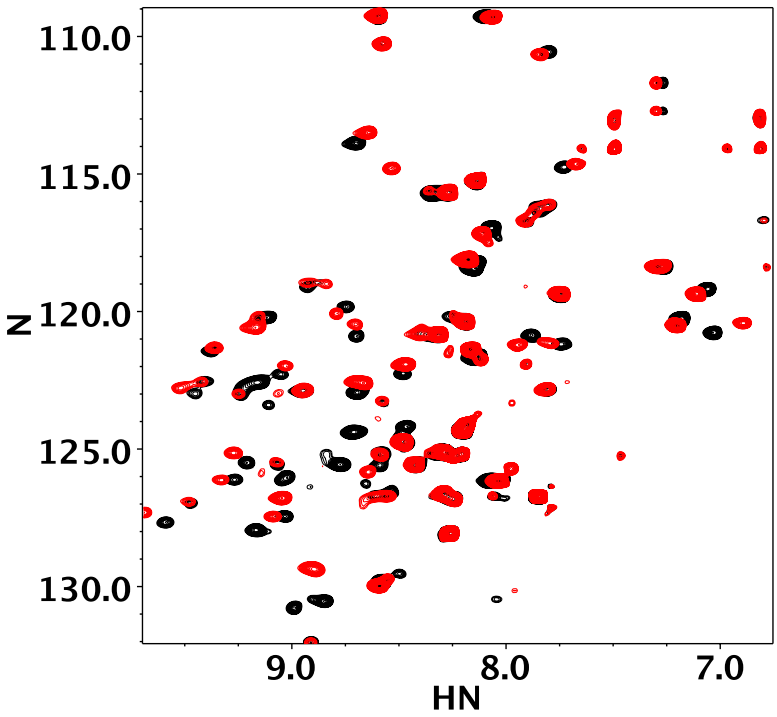

S3. ^{15}N-HSQC Spectrum of ΔN-HSPB6 (500mM) in the absence (black) and presence of a peptide (6-fold excess) mimicking a region of the CTR of HSPB5 (Red). Spectra were collected at 22°C.

```
HSPB1   ---RWRVSLDVNHFAPDELTVKTKDGVVEITGKHEERQDEHGYISRCFTRKYT---LPPG 147
HSPB8   ---PWKVCVNVHSFKPEELMVKTKDGYVEVSGKHEEKQQEGGIVSKNFTKKIQ---LPAE 148
HSPB4   ---KFVIFLDVKHFSPEDLTVKVQDDFVEIHGKHNERQDDHGYISREFHRRYR---LPSN 123
HSPB5   ---RFSVNLDVKHFSPEELKVKVLGDVIEVHGKHEERQDEHGFISREFHRKYR---IPAD 127
HSPB6   ---HFSVLLDVKHFSPEEIAVKVVGEHVEVHARHEERPDEHGFVAREFHRRYR---LPPG 126
HSPB2   ---KFQAFLDVSHFTPDEVTVRTVDNLLEVSARHPQRLDRHGFVSREFCRTYV---LPAD 126
HSPB3   ---HFQILLDVVQFLPEDIIIQTFEGWLLIKAQHGTRMDEHGFISRSFTRQYK---LPDG 123
HSPB7   ---AYEFAVDVRDFSPEDIIVTTSNNHIEVR---AEKLAADGTVMNTFAHKCQ---LPED 131
HSPB9   ---GFQMKLDAHGFAPEELVVQVDGQWLMVTGQQQLDVRDPERVSYRMSQKVHRKMLPSN 109
ODF1    CSSNILGSVNVCGFEPDQVKVRVKDGKVCVSAERENRYDCLGSKKYSYMNICKEFSLPPC 180
                                                          *

HSPB1   VDPTQVSSSLSPEGTLTVEAPMPKLATQSNEITIPVTFESRAQLGGPEAAKSDETAAK-- 205
HSPB8   VDPVTVFASLSPEGLLIIEAPQVPPYSTFGES----SFNNELPQDSQEVTCT-------- 196
HSPB4   VDQSALSCSLSADGMLTFCGPKIQTGLDATHAERAIPVSREEKP--TSAPSS-------- 173
HSPB5   VDPLTITSSLSSDGVLTVNGPRKQ----VSGPERTIPITREEKPAVTAAPKK-------- 175
HSPB6   VDPAAVTSALSPEGVLSI---------------QAAPASAQAPP--PAAAK--------- 160
HSPB2   VDPWRVRAALSHDGILNLEAPRGGRHLDTEVNEVYISLLPAPPDPEEEEEAAIVEP---- 182
HSPB3   VEIKDLSAVLCHDGILVVEVKD--------------PVGTK------------------- 150
HSPB7   VDPTSVTSALREDGSLTIRARR-------------HPHTEHVQQTFRTEIKI-------- 170
HSPB9   LSPTAMTCCLTPSGQLWVRGQCVALALPEAQTGPSPRLGSLGSKASNLTR---------- 159
ODF1    VDEKDVTYSYGLGSCVKIESPCYPCTSPCSPCSPCSPCNPCSPCNPCSPYDPCNPCYPCG 240
              *
```

S4. Sequence alignment of the ACD regions of human sHSPs. The β4/8 groove involved in CTR binding is highlighted in cyan. The β6+7 strand, which defines the ACD-ACD dimer interface is highlighted in green. CTR IxI motifs are italicized. Asterisks mark positions E117 and S135 in HSPB5.

References

1. Bukau, B., Weissman, J., and Horwich, A. (2006) Molecular chaperones and protein quality control. Cell 125, 443–451.
2. Haslbeck, M., Franzmann, T., Weinfurtner, D. and Buchner, J. (2005) Some like it hot: the structure and function of small heat-shock proteins. Nat. Struct. Mol. Biol. 12, 842–846.
3. Ecroyd, H. & Carver, J.A. (2009)Crystallin proteins and amyloid fibrils. Cell. Mol. Life Sci. 66, 62–81.
4. Taylor, R.P., and Benjamin, I.K.J. (2005) Small heat shock proteins: a new classification scheme in mammals. J. Mol. Cell Cardiol. 38, 433-444.
5. Kappé G., Franck E., Verschuure P., Boelens W.C., Leunissen J.A., and de Jong W.W. (2003)The human genome encodes 10 alpha-crystallin-related small heat shock proteins: HspB1-10. Cell Stress Chaperones 8, 53-61.
6. Vicart, P., Caron, A., Guicheney, P., Li, Z., Prévost, M.C., Faure, A., Chateau, D., Chapon, F., Tomé, F., Dupret, J.M., Paulin, D., and Fardeau, M. (1998)A missense mutation in the αB-crystallin chaperone gene causes a desmin-related myopathy. Nat. Genet. 20, 92–95.
7. Rajasekaran, N.S., Connell, P., Christians, E.S., Yan, L.J., Taylor, R.P., Orosz, A., Zhang, X.Q., Stevenson, T.J., Peshock, R.M., Leopold, J.A., Barry, W.H., Loscalzo, J., Odelberg, S.J., and Benjamin, I.J. (2007). Human αB-crystallin mutation causes oxido-reductive stress and protein aggregation cardiomyopathy in mice. Cell 130, 427–439.
8. Liu, Y., Zhang, X., Luo, L., Wu, M., Zeng, R., Cheng, G., Hu, B., Liu, B., Liang, J.J., and Shang, F. (2006) A novel αB-crystallin mutation associated with autosomal dominant congenital lamellar cataract. Invest. Ophthalmol. Vis. Sci. 47, 1069–1075.
9. Selcen, D., and Engel, A.G. (2003) Myofibrillar myopathy caused by novel dominant negative α B-crystallin mutations. Ann. Neurol. 54, 804–810.
10. Vargas-Roig, L.M., Gago, F.E., Tello, O., Anzar, J.C., and Ciocca, D.R. (1998) Heat shock protein expression and drug resistance in breast cancer patients treated with induction chemotherapy. Int. J. Cancer. 79, 468-475.
11. Cornford, P.A., Dodson, A.R., Parsons, K.F., Desmond, A.D., Woolfenden, A., Fordham, M., Neoptolemos, J.P., Ke, Y.Q., and Foster, C.S. (2000) Heat shock protein expression independently predicts clinical outcome in prostate cancer. Cancer Res. 60, 7099-7105.
12. Bagnéris, C., Bateman, O.A., Naylor, C.E., Cronin, N., Boelens, W.C., Keep, N.H., and Slingsby, C. (2009) Crystal structures of alpha-crystallin domain dimers of alphaB-crystallin and Hsp20. J. Mol. Biol. 392, 1242–1252.
13. Jehle, S., van Rossum, B., Stout, J.R., Noguchi, S.R., Falber, K., Rehbein, K., Oschkinat, H., Klevit, R.E., and Rajagopal, P. (2009) alphaB-crystallin: a hybrid solid-state/solution-state NMR investigation reveals structural aspects of the heterogeneous oligomer. J. Mol. Biol. 385, 1481–1497.
14. Langanowsky, A., Benesch, J., Landau, M., Ding, L., Sawaya, M., Cascio, D., Huang, Q., Robinson, C., Horwitz, J., and Eisenberg, D. (2010) Crystal structures of truncated alphaA and alphaB crystallins reveal structural mechanisms of polydispersity important for eye lens function. Protein Sci. 19, 1031–1043.
15. Clark, A.R., Naylor, C.E., Bagnéris, C., Keep, N.H., and Slingsby, C. (2011) Crystal structure of R120G disease mutant of human aB-crystallin domain dimer shows closure of a groove. J. Mol. Biol. 408, 118–134.

16. Aquilina, J.A., Benesch, J.L., Bateman, O.A., Slingsby, C., and Robinson, C.V. (2003) Polydispersity of a mammalian chaperone: mass spectrometry reveals the population of oligomers in alphaB-crystallin. Proc. Natl. Acad. Sci. U.S.A. 19, 10611–10616.
17. Bukach, O.V., Glukhova, A.E., Seit-Nebi, A.S., and Gusev, N.B. (2009) Heterooligomeric complexes formed by human small heat shock proteins HspB1 (Hsp27) and HspB6 (Hsp20). Biochim. Biophys. Acta. 1794, 486–495.
18. Baldwin, A.J., Lioe, H., Hilton, G.R., Baker, L.A., Rubinstein, J.L., Kay, L.E., and Benesch J.L.P. (2011) The Polydispersity of aB-Crystallin Is Rationalized by an Interconverting Polyhedral Architecture. Structure 19, 1855–1863.
19. Kato, K., Goto, S., Inaguma, Y., Hasegawa, K., Morishita, R., and Asano, T. (1994) Purification and characterization of a 20-kDa protein that is highly homologous to alpha B crystallin. J. Biol. Chem. 269,15302–15309.
20. Zantema, A., Verlaan-De Vries, M., Maasdam, D., Bol, S., and van der Eb, A. (1992) Heat shock protein 27 and alpha B-crystallin can form a complex, which dissociates by heat shock. J. Biol. Chem. 267, 12936–12941.
21. Mymrikov, E.V., Seit-Nebi, A.S., and Gusev, N.B. (2012) Heterooligomeric complexes of human small heat shock proteins. Cell Stress Chaperones. 17, 157-169.
22. Braun, N., Zacharias, M., Peschek, J., Kastenmüller, A., Zou, J., and Hanzlik, M. (2011) Multiple molecular architectures of the eye lens chaperone αB-crystallin elucidated by a triple hybrid approach. Proc. Natl. Acad. Sci. U.S.A. 108, 20491-20496.
23. Jehle, S., Vollmar, B.S., Bardiaux, B., Dove, K.K., Rajagopal, P., Gonen, T., Oschkinat, H. and Klevit, R.E. (2011) N-terminal domain of alphaB-crystallin provides a conformational switch for multimerization and structural heterogeneity. Proc. Natl. Acad. Sci. U.S.A. 108, 6409–6414.
24. Sreelakshmi, Y., and Sharma, K.K. (2006) The interaction between alphaA- and alphaB-crystallin is sequence-specific. Mol. Vis. 12, 581-587.
25. Baldwin, A.J., Hilton, G.R., Lioe, H., Bagneris, C., Benesch, J.L.P. and Kay, L.E. (2011) Quaternary Dynamics of αB-Crystallin as a Direct Consequence of Localised Tertiary Fluctuations in the C-Terminus. J. Mol. Biol. 413, 310–320.
26. Delbecq, S.P., Jehle, S. and Klevit, R.E. (2012) Binding determinants of the small heat shock protein, αB-crystallin: recognition of the “IxI” motif. EMBO J 2012 Dec 31, 4587-4594. doi: 10.1038/emboj.2012.318.
27. Schneider, C. A., Rasband, W. S. & Eliceiri, K. W. (2012), "NIH Image to ImageJ: 25 years of image analysis", Nature methods 9, 671-675.
28. Delaglio, F., Grzesiek, S., Vuister, G.W., Zhu, G., Pfeifer, J., and Bax, A. (1995) NMRPipeL a multidimensional spectral processing system based on UNIX pipes. J. Biomol. NMR 6, 277–293.
29. Johnson, B.A. and Blevins, R.A. (1994) NMR View: a computer program for the visualization and analysis of NMR data. J. Biomol. NMR 4, 603–614.
30. Hochberg, G.K., Ecroyd, H., Liu, C., Cox, D., Cascio, D., Sawaya, M.R., Collier, M.P., Stroud, J., Carver, J.A., Baldwin, A.J., Robinson, C.V., Eisenberg, D.S., Benesch, J.L., and Laganowsky A. (2014) The structured core domain of αB-crystallin can prevent amyloid fibrillation and associated toxicity. Proc. Natl. Acad. Sci. U.S.A. 111, 1562-1570. doi: 10.1073/pnas.1322673111.

31. Treweek TM1, Rekas A, Walker MJ, Carver JA. (2010) A quantitative NMR spectroscopic examination of the flexibility of the C-terminal extensions of the molecular chaperones, αA- and αB-crystallin. Exp. Eye Res. 91, 691-699. doi: 10.1016/j.exer.2010.08.015.
32. Jehle, S., Rajagopal, P., Bardiaux, B., Markovic, S., Kühne, R., Stout, J.R., Higman, V.A., Klevit, R.E., van Rossum, B.J., and Oschkinat, H. (2010) Solid-state NMR and SAXS studies provide a structural basis for the activation of alphaB-crystallin oligomers. Nat. Struct. Mol. Biol. 17, 1037–1042.
33. Baldwin, A.J., Walsh, P., Hansen, D.F., Hilton, G.R., Benesch, J.L., Sharpe, S., and Kay, L.E. (2012) Probing dynamic conformations of the high-molecular-weight αB-crystallin heat shock protein ensemble by NMR spectroscopy. J. Am. Chem. Soc. 134, 15343-15350.
34. Hilton, G.R., Hochberg, G.K., Laganowsky, A., McGinnigle, S.I., Baldwin, A.J., and Benesch, J.L.(2013) C-terminal interactions mediate the quaternary dynamics of αB-crystallin. Philos. Trans. R. Soc. Lond. B. Biol. Sci. 368, 20110405. doi:10.1098/rstb.2011.0405.
35. Rajagopal P., Tse E., Borst A.J., Delbecq S.P., Shi L., Southworth D.R., and Klevit R.E. (2015) A conserved histidine modulates HSPB5 structure to trigger chaperone activity in response to stress-related acidosis. Elife. 11:4. doi: 10.7554/eLife.07304.
36. Ito, H., Kamei, K., Iwamoto, I., Inaguma, Y., Nohara, D. and Kato, K. (2001) Phosphorylation-induced change of the oligomerization state of alpha B-crystallin. J. Biol. Chem. 276, 5346–5352.
37. Rogalla, T., Ehrnsperger, M., Preville, X., Kotlyarov, A., Lutsch, G., Ducasse, C., Paul, C., Wieske, M., Arrigo, A.P., Buchner, J., and Gaestel, M. (1999) Regulation of Hsp27 oligomerization, chaperone function, and protective activity against oxidative stress/tumor necrosis factor alpha by phosphorylation. J. Biol. Chem. 274, 18947-18956.
38. Basha E., Friedrich K.L., and Vierling E. (2006) The N-terminal arm of small heat shock proteins is important for both chaperone activity and substrate specificity. J. Biol. Chem. 281, 39943-39952.
39. McHaourab H.S., Lin Y.L., and Spiller B.W. (2012) Crystal structure of an activated variant of small heat shock protein Hsp16.5. Biochemistry. 2012 51, 5105-5112. doi: 10.1021/bi300525x.
40. Skouri-Panet, F., Michiel, M., Férard, C., Duprat, E., and Finet, S. (2012) Structural and functional specificity of small heat shock protein HspB1 and HspB4, two cellular partners of HspB5: role of the in vitro hetero-complex formation in chaperone activity. Biochimie. 94, 975-984. doi: 10.1016/j.biochi.2011.12.018.

CHAPTER 4 Interactions between sHSPS and Clients

Introduction

Small Heat Shock proteins (sHSPs) are a diverse class of ATP-independent molecular chaperones that delay the formation of insoluble protein aggregates through their interactions with destabilized/aggregate-prone proteins (1). Their function has proven beneficial during events of cellular stress including, temperature-related stresses and events of hypoxia and ischemia. Their roles as chaperones have also been implicated in combating diseases tied to protein aggregation such as Alexander disease and tauopathies (2-5). sHSP dysfunction has also been observed through the multiple disease associated mutations that have been identified in human sHSPs, including the R120G mutation in the human sHSP, HSPB5, which is linked to myopathies (6). How sHSPs interact with aggregate-prone proteins (clients) remains relatively undefined across the protein family and is critical for understanding how sHSPs function as well as circumstances where they fail to function.

A fundamental challenge in understanding how sHSPs interact with clients lies within the diversity in both sequence and structure observed in the sHSP family. The central conserved domain, known as the alpha crystallin domain (ACD) defines the sHSP family and is flanked by N and C-terminal regions, which are poorly conserved. When compared across Phyla, the ACD is also poorly conserved in sequence (Figure 1). On the structural level, most sHSPs are known to form oligomers. Structures and pseudo-atomic models of the wheat sHSP, wHSP16.9, the human sHSP, HSPB5, and bacterial *M. jannaschii*, hsp16.5 reveal sHSP oligomers are diverse in both their size and shape (7-10). For example, while wHSP16.9 is known to form relatively monodisperse dodecamers, the human HSPB5 forms polydisperse oligomers ranging from 10-40mers (7,11). The pseudo-atomic model of a tetrahedrally symmetric HSPB5 24mer has an

architecture distinct from wHSP16.9 (Figure 1) (7-9). This raises the questions of how structurally distinct sHSPs can interact with the same client, and what types of interactions between clients and sHSPs are conserved between different sHSPs.

Multiple studies have been directed towards observing and defining interactions between sHSPs and clients. Client binding in plant sHSPs such as wHSP16.9, has been attributed to the N-terminal region of the protein. However, regions involved in client binding remain relatively ill-defined for mammalian sHSPs such as HSPB5, though putative client binding regions have been proposed throughout all regions of mammalian sHSPs (12-20). Further, while some sHSPs including wHSP16.9, have been shown to form complexes with many different clients that are indicative of long-lived and relatively high affinity interactions, interactions between the human sHSP HSPB5 and clients appear much more transient and ill-defined in nature (21-25). Work by Koteiche and others further suggest that sHSPs may interact with client states through distinct modes of either high or low affinity, depending on properties of the client state (26). The fundamental challenge in interpreting these observations in the context of understanding the sHSP family, lies in the fact that these observations have been made across differing systems, where the client and experimental tools used to characterize these interactions are different. The diversity of interactions observed with clients provides impetus to compare how sHSPs with distinct sequences and structures interact with client under common experimental conditions.

Defining interactions with clients has proven a common challenge in characterizing molecular chaperones. Several studies have been directed at characterizing client interactions with ATP-driven chaperones using unfolded proteins that are more amenable to biophysical methods, as they are not susceptible to self-aggregation and remain in an unfolded monomeric

state. These "model clients" include a mutant of staphylococcal nuclease, Δ131Δ, and the *E. coli* phosphatase phoA, and have been used to define client interactions with ATP-driven chaperones HSP90 and Trigger Factor, respectively (27-29). These "model clients" serve as tractable systems to rigorously define interactions between a molecular chaperone and the unfolded monomeric client state.

Here we set to compare how the human sHSP, HSPB5, and the wheat sHSP, wHSP16.9, interact with the model clients Δ131Δ and phoA as well as the in vitro client αlactalbumin (αLac) under conditions where the chaperones are active. We expand on these observations to characterize interactions between these clients and a disease-associated mutation of HSPB5, R120G. Surprisingly, neither WT-HSPB5 nor wHSP16.9 make strong interactions with the unfolded monomeric state of any client tested, while the disease-associated R120G-HSPB5 has a markedly increased affinity for the unfolded monomeric client state. Further, wHSP16.9 has an observable interaction with later state aggregates of αLac which is not observed with HSPB5. These observations highlight the diversity of interactions with client states that exist within the sHSP family and point to mechanisms of client interactions distinct from ATP-driven molecular chaperones.

Results

SHSPs Delay Aggregation Of Model Clients Via Different Mechanisms

sHSPs delay the aggregation of a variety of client proteins *in vitro*, including the protein αLactalbumin (αLac) when it is destabilized by reduction of its disulfide bonds. As shown in Figure 2, large aggregates of αLac are detected by light scattering over time, following the

addition of reducing agent (red trace). The observed aggregation is delayed in the presence of either the human sHSP, HSPB5 or the wheat sHSP, wHSP16.9 (green and black trace respectively). The ability of each sHSP to delay the aggregation of αLac is similar in this assay, raising the question whether these two structurally distinct sHSPs bind the client through common mechanisms.

To detect complex formation between the sHSPs and destabilized αLac, mixtures of either HSPB5 or wHSP16.9 and αLac were analyzed by size exclusion chromatography (SEC). sHSP/client mixtures were incubated for either 2 minutes or 30 minutes following reduction of αLac and then subjected to SEC. SDS-PAGE analysis of elution fractions allowed visualization of the distribution of sHSPs in the presence and absence of the client (Figure 3). After a 2-minute incubation with client, the elution of wHSP16.9 is indistinguishable from that in the absence of a client. In contrast, after a 30-minute incubation with the client, wHSP16.9 elutes significantly earlier (Figure 3). Together the observations indicate that wHSP16.9 interacts with αLac with sufficient affinity to significantly alter its SEC profile, but this interaction does not involve states of the client present at early stages along the aggregation pathway. Using the same SEC method, the distribution of HSPB5 is unaltered by the presence of the client protein at either time point, even though HSPB5 delays the aggregation of destabilized αLac during this timeframe (Figure 3). Thus, while an interaction between HSPB5 and αLac can be inferred on the basis of the observed chaperone activity, the interaction is too transient to be detected by SEC.

The SEC results reveal a clear difference in the ways these two sHSPs interact with a client and indicate that only wHSP16.9 has long-lived, high affinity interactions with αLac states that develop later in the aggregation process (i.e., nucleated states). We sought to determine if wHSP16.9‘s ability to strongly bind later-state aggregates is integral to its chaperone function.

Chaperone assays were performed under conditions where either 1) the sHSP was incubated with αLac prior to reduction-induced aggregation, thereby allowing the sHSP to interact with the client from the initial destabilization of the client or 2) the addition of sHSP was delayed until until initial aggregates of the destabilized client were detected by light-scattering. Under the first condition, where sHSP and client were incubated prior to destabilization, both HSPB5 and wHSP16.9 effectively delay the onset of αLac aggregation as observed by light scattering (Figure 3 bottom green scattering curves). In the second condition, where sHSPs were not added until aggregates are first observed, (figure 3 red scattering curves) HSPB5 fails to delay αLac aggregation, while wHSP16.9 retains its ability to delay the progression of aggregation. Thus, HSPB5 appears to perform its chaperone function by intervening in very early stages of aggregation and is ineffective when faced with nucleated aggregates, while wHSP16.9 is able to intervene by engaging with late-stage species in the progression of αLac aggregation.

Although light scattering assays report on the appearance of very large aggregates, they cannot provide insight into processes that occur prior to this stage along the aggregation pathway, i.e. smaller aggregate states. However, other approaches such as ^{1}H-1D NMR are capable of reporting on earlier states of the destabilized client (24). In this type of experiment 1D NMR spectra are collected as a function of time after the client (αLac) is destabilized by the addition of reducing agent (Supplemental figure 1). The initial destabilized monomeric states of αLac are observable while downstream aggregates form species too large for detection via this conventional NMR technique. The progressive loss of NMR signal from destabilized αLac, monitored as the peak intensity at the region of the spectrum with the greatest initial intensity (0.860 ppm), serves as a metric for observing the transition from monomeric states to oligomers

that occurs early in the aggregation pathway. In fig. 4, the NMR signal for 400μM monomeric αLac can be observed and is sensitive to changes over the time period where light scattering is not detected. In the presence of either 100μM HSPB5 or wHSP16.9, the ^{1}H-1D monomeric αLac NMR signals decay more slowly, indicating the sHSPs act to retain the client in this state (figure 4). Moreover, the addition of either sHSP does not result in an appreciable drop in the NMR signal intensity of αLac as ~90% and ~95% of the predicted intensity ($I_{mixture}/(I_{\alpha Lac\ alone}+I_{sHSP\ alone})$ is retained at the first time point when wHSP16.9 and HSPB5 are present. If destabilized αLac were forming long-lived complexes with the large oligomeric sHSPs, a substantial decrease in spectral intensity would be predicted due to the formation of particles too large to observe by conventional NMR methods. That most of the NMR signal is retained, supports a model where long-lived binding events between the low molecular weight (NMR-observable) αLac and the very large (NMR-invisible) sHSP oligomers do not occur. These observations by NMR, complement our observations made by SEC, which indicate that neither sHSP interacts with the initial unfolded state of αLac with high affinity (Figure 3). Further, that the aggregation of αLac is delayed by their presence implies some weak interaction between the sHSP and client must exist.

sHSP Interactions With Monomeric Unfolded Model Clients

NMR-amenable unfolded proteins have been used to characterize interactions between the client state and ATP-driven HSPs (27-29). These so-called "model clients" do not self-aggregate and remain monomeric in their unfolded states, providing a tractable system for defining interactions between sHSPs and a monomeric unfolded client state. Two such model

clients, a variant of staphylococcal nuclease known as Δ131Δ and the phosphatase phoA, have been used to great effect in studies of other chaperones (27-29).

We characterized interactions between the model client Δ131Δ and fragments of phoA with wHSP16.9 and HSPB5 by 2D-NMR. ^{13}C-HSQC spectra of 50μM Δ131Δ were collected at 310K, pH 7.5 in the presence and absence of a 10-fold excess (500μM) of each sHSP. At a 10-fold excess of wHSP16.9, only an ~8% decrease in spectral intensity is observed in the Δ131Δ ^{13}C-HSQC, while in the presence of HSPB5, ~56% of the intensity in the Δ131Δ ^{13}C-HSQC spectrum is lost (Figure 5). Additional,^{15}N HSQC spectra of 50μM Δ131Δ and two fragments of PhoA at 50μM, were also collected in the absence and presence of sHSP at 283K, and 295K, respectively. Together, these proteins represent a total of 352 residues of unfolded protein sequence that could interact with sHSPs. Addition of a 5-fold excess of HSPB5 or wHSP16.9 does not dramatically alter the ^{15}N HSQC spectra of the model clients, under these conditions (Supplemental figure 2). Under these conditions, the average loss of peak intensity is ~4% and ~6% in the presence of wHSP16.9 and HSPB5, respectively. For all clients, the broadening observed in the presence of HSPB5 is greater than broadening observed in the presence of wHSP16.9. Overall, the observations are consistent with weak and transient interactions between client states and HSPB5. If wHSP16.9 interacts with these client states, the impact on the model client spectra is minor.

The Disease Associated R120G-HSPB5 Has an Altered Affinity For Clients

The inherited HSPB5 mutation, R120G, is associated with cataracts and cardiomyopathies (6). How this mutation impacts interactions with clients is of great interest. Interactions between R120G-HSPB5 and αLac as followed by both light scattering and 1D NMR

have been previously reported (30,31). In light scattering-based assays, R120G-HSPB5 is a much poorer chaperone than the wt-HSPB5 (Supplemental figure 3) (31). In time-dependent ^{1}H 1D ^{1}H NMR spectra of DTT-destabilized αLac, accelerated loss of intensity has been observed in the presence of R120G-HSPB5, suggesting an interaction distinct from that observed with wt HSPB5, occurs between destabilized αLac and the mutant sHSP (30). We have reproduced this result and find that the disease-associated mutant has an altered and higher affinity for αLac (Supplemental figure 4). Importantly, for spectra of 400μM destabilized αLac, in the presence of a 0.25 molar equivalents of R120G-HSPB5, only ~75% of the predicted 1D H NMR Intensity ($I_{mixture}/(I_{\alpha Lac\ alone}+I_{sHSP\ alone})$ is observed, in comparison to the ~95% and ~90% of signal retained in the presence of wt HSPB5 and wHSP16.9, under the same conditions. This demonstrates the mutant has an altered higher affinity for early-unfolded client state of αLac that is distinct from the interactions we observe with either wt sHSP.

To obtain more information regarding the modes of client interactions, R120G-HSPB5 oligomer binding to the model client Δ131Δ was compared with wt HSPB5 oligomers. In presence of 10-fold excess of R120G-HSPB5, broadening in the ^{13}CHSQC spectrum of 50μM Δ131Δ is observed which is greater than the broadening observed with wt HSPB5 and wHSP16.9 oligomers by ~2 fold and ~8 fold respectively (Figure 5). The greater loss of intensity in the Δ131Δ spectrum also suggests that R120G-HSPB5 oligomers have a bolstered affinity for the monomeric model client distinct from either wt sHSP. Yet, this increase in affinity for client manifests as poor chaperone activity.

The R120G Mutation Alters Client Binding Within The ACD Region

The R120G mutation falls within the conserved alpha crystallin domain (ACD). Therefore, we set to determine whether the mutation alters client binding within the ACD region. The isolated, dimeric ACD region of HSPB5 has served as a model for characterizing protein-protein interactions within this conserved region of the protein and is amenable to solution NMR (32). ^{15}N-HSQC NMR spectra of 400μM wt-HSPB5 ACD and the R120G-HSPB5 ACD were collected in the presence and absence of 400μM destabilized αLac. In the presence of destabilized αLac only very subtle changes were observed in the wt-HSPB5 ACD spectrum, indicating the interaction(s) between the client and the ACD are weak and highly transient (Figure 6). In striking contrast, broadening in the R120G-HSPB5-ACD spectrum is observed in the presence of destabilized αLac, which results in a ~66% loss in intensity in the R120G-HSPB5-ACD spectrum (Figure 6). Due to limited spectral assignments and the observed broadening, the region(s) of the R120G-HSPB5-ACD involved in this interaction could not be identified. Such broadening is indicative of an interaction with destabilized αLac that is stronger/longer-lived and distinct from what is observed with the wt HSPB5-ACD.

From experiments with full-length proteins, it is clear FL HSPB5 and FL R120G-HSPB5 have distinct interactions with the monomeric model client Δ131Δ. Using the same rationale as binding experiments between ACDs and destabilized αLac, we set to determine whether the R120G mutation alters the ACD interaction with Δ131Δ. ^{15}N HSQC spectra of Δ131Δ in the presence and absence of the HSPB5-ACD reveal specific binding between the two proteins, with select resonances showing shifts and/or broadening (Figure 7). In contrast to the differences in binding observed with destabilized αLac, the binding to Δ131Δ by the R120G-HSPB5 ACD is indistinguishable from the WT-ACD (Figure 7). Partial assignments of the ^{15}N HSQC Δ131Δ spectrum are available, allowing identification of the affected residues of Δ131Δ in a region

containing the sequence $I^{71}EV$ (28,33). This sequence corresponds to a so-called IXI/V-motif, which is found in the C-terminal regions (CTR) of many sHSPs. In the context of a sHSP CTR, this motif is known to bind to the β4/8 groove of the ACD in an interaction observed in sHSP oligomers (See thesis chapter 2, ref.32). . To confirm binding to Δ131Δ occurs via the β4/8 groove, we introduced a mutation, S135Q, into the HSPB5-ACD (32). This mutation has previously been shown to block IXI-based interactions with an ACD β4/8 groove. The groove-blocking mutation abrogates the observed interaction demonstrating that other than binding to the β4/8 groove, interactions between the ACD and this model client are relatively limited (Figure 7). Further, mutation of the $I^{71}EV$ sequence in Δ131Δ to $I^{71}EA$ (V73A- Δ131Δ) also, abrogates much of the observed binding to the HSPB5-ACD (Supplemental Figure5).

ACDs Show Some Confounding Properties

A growing body of work has been directed towards characterizing the chaperone activity of ACDs, largely because they prove much more experimentally tractable than full-length oligomers. In many cases, the chaperone activity of ACDs has been proposed to be similar to that of full-length oligomers. Though the wt HSPB5-ACD retains some chaperone activity with αLac, the HSPB5 oligomer proves a more potent chaperone for destabilized αLac under the chaperone conditions presented here (Supplemental figure 6). We were surprised to find that R120G-HSPB5-ACD is a more effective chaperone for αLac in comparison to HSPB5-ACD (Supplemental figure 6). This result was not anticipated based on results with full-length proteins, where the mutation has the opposite effect and results in poorer chaperone function. Additionally, binding between Δ131Δ and oligomeric HSPB5 is weak relative to the ACD/Δ131Δ binding experiments (compare Figure S2 and 7). It is likely the interaction with the

ACD β4/8 groove may be consequence of studying ACDs in isolation or in the least is an overrepresentation of an interaction less abundant in the context of sHSP oligomers. That we observe ACD function and binding that do not trend with the oligomers suggests studies directed at characterizing the function of ACDs in isolation should be interpreted with caution.

Discussion

By multiple methods we set to compare how two sHSPs, wHSP16.9 and HSPB5, interact with clients. Our results show the two sHSPs interact with clients through distinct modes to delay protein aggregation; one being weak interactions observed with HSPB5 and the other a longer-lived and higher affinity interaction only observed between wHSP16.9 and αLac aggregates that manifest later in its aggregation (Figures 3,4 and 8). Though it is surprising that a common mechanism of client binding is not conserved, an explanation for their difference in function may lie in the divergent sequence and structure observed between the two sHSPs (Figure 1). Why nature would select for two distinct binding modes remains to be answered. However, it is clear both modes of interactions can be effective in delaying protein aggregation (Figure 2). It is important to note the binding observations made here are with a limited number of clients and were made under a limited set of solution conditions. It is possible, if not likely, that different clients and/or different solution conditions may result in interactions between clients and sHSPs that are distinct from those observed here. Further investigation with other clients, using strategies like those presented here, will prove informative in understanding the contributions of the client in sHSP/client interactions.

Transient Interactions Are Sufficient For Chaperone Function

We are unable to detect long-lived interactions between destabilized αLac and either full-length HSPB5-oligomers or ACD dimers under conditions where chaperone function occurs (Figure 3,4, and 6). This observation is consistent with other studies directed at characterizing the interaction between HSPB5, αLac and other clients including gamma-crystallin and apo-myogolobin (24,25). That we fail to detect strong interactions between phoA and Δ131Δ and HSPB5 complements these observations and suggests HSPB5 operates predominantly through transient interactions with the client state (Figure 5, S2). Consistent with these observations with model clients, weak interactions with client states of T4 lysozyme and HSPB5 have also been previously reported (26). Multiple regions of HSPB5 have been identified as potential client binding sites (14-20). That these studies fail to converge on a single region of HSPB5 suggests interactions with clients occur through multiple surfaces/regions of the sHSP. The presence of multiple low affinity binding sites may also explain why binding to the unfolded monomeric state is difficult to detect and quantify.

That the interaction between HSPB5 and clients is weak suggests HSPB5 competes with aggregation binding events through the kinetics of binding rather than the thermodynamics of binding. Therefore the efficacy of HSPB5 chaperone function is likely dependent on the aggregation kinetics of the client. The failure of HSPB5 to prevent aggregation of αLac once nucleated aggregates are formed, further supports this model and suggests that the initial stages of αLac aggregation are distinct from aggregation events that occur after nucleated species have formed (Figure 3).

Whether wHSP16.9 also operates through transient interactions with the client state remains unclear. It is apparent that the binding between wHSP16.9 and the model clients phoA, Δ131Δ, or the initial destabilized state of αLac is weak, at best (Figure 3, 5 and S2). Therefore,

the properties of the client needed for long-lived interactions with wHSP16.9 are not present in these client states. However, sHSPs known to form long-lived interactions with clients have also been shown to bind clients transiently, under certain solution conditions (22). It is therefore possible transient interactions between wHSP16.9 and clients occur but it is difficult to infer their function due to the presence of long-lived interactions with later stage aggregates of αLac.

The transient mode of client binding observed is likely too weak to induce changes in the global structure/distribution of oligomers. This is consistent with the observation that destabilized αLac does not alter the distribution of HSPB5 (Figure 3). Previous SAXS studies with HSPB5 and αLac also support the absence of global changes in the oligomer in the presence of the *in vitro* client (23). The relatively slow rate of subunit exchange observed for HSPB5 in the order of $10^{-3}sec^{-1}$, also suggest global changes in HSPB5 oligomers likely occur on a timescale too slow to be relevant for chaperone function and that the native distribution of oligomers is a functional chaperoning unit (34). Therefore, it is most likely that the native distribution of HSPB5 oligomers act as chaperoning units and do not require structural rearrangement for weak client binding interactions.

Strong Interactions With Client Proteins

Though sHSPs are able to operate through transient binding interactions with the client, stronger binding interactions also occur between clients and some sHSPs, such as wHSP16.9. This is clear for wHSP16.9, which forms longer-lived complexes with destabilized αLac during later stages in its aggregation (Figure 3). Other long-lived complexes with multiple clients have been observed with wHSP16.9 (13). It is apparent longer-lived interactions can impart advantages during chaperone function such as delaying aggregation events that HSPB5 fails to

disrupt (figure 3). Much of the client binding in wHSP16.9 and other plant sHSPs has been attributed to the N-terminal region of the proteins (12,13). Differences in structure and sequence in this region are substantial between plant and human sHSPs and likely impact client interactions (Figure 1). It is still unclear which differences in the sHSPs are important in client binding occur.

The R120G Disease Associated Mutation

We are able to demonstrate that the full-length R120G-HSPB5 and the R120G-HSPB5-ACD have stronger interactions with clients than the wild-type HSPB5 constructs (Figure 5, 6 and S4). Both the R120G-ACD and R120G HSPB5-oligomer have notably higher affinity for destabilized αLac (Figure S4 and 6). The enhanced binding with the R120G-ACD suggests the mutation alters how the ACD region interacts with destabilized αLac. Likely, this altered interaction within the ACD region also manifests in the context of the mutant oligomer. However, the R120G-HSPB5 oligomer also has an increased affinity for Δ131Δ that cannot be explained by alterations in the ACD region alone (Figures S2 and 7). Thus, the disease-associated mutant impacts client interactions both within and outside the ACD region, in the context of the R120G-oligomer. Importantly, based on 1D-nmr experiments, the longer-lived interaction between R120G-HSPB5 and αLac, which involves initial unfolded states of αLac, is distinct from the longer-lived interactions observed with wHSP16.9, which binds species of αLac that appears later in the αLac aggregation pathway (Figure 4 and S4). The enhanced affinity observed with R120G also demonstrates that not all interactions with a client lead to chaperone function and importantly, we do not observe a correlation between the affinity for the client and chaperone function.

ACD Interactions With A Client

Multiple regions within the ACD have been identified as putative client binding regions and under limited conditions, with a limited number of clients such as αLac, the ACD retains some chaperone activity (35, 36). Here we are able to demonstrate the model client Δ131Δ can bind to the β4/8 groove of the ACD through an IXI/V motif within Δ131Δ (Figure 7 and S5). This region has been previously implicated in interactions with clients (15, 16, 19, 37). That Δ131Δ can bind the groove demonstrates a client can in principle, interact with the groove through an IXI/V motif. However, this interaction is not readily apparent with full-length oligomeric HSPB5, suggesting access to the β4/8 groove is limited for client binding in HSPB5-oligomers under the solution conditions tested here (Figure 4). Within the HSPB5 oligomer, access to the β4/8 groove is likely limited by interactions involved in oligomer assembly, including interactions with a C-terminal IXI motif found in many sHSPs, which also binds the β4/8 groove. However, changes in solution conditions such as acidification and temperature are known to alter the accessibility of the groove and may make it available for client interactions under these stress conditions (38, 39).

Interplay Between Molecular Chaperones

There is evidence that sHSPs work in concert with ATP-driven chaperones by preventing aggregation and "handing off" clients to ATP-driven chaperones, which then drive protein refolding (22, 40-44). How sHSPs may "hand off" clients remains poorly defined. In the context of sHSPs that bind clients transiently, it is likely that rather than a physical "hand off" of clients between a sHSP and an ATP-driven HSPs, the interplay is a product of differences in binding affinities, favoring client association with ATP-driven "refolding" chaperones. This model is

supported by the observation that the native sHSPs in this study do not interact strongly with the model client Δ131Δ and phoA, which interact with the ATP-driven chaperones HSP90 and Trigger factor with Kds in the tens of μM range (28, 29). In the context of the longer-lived interactions we observe between wHSP16.9 and αLac, it seems likely clients in complex with the sHSP may be limited in their ability to interact with ATP-driven chaperones. This may or may not be the case, as it has been demonstrated that many of these longer-lived interactions between sHSPs and clients can be disrupted by ATP-driven chaperones (22, 40-44). The mechanism of this process remains unclear. However, observations with model clients made here and by others, demonstrate that ATP-driven chaperones and sHSPs recognize different regions/properties of a client (28,29). This difference likely has a role in the interplay between sHSPs and other molecular chaperones.

Here, we have demonstrated that two different sHSPs interact with the same client in distinct ways. Surprisingly, both sHSPs have remarkably weak affinity for the unfolded monomeric state of αLac, Δ131Δ and phoA. This shows that sHSPs operate through client interactions that are distinct from many of the ATP-driven molecular chaperones. In the case of wHSP16.9, we are able to detect a longer-lived interaction with αLac aggregates that form later in the client's aggregation and show that this interaction contributes to chaperone function. This demonstrates sHSPs can interact with different client states that manifest during aggregation. Importantly, it is also apparent that not all interactions with clients are functionally beneficial as is most apparent with the disease-associated R120G-HSPB5. The variability in how sHSPs interact with a client further highlights the diversity in sequence, structure and function observed across the sHSP family.

Materials And Methods

Protein constructs expression and purification

All protein constructs and methods for their expression and purification have been previously described. Briefly, all proteins were expressed and purified BL21 *E. coli*. Expression was induced through the addition of IPTG and cultures were grown for 16 hours at either 16°C or 22°C. Full-length sHSPs were purified through anion exchange and SEC chromatography, using methods previously described. HSPB5 ACDs (Residues 64-152) were purified from TEV protease-cleavable His-tagged constructs using Ni^{2+} Affinity, anion exchange chromatography and size exclusion chromatography, as previously described. PhoA fragments were, purified from TEV cleavable MBP fusions using Ni^{2+} affinity chromatography and SEC. Δ131Δ was purified through ethanol precipitation in Urea and cation exchange chromatography, as previously described.

Chaperone Assays by light scattering. Light scattering chaperone assays were performed in with PBS solutions at pH 7.5 and 250µL well volumes. DTT-denatured bovine α-Lactalbumin (Sigma L6010) was used as the model substrate and light scattering at A_{360} nm was used to monitor protein aggregation in the presence and absence of sHSPs at 42 ºC. A ratio of 20µM sHSP (subunit concentration) to 600µM aLac was used. Aggregation of aLac was induced by the addition of EDTA and DTT to final concentrations of 5mM. For assays where the addition of sHSPs was delayed allowing aggregates of αLac to form, sHSPs were added to aggregating αLac when ~5% of the final observed light scattering was detected.

SEC of reduced αLac and sHSPs. All SEC experiments were performed on an GE Akta Purifier equipped with a 24ml Superdex 200 preparatory grade column (GE Life Sciences) and a 100µl

sample loop in PBS 7.5. SEC experiments were performed at room temperature (~25°C) with 600μM αLac and 100μM HSPB5 or wHSP16.9. Mixtures at 42°C, were incubated for either 2-minutes or 30-minutes after the addition of 5mM DTT and 5mM EDTA, then subject to SEC. Fractionated elutions were visualized by SDS-PAGE.

1D NMR spectra of destabilized αLac. Watergated ^{1}H-1D NMR spectra of 400μM αLac in the presence of 5mM DTT and 5mM EDTA were collected at 310K over time in the absence and presence of 100μM HSPB5, R120G HSPB5 or wHSP16.9. The progressive loss of intensity due to aggregation was monitored at 0.860ppm, which provides the strongest signal in the destabilized αLac spectrum (Supplemental figure 1). The expected intensity $I_{\alpha Lac\ alone}+I_{sHSP\ alone}$ was compared to mixtures of destabilized αLac and a sHSP ($I_{mixture}$) and the retained intensity in the mixture was reported ($I_{mixture}/(I_{\alpha Lac\ alone}+I_{sHSP\ alone})$ as a percentage of the predicted intensity $I_{\alpha Lac\ alone}+I_{sHSP\ alone}$.

2D NMR spectra of model clients. ^{15}N TROSY-HSQC spectra of Δ131Δ and fragments of PhoA at pH 7.0, were collected on a Bruker Avance II 600 MHz spectrometer equipped with a triple resonance, z-gradient cryoprobe at 283K, and 295K respectively. All ^{15}N TROSY-HSQC spectra of model clients were collected on samples containing 50μM client protein and when present, 250μM sHSP or ACD. Additional ^{13}C HSQC Spectra of 50μM Δ131Δ were collected at pH 7.5 310K in the presence and absence of 500μM HSPB5, R120G HSPB5 and wHSP16.9.

2D NMR Spectra of ACDs. ^{15}N TROSY-HSQC spectra of ACDs and ACD mutants were collected on a Bruker 500 MHz Avance III spectrometer equipped with a 5-mm z axis gradient, triple resonance probe. All samples were in PBS pH 7.5 10% D_2O. Spectra of 600μM HSPB5-ACD were collected at 295K in the presence and absence of 150μM Δ131Δ and Δ131Δ mutants.

Additional spectra of 400μM HSPB5-ACD and R120G HSPB5-ACD were collected in the presence and absence of 400μM destabilized αLac. Spectra of ACDs in the presence of destabilized αLac were collected over the 1hr following the addition of DTT and EDTA to the NMR sample.

Figures

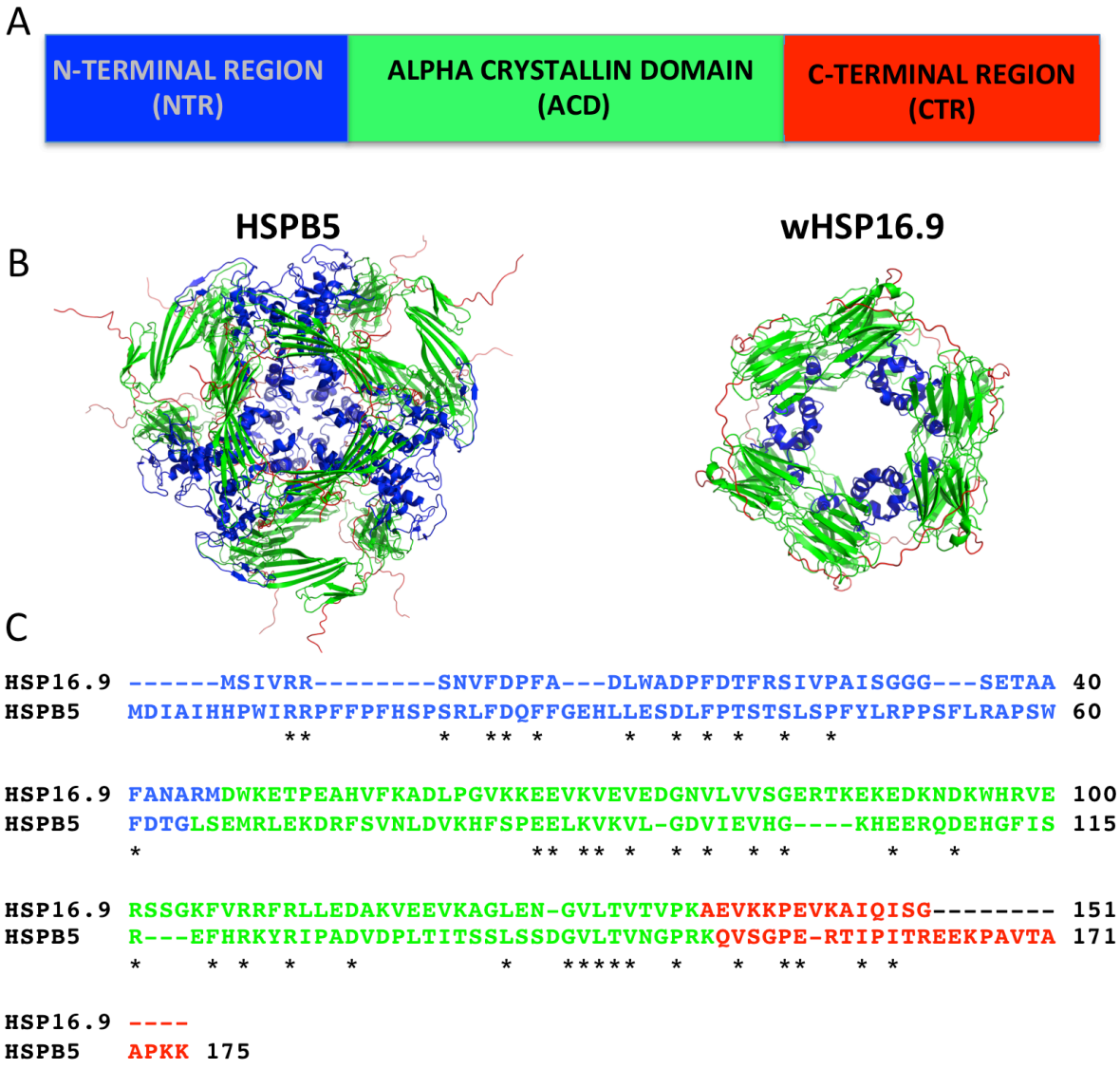

Figure 1. A) Domain architecture of sHSPs HSPB5 and wHSP16.9. The conserved alpha crystallin domain (green) is flanked by N-terminal (blue) and C-terminal (red) regions. B) Comparison of a pseudo-atomic model of the HSPB5 24mer (left) and the structure of the wHSP16.9 dodecamer (right). The N-terminal regions (blue), ACDs (green) and C-terminal regions (red) are highlighted. ~50% of the N-terminal regions are not resolved in the wHSP16.9 structure (PDB ID 1GME) C) Primary sequence alignments of HSPB5 and wHSP16.9 with regions highlighted in colors previously defined in A.

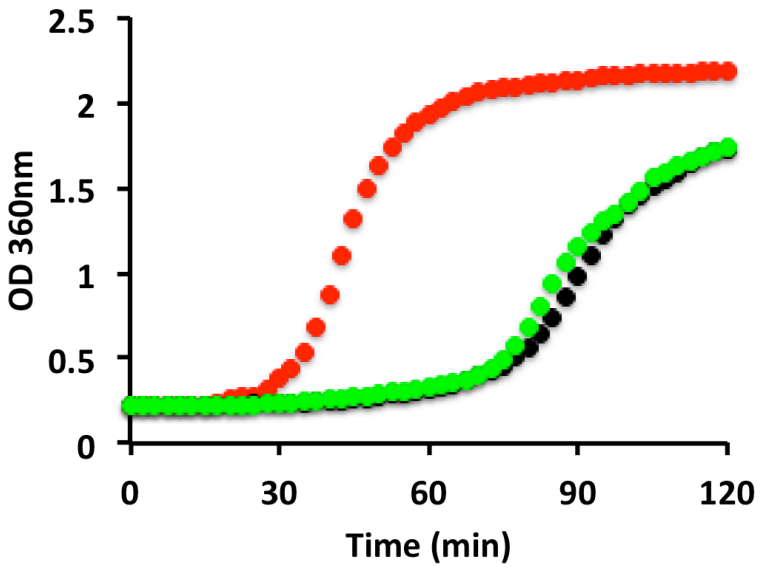

Figure 2. *Chaperone activity of HSPB5 and wHSP16.9 with destabilized αLac by light scattering*. The aggregation of 600μM αLac, destabilized by the addition of DTT can be monitored by the increase in light scattering at 360nm as a function of time (red curve). The presence of either 20μM HSPB5 (green curve) or 20μM wHSP16.9 (black curve) delays the onset of aggregation.

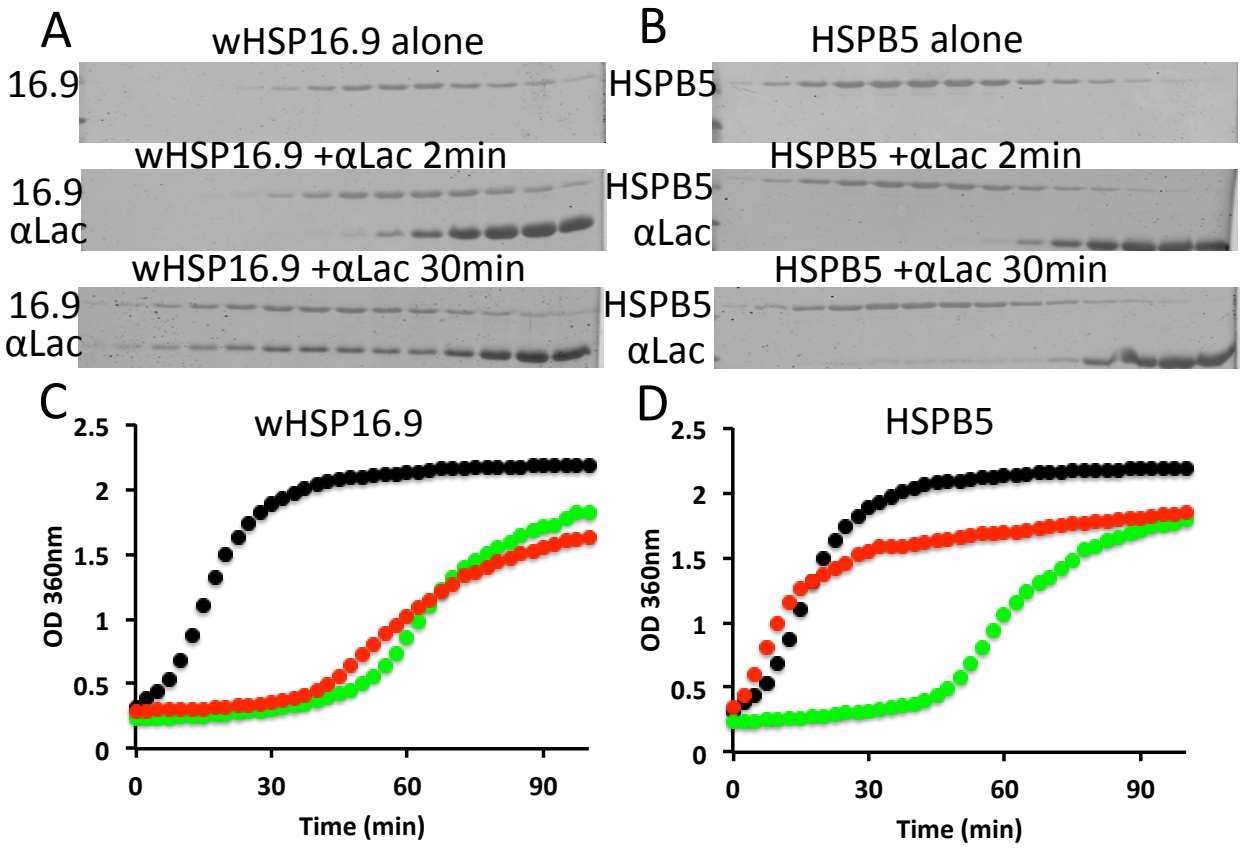

Figure 3. *SEC elutions of sHSP/Client mixtures*. A) SDS-PAGE Gels of SEC fractionated elutions of wHSP16.9 alone (A, top) and mixtures of wHSP16.9 and DTT destabilized αLac incubated at 42°C for 2 minutes (A, middle) and 30minutes (A, bottom) after αLac is reduced. B) SDS-PAGE Gels of SEC fractionated elutions of HSPB5 alone (B, top) and mixtures of HSPB5 and DTT destabilized αLac incubated at 42°C for 2minutes (B, middle) and 30minutes (B, bottom) after αLac is reduced. C,D) The aggregation of 600μM αLac, destabilized by the addition of DTT monitored by light scattering (black curve). If 20μM HSPB5 or 20μM wHSP16.9 are present at the addition of DTT chaperone function with both sHSPs is observed (green curves). If the addition of the sHSPs is delayed until aggregates of DTT destabilized αLac are detected, wHSP16.9 effectively delays aggregation (C red curve) while HSPB5 no longer acts as an effective chaperone (D red curve).

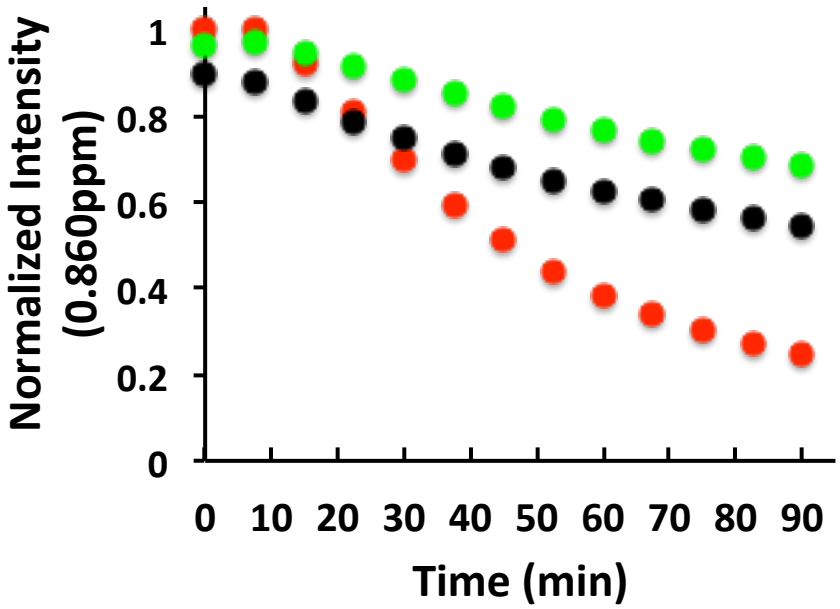

Figure 4. *The aggregation of destabilized αLac observed by 1D NMR*. The peak intensity at 0.860ppm of 400μM DTT destabilized αLac measured as a function of time (red curve). The peak intensity at 0.860ppm of 400μM DTT destabilized αLac in the presence of 100μM HSPB5 (green curve) and wHSP16.9 (black curve) measured as a function of time. Intensities for were normalized to the value ($I_{\alpha Lac\ alone}+I_{sHSP\ alone}$) at 0.860ppm which varied depending on the sHSP in each mixture.

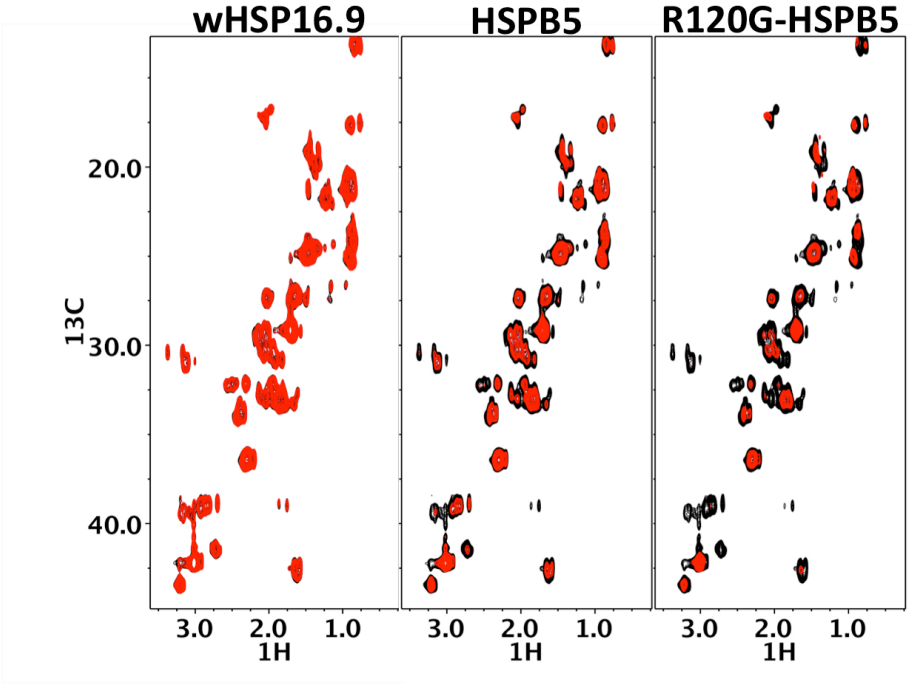

Figure 5. *sHSP interactions with Δ131Δ*. ^{13}C-HSQC spectra of 50μM Δ131Δ at 310K pH 7.5 in the absence (black) and presence (red) of a 500μM of full-length wHSP16.9 (left), HSPB5 (middle) and R120G HSPB5 (right).

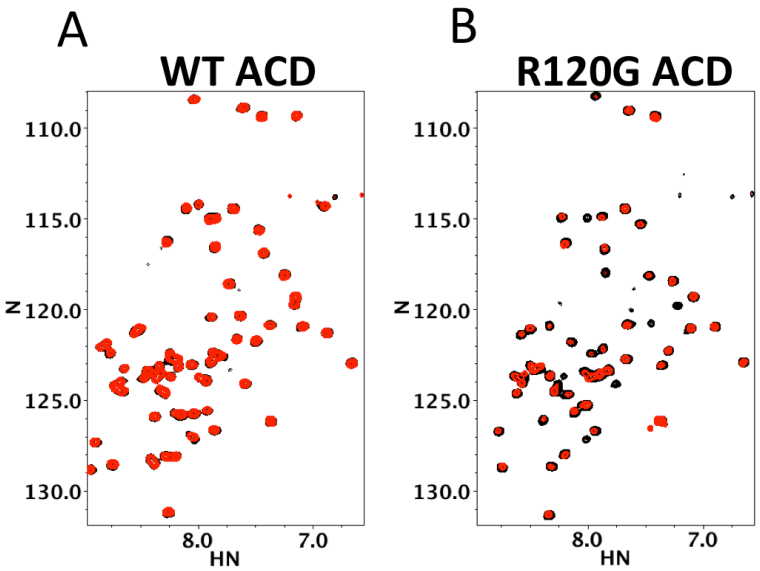

Figure 6. *ACD interactions with destabilized αLac*. ^{15}N HSQC Spectra at 310K pH 7.5 of A. 400µM ^{15}N-WT HSPB5-ACD in the absence (black) and presence (red) of 400µM destabilized αLac. B 400µM ^{15}N-R120G HSPB5-ACD in the absence (black) and presence (red) of 400µM destabilized αLac.

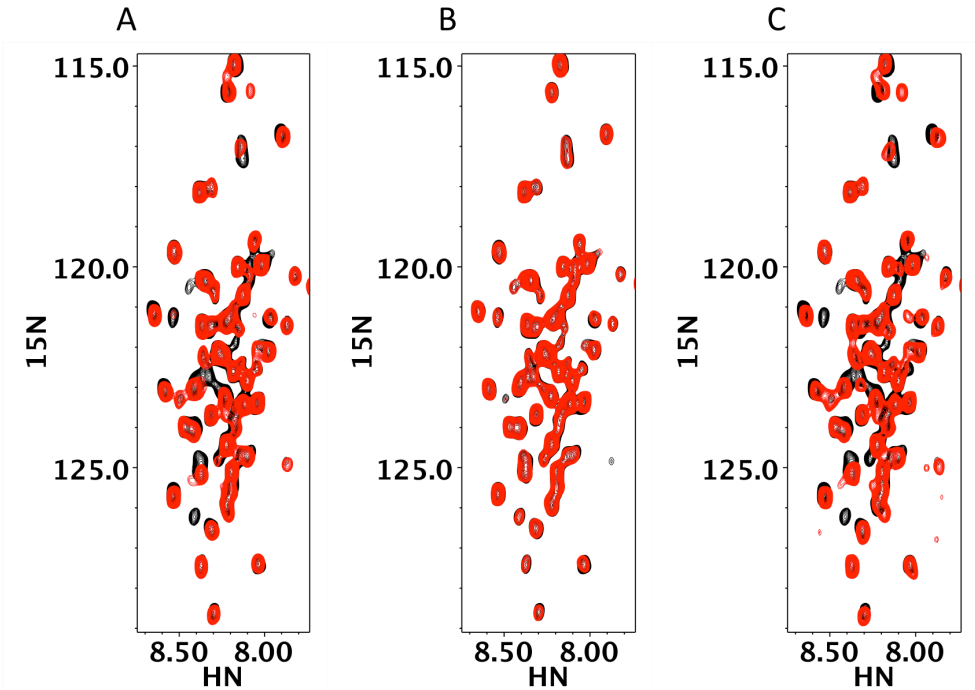

Figure 7 *ACD interactions with Δ131Δ*. ^{15}N-HSQC spectra of 50µM Δ131Δ in the absence (black) and presence (red) of a 250µM of A) wt-HSPB5 ACD B) S135Q HSPB5 ACD and C) R120G-HSPB5 ACD. Spectra were collected at 283K, pH 7.0.

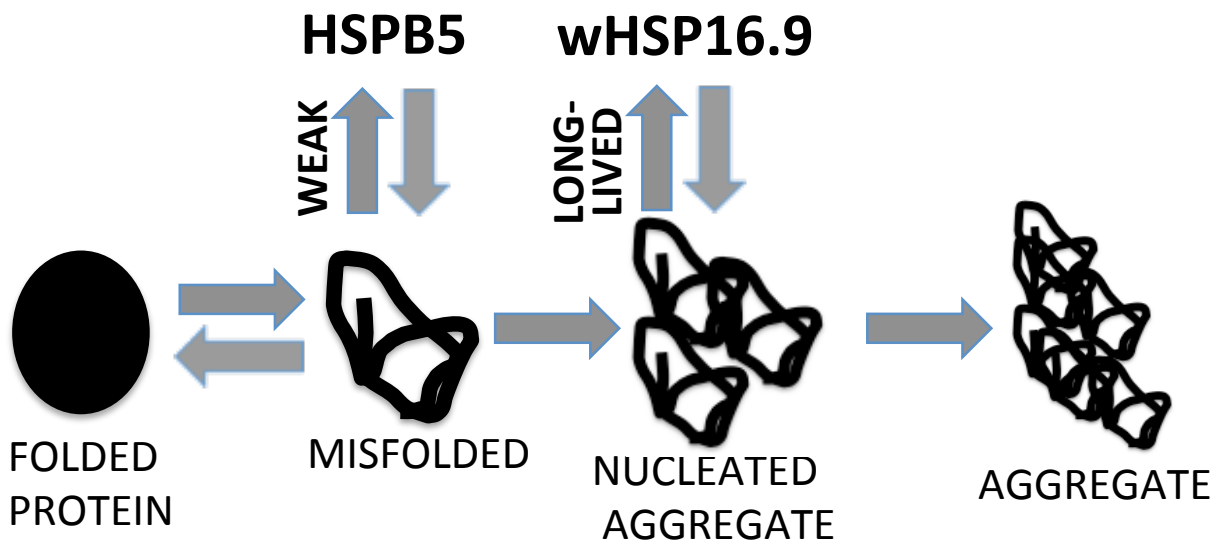

Figure 8. Cartoon diagram of different client interactions observed with HSPB5 and wHSP16.9. HSPB5 and wHSP16.9 interact with different states of statbilized αLac with different affinities. While HSPB5 binds early misfolded states through weak interactions, wHSP16.9 binds to late state aggregates through longer-lived higher affinity interactions.

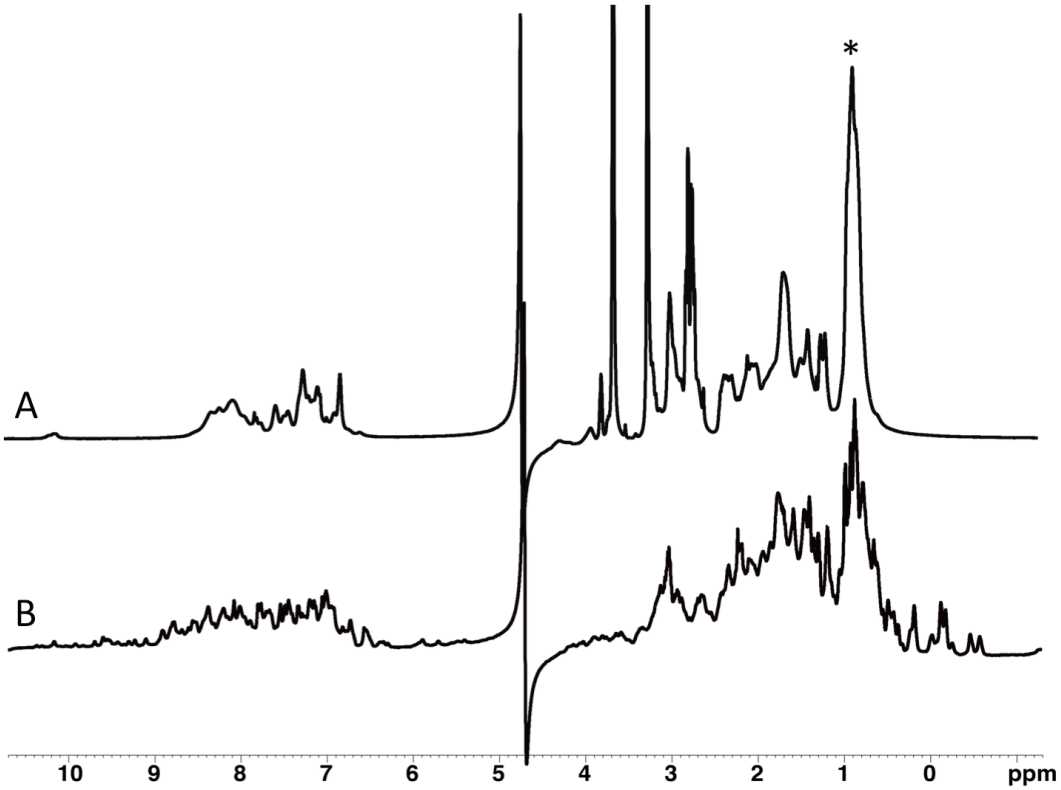

Supplemental Figure 1. 1D-NMR Spectra of A) 400μM DTT destabilized αLac. The peak used for intensity measurements at 0.860 ppm is highlighted with an asterisk. B) 400μM αLac under non-reducing conditions.

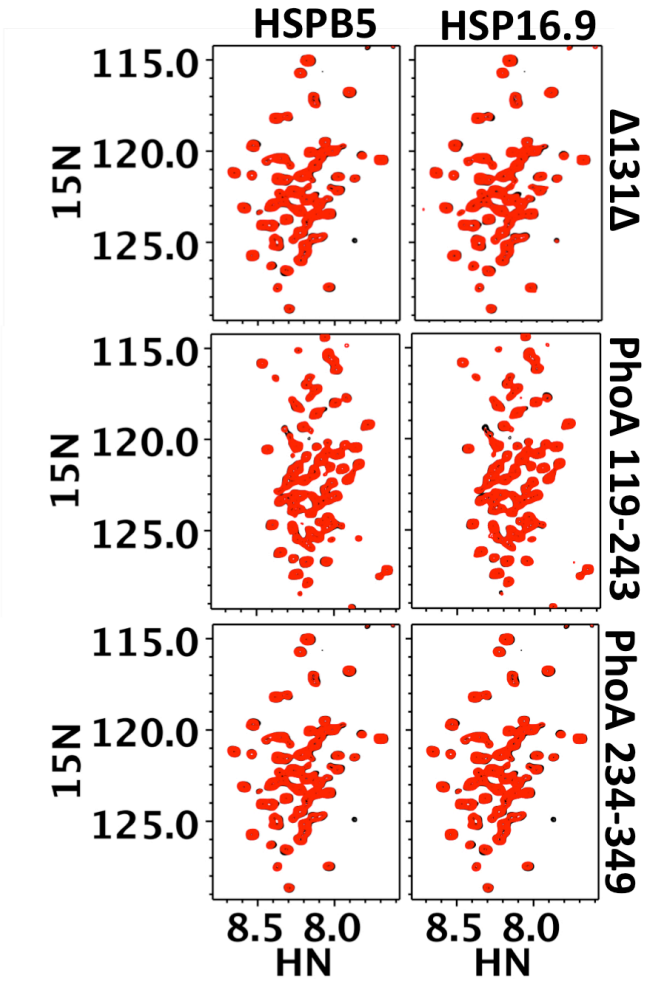

Supplemental Figure 2. Overlays of ^{15}N HSQC Spectra of 50µM Δ131Δ (top row), PhoA 119-243 (middle row) and PhoA 234-349 (bottom row) in the absence (black) and presence (red) of 250µM HSPB5 (left column) and wHSP16.9 (right column). Δ131Δ spectra were collected at 283K and PhoA spectra were collected at 295K.

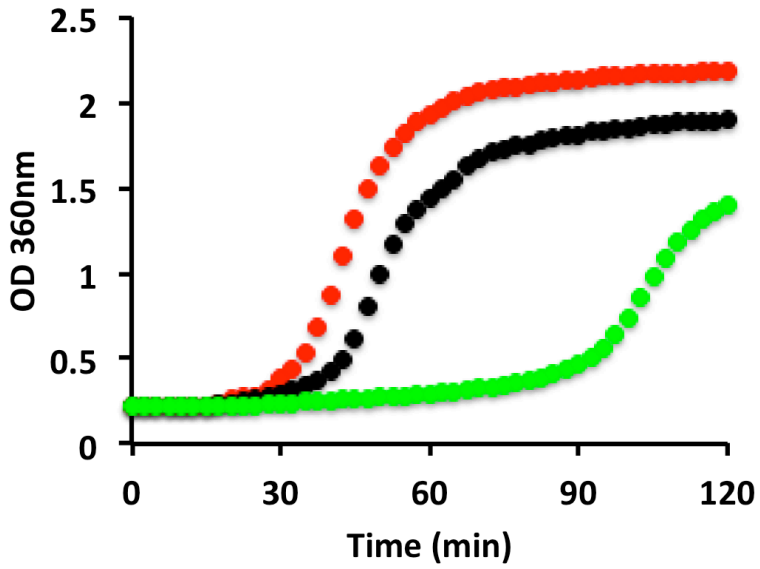

Supplemental Figure 3. . *Chaperone activity of HSPB5 and R120G-HPSB5 with destabilized αLac by light scattering*. The aggregation of 600μM αLac, destabilized by the addition of DTT monitored by the increase in light scattering at 360nm as a function of time (Red curve). The presence of 20μM HSPB5 (green curve) delays the onset of aggregation. Much poorer chaperone activity is observed with the mutant R120G-HSPB5 (black curve).

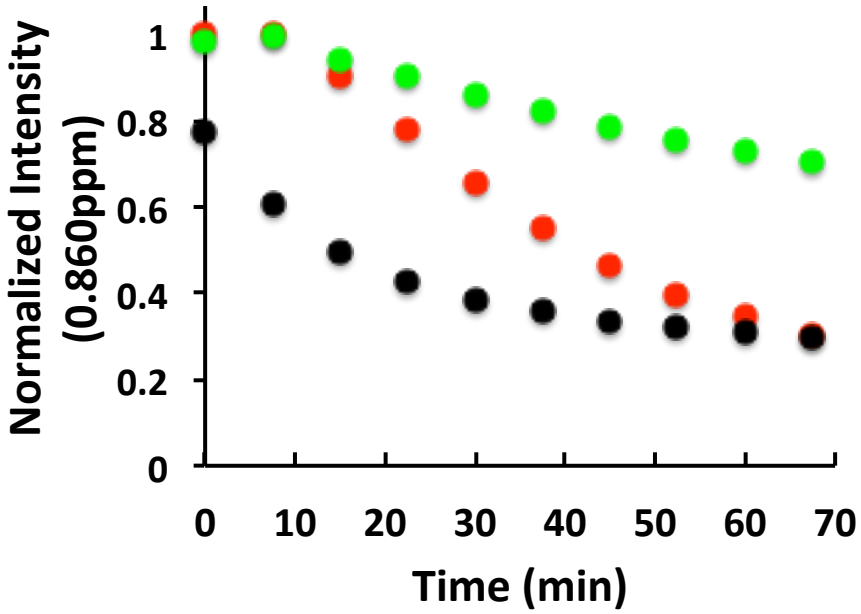

Supplemental Figure 4. *R120G interactions with destabilized αLac by 1D NMR*. The peak intensity at 0.860ppm of 400μM DTT destabilized αLac was measured as a function of time (red curve). The peak intensity at 0.860ppm of 400μM DTT destabilized αLac in the presence of 100μM HSPB5 (green curve) and R120G HSPB5 (black curve) measured as a function of time. Intensities for were normalized to the value ($I_{\alpha Lac\ alone}+I_{sHSP\ alone}$) at 0.860ppm which varied, depending on the sHSP in each mixture.

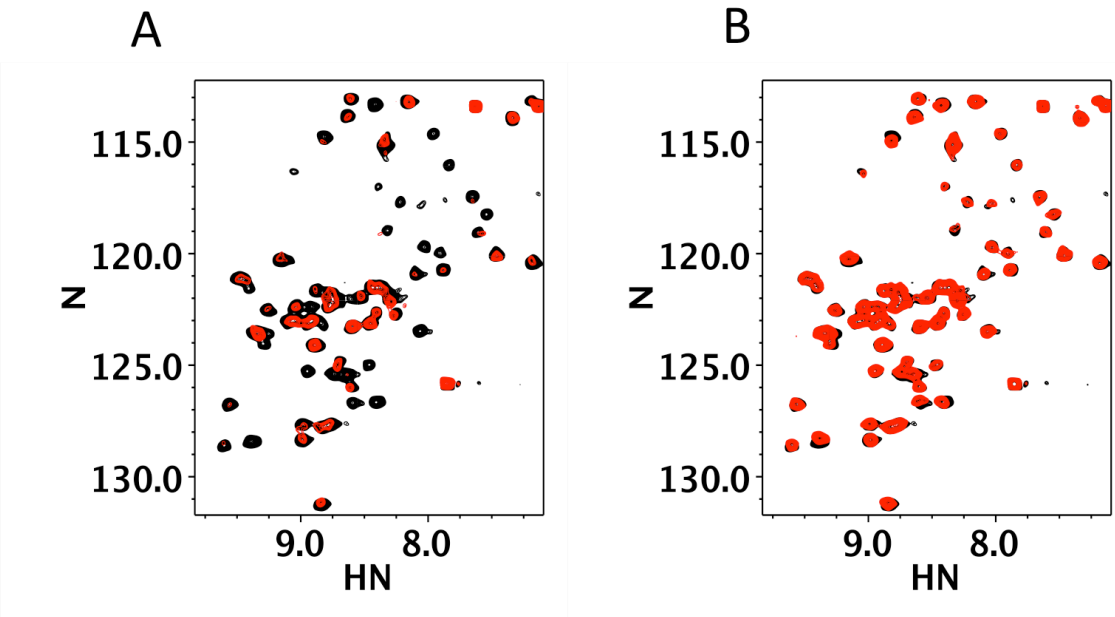

Supplemental Figure 5 Binding of Δ131Δ and IXA Δ131Δ to wt HSPB5 ACD. ^{15}NHSQC spectra of 600μM wt HSPB5-ACD in the absence (black) and presence (red) of A) 150μM Δ131Δ and B) 150μM V73A Δ131Δ. Spectra were collected at 295K pH 7.5.

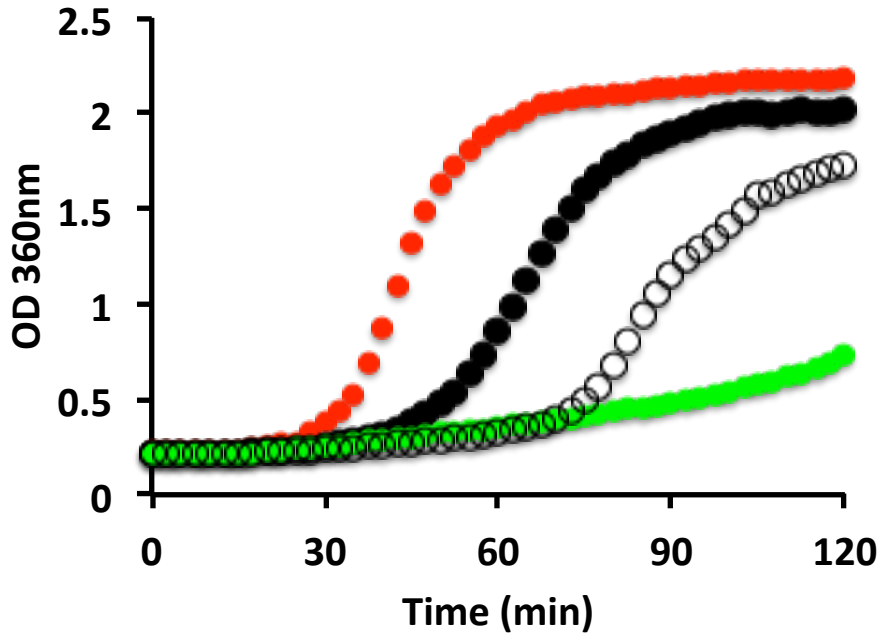

Supplemental Figure 6. *Chaperone activity of HSPB5-ACD and R120G-HSPB5-ACD with destabilized αLac by light scattering*. The aggregation of 600μM αLac, destabilized by the addition of DTT can be monitored by the increase in light scattering at 360nm as a function of time (red curve). The presence of either 20μM HSPB5-ACD (black curve) or 20μM R120G-HSPB5-ACD (green curve) delays the onset of aggregation. Aggregation of αLac in the presence of full-length HSPB5 is also shown (open circles).

References

1 Horwitz, J. (1992) Alpha-crystallin can function as a molecular chaperone. Proc Natl Acad Sci USA 89:10449–10453.

2 Goldstein, L.E., Muffat, J.A., Cherny, R.A., Moir, R.D., Ericsson, M.H., Huang, X., Mavros, C., Coccia, J.A., Faget, K.Y., Fitch, K.A., Masters, C.L., Tanzi, R.E., Chylack, L.T. Jr, and Bush, A.I. (2003) Cytosolic beta-amyloid deposition and supranuclear cataracts in lenses from people with Alzheimer's disease. Lancet 361:1258–1265.

3 Kato, K., Inaguma, Y., Ito, H., Iida, K., Iwamoto, I., Kamei, K., Ochi, N., Ohta, H., and Kishikawa, M. (2001) Ser-59 is the major phosphorylation site in alphaB-crystallin accumulated in the brains of patients with Alexander's disease. J Neurochem 76:730–736.

4 Velotta, J.B., Kimura, N., Chang, S.H., Chung, J., Itoh, S., Rothbard, J., Yang, P.C., Steinman, L., Robbins, R.C., and Fischbein, M.P. (2011) αB-crystallin improves murine cardiac function and attenuates apoptosis in human endothelial cells exposed to ischemia-reperfusion. Ann Thorac Surg 91:1907-1913.

5.Björkdahl, C., Sjögren, M.J., Zhou, X., Concha, H., Avila, J., Winblad, B., Pei, J.J. (2008) Small heat shock proteins Hsp27 or alphaB-crystallin and the protein components of neurofibrillary tangles: tau and neurofilaments. Neurosci Res. 86:1343-1352.

6 Vicart, P., Caron, A., Guicheney, P., Li, Z., Prévost, M.C., Faure, A., Chateau, D., Chapon, F., Tomé, F., Dupret, J.M., Paulin, D., and Fardeau, M. (1998) A missense mutation in the alphaB-crystallin chaperone gene causes a desmin-related myopathy. Nat Genet 20:92–95.

7.van Montfort, R.L., Basha, E., Friedrich, K.L., Slingsby, C., and Vierling, E. (2001) Crystal structure and assembly of a eukaryotic small heat shock protein. Nat Struct Biol. 8:1025-1030.

8 Braun, N., Zacharias, M., Peschek, J., Kastenmüller, A., Zou, J., and Hanzlik, M. (2011) Multiple molecular architectures of the eye lens chaperone αB-crystallin elucidated by a triple hybrid approach. Proc. Natl. Acad. Sci. U.S.A. 108: 20491-20496.

9. Jehle, S., Vollmar, B.S., Bardiaux, B., Dove, K.K., Rajagopal, P., Gonen, T., Oschkinat, H. and Klevit, R.E. (2011) N-terminal domain of alphaB-crystallin provides a conformational switch for multimerization and structural heterogeneity. Proc. Natl. Acad. Sci. USA 108: 6409–6414.

10. Kim, K.K., Kim, R., and Kim, S.H. (1998) Crystal structure of a small heat-shock protein. Nature. 394: 595-599.

11. Aquilina, J.A., Benesch, J.L., Bateman, O.A., Slingsby, C., and Robinson, C.V. (2003) Polydispersity of a mammalian chaperone: mass spectrometry reveals the population of oligomers in alphaB-crystallin. Proc. Natl. Acad. Sci. U.S.A. 19, 10611–10616.

12 Jaya, N., Garcia, V., and Vierling E. (2009) Substrate binding site flexibility of the small heat shock protein molecular chaperones. Proc. Natl. Acad. Sci. U S A. 106:15605-9

13 Basha, E., Friedrich, K.L., and Vierling, E. (2006) The N-terminal arm of small heat shock proteins is important for both chaperone activity and substrate specificity. J. Biol. Chem. 28: 39943-52.

14. Ghosh, J.G., Shenoy, A.K. & Clark, J.I. N- and C-Terminal motifs in human alphaB crystallin play an important role in the recognition, selection, and solubilization of substrates. Biochemistry 45:13847-54(2006).

15. Santhoshkumar, P., and Sharma, K.K. (2006) Conserved F84 and P86 residues in aB-crystallin are essential to effectively prevent the aggregation of substrate proteins. Protein Sci 15:2488-2498.

16. Bhattacharyya, J., Padmanabha Udupa, E.G., Wang, J., and Sharma, K.K. (2006) Mini-alphaB-Crystallin: A Functional Element of aB-Crystallin with Chaperone-like Activity. Biochemisrty 45: 3069- 3076..

17. Aquilina, J.A. and Watt, S.J. (2007) The N-terminal domain of aB-crystallin is protected from proteolysis by bound substrate. Biochem. Biophys. Res. Commun. 353: 1115-1120.

18. Sharma, K., Kumar, G.S., Murphy, A.S., and Kester, K. (1998) Identification of 1,1'-bi(4-anilino)naphthalene-5,5'-disulfonic acid binding sequences in alpha-crystallin. Biochemistry 273:15474 -15478.

19. Ghosh, J.G., Estrada, M.R., and Clark, J.I. (2005) Interactive domains for chaperone activity in the small heat shock protein, human alphaB crystallin. Biochemistry 44: 14854-69.

20. Sharma, K.K., Kaur, H. and Kester, K. (1997) Functional Elements in Molecular Chaperone a - Crystallin : Identification of Binding Sites in a B- Crystallin. Biochemical and Biophysical Research Communications 222, 217-222.

21 Cheng, G., Basha, E., Wysocki, V.H., and Vierling, E. (2008) Insights into small heat shock protein and substrate structure during chaperone action derived from hydrogen/deuterium exchange and mass spectrometry. J. Biol. Chem. 283: 26634-42.

22. Lee, G.J., Roseman, A.M., Saibil, H.R., and Vierling, E. (1997) A small heat shock protein stably binds heat-denatured model substrates and can maintain a substrate in a folding-competent state. EMBO J. 16:659-71.

23. Regini, J.W., Ecroyd, H., Meehan, S., Bremmell, K., Clarke, M.J., Lammie, D., Wess, T., and Carver J.A. (2010) The interaction of unfolding α-lactalbumin and malate dehydrogenase with the molecular chaperone αB-crystallin: a light and X-ray scattering investigation. Mol Vis. 16:2446-2456.

24. Lindner, R.A., Kapur, A., and Carver, J.A. (1997) The interaction of the molecular chaperone, alpha-crystallin, with molten globule states of bovine alpha-lactalbumin. J Biol Chem. 272: 27722-27729.

25. Treweek, T.M., Lindner, R.A., Mariani, M., and Carver, J.A. (2000) The small heat-shock chaperone protein, alpha-crystallin, does not recognize stable molten globule states of cytosolic proteins. Biochim Biophys Acta. 1481:175-188.

26. Koteiche, H.A., and McHaourab, H.S. (2003) Mechanism of chaperone function in small heat-shock proteins. Phosphorylation-induced activation of two-mode binding in alphaB-

crystallin. J Biol Chem. 278:10361-10367.

27 Street, T.O., Zeng, X., Pellarin, R., Bonomi, M., Sali, A., Kelly, M.J., Chu, F., and Agard, D.A. (2014) Elucidating the mechanism of substrate recognition by the bacterial Hsp90 molecular chaperone. J Mol Biol 426: 2393-2404.

28 Street, T.O., Lavery, L.A., and Agard, D.A. (2011) Substrate binding drives large-scale conformational changes in the Hsp90 molecular chaperone. Mol Cell. 42: 96-105.

29. Saio, T., Guan, X., Rossi, P., Economou, A., and Kalodimos C.G. (2014) Structural basis for protein antiaggregation activity of the trigger factor chaperone. Science. 344:1250494.

30 Treweek, T.M., Rekas, A., Lindner, R.A., Walker, M.J., Aquilina, J.A., Robinson, C.V., Horwitz, J., Perng, M.D., Quinlan, R.A., and Carver, J.A. (2005) R120G alphaB-crystallin promotes the unfolding of reduced alpha-lactalbumin and is inherently unstable. FEBS J. 272: 711-24.

31 Bova M.P Yaron O, Huang Q, Ding L, Haley DA, Stewart PL, Horwitz J. (1999) Mutation R120G in αB-Crystallin, which is linked to desmin-related myophathy, results in an irregular structure and defective chaperone-like function. Proc. Natl. Acad. Sci. U S A. 96: 6137-6142.

32 Delbecq, S.P., Jehle, S., and Klevit R.E. (2012) Binding determinants of the small heat shock protein, αB-crystallin: recognition of the 'IxI' motif. EMBO J. 31:4587-4594.

33 Alexandrescu, A.T., Abeygunawardana, C., and Shortle, D. (1994) Structure and dynamics of a denatured 131-residue fragment of staphylococcal nuclease: a heteronuclear NMR study. Biochemistry 33:1063-1072.

34 Baldwin, A.J., Lioe, H., Hilton, G.R., Baker, L.A., Rubinstein, J.L., Kay, L.E., and Benesch J.L.P. (2011) The Polydispersity of aB-Crystallin Is Rationalized by an Interconverting Polyhedral Architecture. Structure 19, 1855–1863.

35. Laganowsky, A., Benesch, J.L., Landau, M., Ding, L., Sawaya, M.R., Cascio, D., Huang, Q., Robinson, C.V., Horwitz, J., and Eisenberg, D. (2010) Crystal structures of truncated alphaA and alphaB crystallins reveal structural mechanisms of polydispersity important for eye lens function. Protein Sci. 19:1031-1043

36 Hochberg, G.K., Ecroyd, H., Liu, C., Cox, D., Cascio, D., Sawaya, M.R., Collier, M.P., Stroud, J., Carver, J.A., Baldwin, A.J., Robinson, C.V., Eisenberg, D.S., Benesch, J.L., and Laganowsky, A. (2014) The structured core domain of αB-crystallin can prevent amyloid fibrillation and associated toxicity. Proc Natl Acad Sci U S A 111: 1562-1570.

37 Ghosh, J.G., Estrada, M.R., and Clark, J.I. (2006) Structure-based analysis of the beta8 interactive sequence of human alphaB crystallin. Biochemistry 45: 9878-9886.

38 Jehle, S., Rajagopal, P., Bardiaux, B., Markovic, S., Kühne, R., Stout, J.R., Higman, V.A., Klevit, R.E., van Rossum, B.J., and Oschkinat, H. (2010) Solid-state NMR and SAXS studies provide a structural basis for the activation of alphaB-crystallin oligomers. Nat. Struct. Mol. Biol. 17, 1037–1042.

39. Baldwin, A.J., Walsh, P., Hansen, D.F., Hilton, G.R., Benesch, J.L., Sharpe, S., and Kay,

L.E. (2012) Probing dynamic conformations of the high-molecular-weight αB-crystallin heat shock protein ensemble by NMR spectroscopy. J. Am. Chem. Soc. 134, 15343-15350.

40 Lee, G.J., and Vierling, E. (2000) A small heat shock protein cooperates with heat shock protein 70 systems to reactivate a heat-denatured protein. Plant Physiol. 122, 189–198.

41.Wang, K., and Spector, A. (2000) alpha-crystallin prevents irreversible protein denaturation and acts cooperatively with other heat-shock proteins to renature the stabilized partially denatured protein in an ATP-dependent manner. Eur. J. Biochem. 267, 4705–4712.

42. Mogk, A., Deuerling, E., Vorderwulbecke, S., Vierling, E. & Bukau, B. (2003) Small heat shock proteins, ClpB and the DnaK system form a functional triade in reversing protein aggregation. Mol. Microbiol. 50, 585–595.

43. Haslbeck, M., Miess, A., Stromer, T., Walter, S. and Buchner, J. (2005) Disassembling protein aggregates in the yeast cytosol: The cooperation of Hsp26 with Ssa1 and Hsp104. J. Biol. Chem. 280, 23861–23868 .

44. Cashikar, A.G., Duennwald, M.L. and Lindquist, S.L. (2005) A chaperone pathway in protein disaggregation: Hsp26 alters the nature of protein aggregates to facilitate reactivation by Hsp104. J. Biol. Chem. 280, 23869–23875.